Angewandte Chemie
Eine Zeitschrift der Gesellschaft Deutscher Chemiker

Supporting Information

A Chemiluminescent Tetraaryl Diborane(4) Tetraanion

*Hendrik Budy, Thomas Kaese, Michael Bolte, Hans-Wolfram Lerner, and Matthias Wagner**

anie_202106980_sm_miscellaneous_information.pdf
anie_202106980_sm_Video.mp4

Table of contents

1. Experimental details and characterization data

General considerations: All reactions, manipulations, and analyses were carried out under an atmosphere of dry argon in a glovebox or by applying standard Schlenk techniques. THF, Et_2O, 1,4-dioxane, toluene, and C_6H_6 were dried over Na/benzophenone; *n*-pentane and *n*-hexane were dried over Na; 1,2-dimethoxyethane (DME), [D_8]THF, and C_6D_6 were dried over Na-K alloy without benzophenone. Prior to use, the solvents were distilled from the drying agent and then degassed by applying three freeze-pump-thaw cycles. 1-Chlorobutane was degassed by applying three freeze-pump-thaw cycles prior to use. [*n*Bu_4N][PF_6] (room temperature) and [Me_4N]Cl (80 °C) were dried *in vacuo* prior to use. Compounds 2,7-di-*tert*-butyl-9-bromo-9-borafluorene,[S1] **1**,[S2] and Li[**2**H][S3] were synthesized according to literature procedures.

NMR spectra were recorded at 298 K using Bruker DPX 250, Avance II 300, Avance III 500 HD, or DRX 600 spectrometers. Chemical shift values are referenced to (residual) solvent signals ($^1H/^{13}C\{^1H\}$; [D_8]THF: δ = 3.58/67.21 ppm[S4] or C_6D_6: δ = 7.16/128.06 ppm[S4]), or $BF_3{\cdot}Et_2O$ ($^{11}B/^{11}B\{^1H\}$), or external LiCl in D_2O (^7Li),. Abbreviations: s = singlet, d = doublet, t = triplet, q = quartet, vt = virtual triplet, vq = virtual quartet, vquint = virtual quintet, br = broad, n.o. = not observed, n.r. = multiplet expected in the NMR spectrum but not resolved. Resonances of carbon atoms attached to boron atoms were typically broadened and sometimes only observed in ^1H-^{13}C-HMBC experiments due to the quadrupolar relaxation of boron. The alkali metal salts Li[**5**], Na_2[**3**], Na_2[**2**], and Na_4[**3**] were isolated as THF and/or DME solvates, which were dried in a dynamic vacuum (oil pump; approximately 10^{-3} torr, room temperature, 10 – 20 min.). After this drying process, the number of remaining THF and/or DME ligands typically varies between individual samples and with respect to the THF and/or DME content of corresponding single-crystalline material (cf. the X-ray crystal structure analyses). It is therefore advisable to determine the individual THF and/or DME content of each sample by means of ^1H NMR spectroscopy.

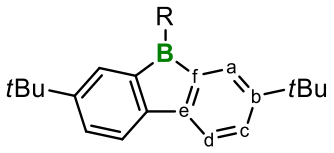

Figure S1. Numbering scheme used for the assignment of the ^1H and $^{13}C\{^1H\}$ NMR resonances.

UV/vis absorption spectra were recorded at room temperature using a Varian Cary 60 Scan UV/vis spectrophotometer. Chemiluminescence spectra were recorded at room temperature using a *Jasco* FP-8300 spectrofluorometer equipped with a calibrated *Jasco* ILF-835 100 mm diameter integrating sphere and analyzed using the *Jasco* FWQE-880 software. GC-MS (gas chromatography - mass spectrometry) data were recorded using a Shimadzu GCMS-QP 2010SE. The stationary phase (Restek) had a length of 60 m with an inner diameter of 0.32 mm. The analyte was diluted with THF prior to measurement. To avoid overloading the MS, a solvent cut was used. Samples were injected at 200 °C and 1/10 thereof was transferred onto column with a flow rate of 1.86 mL/min, carried by helium gas. The oven was heated from 50 °C for 1 min, the temperature was subsequently elevated at a rate of 20 °C/min up to 250 °C and held for 40 min, then elevated again at a rate of 25 °C/min up to 270 °C and held for 10 min. After exiting the column, substances were ionized with 70 eV and cationic fragments were measured within a range of m/z = 35-800 (mass per charges).

1.1 Synthetic procedures

1.1.1 Synthesis of 4

2,7-di-*tert*-butyl-9-bromo-9-borafluorene (2.460 g, 6.926 mmol) was dissolved in *n*-pentane (100 mL) and neat Me_3SiOMe (2.0 mL, 14.5 mmol, 2.1 equiv) was added *via* syringe. The solution was stirred overnight and then all volatiles were removed under reduced pressure to afford **4** as a colorless solid. Yield: 2.099 g (6.854 mmol, 99%).

Single crystals of **4** were grown from a solution of **4** in pentane at –30 °C.

^{1}H NMR (500.2 MHz, C_6D_6): δ = 7.76 (d, ^4J(H,H) = 1.9 Hz, 2H; H-a), 7.39 (d, ^3J(H,H) = 7.9 Hz, 2H; H-d), 7.31 (d, ^3J(H,H) = 7.9 Hz, ^4J(H,H) = 1.9 Hz, 2H; H-c), 3.87 (s, 3H; OCH_3), 1.26 ppm (s, 18H, C(CH_3)$_3$).

^{11}B NMR (160.5 MHz, C_6D_6): δ = 45.8 ppm ($h_{1/2}$ ≈ 350 Hz).

^{13}C{^{1}H} NMR (125.8 MHz, C_6D_6): δ = 150.7 (C-e), 150.3 (C-b), 137.2 (br; C-f), 129.7 (C-a or C-c), 129.6 (C-c or C-a), 119.6 (C-d), 55.7 (O*C*H$_3$), 34.7 (*C*(CH$_3$)$_3$), 31.5 ppm (C(*C*H$_3$)$_3$).

^{1}H NMR (500.2 MHz, [D_8]THF): δ = 7.60 (d, ^4J(H,H) = 1.9 Hz, 2H; H-a), 7.36 (d, ^3J(H,H) = 7.9 Hz, 2H; H-d), 7.33 (d, ^3J(H,H) = 7.9 Hz, ^4J(H,H) = 1.9 Hz, 2H; H-c), 4.29 (s, 3H; OCH_3), 1.32 ppm (s, 18H, C(CH_3)$_3$).

^{11}B NMR (160.5 MHz, [D_8]THF): δ = 46.1 ppm ($h_{1/2}$ ≈ 400 Hz).

^{13}C{^{1}H} NMR (125.8 MHz, [D_8]THF): δ = 150.8 (C-e), 150.5 (C-b), 137.3 (br; C-f), 129.6 (C-a), 129.6 (C-c), 119.5 (C-d), 56.1 (O*C*H$_3$), 35.0 (*C*(CH$_3$)$_3$), 31.5 ppm (C(*C*H$_3$)$_3$).

An alternative synthesis of **4** has been described earlier.[S5]

1.1.2 Synthesis of Li[5]

A solution of **4** (585 mg, 1.91 mmol) in DME (15 mL) was cooled to –30 °C. Pre-cooled (–30 °C) Li granules (719 mg, 103.6 mmol, 54 equiv) were added, and the reaction mixture was stored at –30 °C for 5 d during which time Li[**5**] crystallized in the form of orange blocks (*vide infra*). The excess Li granules were removed manually and the crystal-containing mother liquor was stored again at –30 °C for 1 d. Afterwards, the mother liquor was removed *via* syringe,

the orange crystalline solid was washed with DME (2 x 1 mL), and dried *in vacuo*. Molecular formula of the solvated salt according to ^{1}H NMR spectroscopy: [Li(dme)$_{3.5}$][**5**]. Yield: 452 mg (0.500 mmol, 79%). *Note:* The yield is calculated under the assumption that the liberated LiOMe (1 equiv) consumes 1 equiv of **4** in a Lewis acid-base reaction to give Li[**4**OMe]. As a consequence, 3 equiv of **4** are necessary to yield 1 equiv of Li[**5**].

Single crystals of [Li(dme)$_3$][**5**](DME) were obtained directly from the reaction mixture as described above (*note:* working at higher concentrations should be avoided to prevent co-crystallization of orange [Li(dme)$_3$][**5**](DME) and colorless [Li(dme)$_{1.5}$][**4**OMe]; see below). Single crystals of [Li(thf)$_4$][**5**](THF)$_2$ were grown from a THF solution of Li[**5**] at –30 °C.

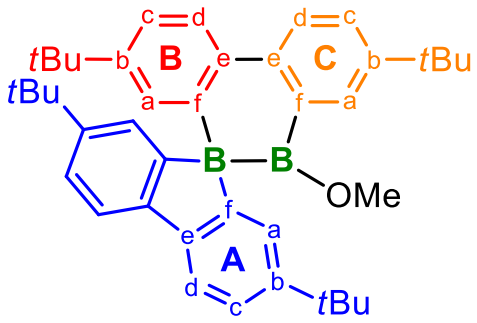

Figure S2: Structure and numbering scheme for the NMR assignment of Li[**5**].

^{1}H NMR (500.2 MHz, [D$_8$]THF): δ = 7.75 (d, ^{3}J(H,H) = 8.2 Hz, 1H; H-Cd), 7.50 (d, ^{3}J(H,H) = 8.0 Hz, 1H; H-Bd), 7.50 (d, ^{4}J(H,H) = 2.4 Hz, 1H; H-Ba), 7.43 (d, ^{3}J(H,H) = 7.8 Hz, 2H; H-Ad), 7.43 (d, ^{4}J(H,H) = 2.4 Hz, 1H; H-Ca), 7.35 (dd, ^{3}J(H,H) = 8.2 Hz, ^{4}J(H,H) = 2.4 Hz, 1H; H-Cc), 7.23 (d, ^{4}J(H,H) = 2.0 Hz, 2H; H-Aa), 6.87 (dd, ^{3}J(H,H) = 8.0 Hz, ^{4}J(H,H) = 2.4 Hz, 1H; H-Bc), 6.84 (dd, ^{3}J(H,H) = 7.8 Hz, ^{4}J(H,H) = 2.0 Hz, 2H; H-Ac), 2.95 (s, 3H; OCH_3), 1.29 (s, 9H; C(CH_3)$_3$-C), 1.18 (s, 9H; C(CH_3)$_3$-B), 1.17 ppm (s, 18H; C(CH_3)$_3$-A).

^{11}B NMR (160.5 MHz, [D$_8$]THF): δ = n.o. (s; B–*B*–OMe), –11.0 ppm (s; *B*–B–OMe).

^{13}C{^{1}H} NMR (125.8 MHz, [D$_8$]THF): δ = 167.5 (br; C-Af), 159.5 (br; C-Bf), 147.6 (C-Ce), 146.1 (C-Ae), 145.8 (C-Cb), 145.7 (C-Bb), 144.3 (C-Ab), 141.2 (br; C-f), 140.2 (C-Be), 131.3 (C-Ba), 129.0 (C-Aa), 126.9 (C-Ca), 126.2 (C-Cc), 124.4 (C-Bd), 123.8 (C-Cd), 119.3 (C-Bc), 118.1 (C-Ac), 117.4 (C-Ad), 56.1 (O*C*H$_3$), 34.8 (*C*(CH$_3$)$_3$-B), 34.7 (*C*(CH$_3$)$_3$-C), 34.7 (*C*(CH$_3$)$_3$-A), 32.3 (C(*C*H$_3$)$_3$-A), 32.1 (C(*C*H$_3$)$_3$-B), 32.0 ppm (C(*C*H$_3$)$_3$-C).

In the ^{1}H and ^{13}C{^{1}H} NMR spectra ([D$_8$]THF), Li[**5**] gives rise to three sets of C_6H_3tBu signals with relative proton-integral ratios of 2:1:1. Fast librational motion in solution obviously renders the two aryl rings of the chelating 2,2'-biphenyldiyl fragment chemically equivalent. The tetracoordinated B nucleus resonates at $\delta(^{11}B)$ = −11.0 ppm, whereas the signal of the tricoordinated one was not detectable, probably due to aggravated quadrupolar broadening.

1.1.3 Isolation of Li[4OMe] from its co-crystallizate with [Li(dme)$_3$][5](DME)

A solution of **4** (560 mg, 1.83 mmol) in DME (5 mL) was cooled to –30 °C. Pre-cooled (–30 °C) Li granules (120 mg, 17.3 mmol, 9.5 equiv) were added, and the reaction mixture was stored at –30 °C for one day, whereupon [Li(dme)$_3$][**5**](DME) formed (*vide supra*). Colorless crystals of [Li(dme)$_{1.5}$][**4**OMe] grew together with orange crystals of [Li(dme)$_3$][**5**](DME). The crystals of [Li(dme)$_{1.5}$][**4**OMe] were manually collected and analyzed by means of X-ray diffraction and NMR spectroscopy.

^{1}H NMR (500.2 MHz, [D$_8$]THF): δ = 7.32 (d, ^{3}J(H,H) = 7.8 Hz, 2H; H-d), 7.30 (d, ^{4}J(H,H) = 2.1 Hz, 2H; H-a), 7.05 (dd, ^{3}J(H,H) = 7.8 Hz, ^{4}J(H,H) = 2.1 Hz, 2H; H-c), 2.81 (s, 6H; OCH_3), 1.31 ppm (s, 18H, C(CH_3)$_3$).

^{11}B NMR (160.5 MHz, [D$_8$]THF): δ = 9.5 ppm (s).

^{13}C{^{1}H} NMR (125.8 MHz, [D$_8$]THF): δ = 154.6 (br; C-f), 148.0 (C-e), 147.2 (C-b), 126.3 (C-a), 123.3 (C-c), 117.8 (C-d), 50.2 (O*C*H$_3$), 34.8 (*C*(CH$_3$)$_3$), 32.1 ppm (C(*C*H$_3$)$_3$).

1.1.4 Synthesis of Na$_2$[3]

A solution of [Li(dme)$_{3.5}$][**5**] (200 mg, 221 μmol) in THF (2 mL) was stirred with Na metal (160 mg, 6.96 mmol, 32 equiv) for 3 h at room temperature to give a brown-red solution of Na$_4$[**3**] (*vide infra* for its isolation and characterization). The excess Na metal was removed manually and [Li(dme)$_{3.5}$][**5**] (200 mg, 221 μmol, 1 equiv) in THF (2 mL) was added dropwise with stirring. The resulting deep blue mixture was filtered by using a frit (G4) and the filter cake was washed with THF (2 x 0.5 mL). The combined filtrates were evaporated to dryness under reduced pressure to give a solid (382 mg) that consisted mainly of Na$_2$[**3**] (90% according to ^{1}H NMR spectroscopy, which was conducted on a sample of 10 mg). Recrystallisation from DME at –30 °C (372 mg of the crude product was dissolved in 2.5 mL) and subsequent drying of the

crystals gave $[Na_2(dme)_{3.75}][\mathbf{3}]$ (> 97% according to ^{1}H NMR spectroscopy; the major contaminant (approx. 1%) was the isomer $Na_2[\mathbf{2}]$). Yield: 264 mg (283 μmol, 62%).

Very dark single crystals of $[Na(dme)_2]_2[\mathbf{3}]$, which showed red reflections at their crystal faces, were obtained from a deep blue solution of $Na_2[\mathbf{3}]$ in DME at –30 °C; single crystals of $[Na(thf)_3{\cdot}thf][Na(thf)(dme)][\mathbf{3}]$ were obtained from a THF solution of $Na_2[\mathbf{3}]$ at –30 °C.

^{1}H NMR (500.2 MHz, [D$_8$]THF): δ = 8.88 (d, ^4J(H,H) = 1.9 Hz, 4H; H-a), 7.57 (d, ^3J(H,H) = 7.9 Hz, 4H; H-d), 6.91 (d, ^3J(H,H) = 7.9 Hz, ^4J(H,H) = 1.9 Hz, 4H; H-c), 1.46 ppm (s, 36H, C(CH_3)$_3$).

^{11}B NMR (160.5 MHz, [D$_8$]THF): δ = 35.3 ppm ($h_{1/2}$ ≈ 450 Hz).

^{13}C{^{1}H} NMR (125.8 MHz, [D$_8$]THF): δ = 158.0 (br; C-f), 144.3 (C-b), 142.5 (C-e), 128.7 (C-a), 117.8 (C-c), 117.6 (C-d), 35.3 (*C*(CH$_3$)$_3$), 32.9 ppm (C(*C*H$_3$)$_3$).

1.1.5 Synthesis of Na_4[3]

Method A: In an NMR tube, $[Li(dme)_{3.5}][\mathbf{5}]$ (15 mg, 16 μmol) was dissolved in [D$_8$]THF (0.5 mL) and treated with Na metal (2 mg, 0.09 mmol, 5 equiv). The NMR tube was flame-sealed. After 1 d at room temperature, the reaction solution consisted mainly of $Na_4[\mathbf{3}]$ (approx. 93%). $Na_2[\mathbf{3}]$ (approx. 4%) and $Na_2[\mathbf{2}]$ (approx. 1% according to ^{1}H NMR spectroscopy) were formed as minor components (see Figure S21).

Method B: $[Na_2(dme)_{3.75}][\mathbf{3}]$ (60 mg, 64 μmol) was dissolved in THF (2 mL) and Na metal (77 mg, 3.4 mmol, 52 equiv) was added. The solution was set to rest for 2 d at room temperature, whereupon its color changed from deep blue to brown-red. The excess alkali metal was removed manually and the solution was evaporated to dryness under reduced pressure to give a solid (64 mg) consisting mainly of $[Na_4(thf)_2(dme)][\mathbf{3}]$ (approx. 90%). Minor components were $Na_2[\mathbf{3}]$ (approx. 5%) and $Na_2[\mathbf{2}]$ (approx. 3% according to ^{1}H NMR spectroscopy).

Note: Solutions of the tetraanion salt $Na_4[\mathbf{3}]$ are extremely sensitive to oxidation. Due to the pronouncedly different colors of $Na_4[\mathbf{3}]$ (brown-red in THF) and its oxidation product $Na_2[\mathbf{3}]$ (deep blue in THF), the oxidation process can easily be followed by the naked eye. Even when working in an argon-filled glovebox (H_2O, O_2 < 1 ppm), the characteristic blue color of $Na_2[\mathbf{3}]$ solutions was observed when thin liquid films of $Na_4[\mathbf{3}]$ formed on glass surfaces. Oxidation also seems to occur rapidly on metal surfaces (spatula or syringe needles). THF solutions of $Na_4[\mathbf{3}]$ contained in flame-sealed NMR tubes are stable for several weeks or even months.

Single crystals of {[Na(thf)(dme)$_{0.5}$]$_2$[Na(thf)]$_{0.5}$[Na]$_{1.5}$[**3**]}$_2$ were grown by gas-phase diffusion of *n*hexane into a THF solution of Na$_4$[**3**]. The quality of the crystals was poor so that only the general constitution of the anion could be confirmed. Even though we undertook multiple attempts to grow better crystals, we were not successful.

^{1}H NMR (500.2 MHz, [D$_8$]THF): δ = 8.17 (n.r., 4H; H-a), 7.89 (d, ^3J(H,H) = 7.9 Hz, 4H; H-d), 6.18 (d, ^3J(H,H) = 7.9 Hz; H-c), 1.37 ppm (s, 36H, C(C*H*$_3$)$_3$).

^{11}B NMR (160.5 MHz, [D$_8$]THF): δ = 14.3 ppm ($h_{1/2}$ ≈ 600 Hz).

^{13}C{^{1}H} NMR (125.8 MHz, [D$_8$]THF): δ = 139.3 (br; C-f), 131.3 (br; C-b), 125.0 (br; C-a), 121.7 (C-e), 119.7 (C-d), 103.7 (br; C-c), 35.1 (*C*(CH$_3$)$_3$), 33.1 ppm (C(*C*H$_3$)$_3$).

1.1.6 Synthesis of Na$_2$[2]

[Na$_2$(dme)$_{3.75}$][**3**] (157 mg, 168 μmol) was dissolved in THF (4 mL). HCl in Et$_2$O (2 mol/L, 0.5 μL, 1 μmol, 0.006 equiv) was added at room temperature. Initially, the solution retained its deep blue color, but turned deep red when stirred overnight. An NMR spectrum recorded on the reaction solution revealed essentially the resonances of Na$_2$[**2**] (cf. Figure S25). Single crystals of [Na(thf)$_3$]$_2$[**2**] grew upon storing the reaction mixture at –30 °C.

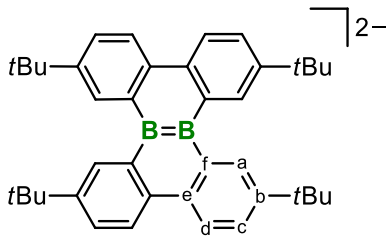

Figure S3. Numbering scheme for the assignment of the ^{1}H and ^{13}C{^{1}H} NMR resonances of [**2**]$^{2–}$.

^{1}H NMR (500.2 MHz, [D$_8$]THF): δ = 9.26 (d, ^4J(H,H) = 2.3 Hz, 4H; H-a), 8.75 (d, ^3J(H,H) = 8.7 Hz, 4H; H-d), 7.14 (dd, ^3J(H,H) = 8.7 Hz, ^4J(H,H) = 2.3 Hz, 4H; H-c), 1.54 ppm (s, 36H, C(C*H*$_3$)$_3$).

^{11}B NMR (160.5 MHz, [D$_8$]THF): δ = 32.2 ppm ($h_{1/2}$ ≈ 500 Hz).

^{13}C{^{1}H} NMR (125.8 MHz, [D$_8$]THF): δ = 146.1 (br; C-f), 141.8 (C-b), 134.0 (C-e), 126.9 (C-a), 125.3 (C-d), 116.2 (C-c), 35.1 (*C*(CH$_3$)$_3$), 32.7 ppm (C(*C*H$_3$)$_3$).

1.1.7 Synthesis of Li_4[6]

A solution of **6** (21 mg, 0.051 mmol) in [D_8]THF (0.8 mL) was treated with Li granules (21 mg, 3.0 mmol, 59 equiv) and the mixture was stirred for 5 h at room temperature. The excess Li metal was removed manually and the solution was placed in an NMR tube. The tube was flame-sealed under vacuum and the sample thereafter investigated by NMR spectroscopy at room temperature (cf. Figure S29). ^{1}H NMR spectroscopy revealed the formation of Li_4[**6**] (approx. 86%) and Li_2[**6**] (approx. 6%). The reaction solution was evaporated to dryness and the residue dissolved in Et_2O. A few single crystals of [Li(Et_2O)][Li(thf)]$_2$[Li(thf)(Et_2O)][**6**] were obtained by slow evaporation of the solvent at −30 °C and fully consumed for X-ray crystallography.

^{1}H NMR (500.2 MHz, [D_8]THF): δ = 8.19 (d, ^3J(H,H) = 8.2 Hz, 4H; H-a), 7.84 (d, ^3J(H,H) = 8.2 Hz, 4H; H-d), 6.35 (vt, 4H; H-b), 6.09 (vt, 4H; H-c), 2.89 (d, ^3J(H,H) = 5.8 Hz, 2H; CHCH_2C(CH_3)$_3$), 2.83 (t, ^3J(H,H) = 5.8 Hz, 1H; CHCH_2C(CH_3)$_3$), 1.13 ppm (s, 9H; CHCH_2C(CH_3)$_3$).

^{7}Li NMR (194.4 MHz, [D_8]THF): δ = −7.4 ppm (s).

^{11}B NMR (160.5 MHz, [D_8]THF): δ = 18.5 ppm ($h_{1/2}$ ≈ 750 Hz).

^{13}C{^{1}H} NMR (125.8 MHz, [D_8]THF): δ = 128.7 (C-a), 121.5 (C-d), 121.3 (br; C-f), 115.0 (C-e), 114.8 (C-b), 108.6 (C-c), 53.6 (CHCH$_2$C(CH_3)$_3$), 34.1 (CHCH_2C(CH_3)$_3$), 30.9 (CHCH_2C(CH$_3$)$_3$), 10.7 ppm (br; CHCH_2C(CH_3)$_3$).

Note: Due to the almost overlapping resonances of C-d/C-f and C-e/C-b, an unambiguous assignment of the signals of Li_4[**6**] was not possible on the basis of ^{1}H-^{13}C-HSQC and ^{1}H-^{13}C-HMBC NMR experiments alone. We therefore also relied on analogies to the spectra of Li_4[**6**].

1.2 Studies on the reduction chemistry of the borafluorene derivatives 1, 2,7-di-*tert*-butyl-9-bromo-9-borafluorene, 4, Li[5], and Na_2[3] that paved the way for the selective synthesis of Li[5], Na_2[3], and Na_4[3] described in chapter 1.1

1.2.1 Reductions of 1 with Li metal in THF and DME

1 was stirred with Li granules in THF or DME at room temperature. Both reactions gave complex mixtures that contained (among other compounds) Li_2[**2**],[S5] Li_2[**1**],[S6] and Li_4[**3**], which could only be separated by manual crystal picking.

Reduction in THF: **1** (200 mg, 724 μmol) was dissolved in THF (3 mL). Li granules (126 mg, 18.2 mmol, 25 equiv) were added, the mixture was stirred for 1 h at room temperature, and filtered by using a frit (G4). ^{1}H NMR spectroscopy on the filtrate revealed that Li_4[**3**] had been formed as a minor product (approx. 3%). Upon storage of the filtrate at –30 °C, single crystals of $[Li_2(thf)_3]$[**1**][S6] and $[Li(thf)_2]_2[Li_2(thf)_3]$[**3**] were obtained, separated manually, and analyzed by X-ray diffraction and NMR spectroscopy.

Reduction in DME: **1** (100 mg, 362 μmol) was dissolved in DME (1.5 mL). Li granules (60 mg, 8.6 mmol, 24 equiv) were added at room temperature, the mixture was stirred overnight, and filtered by using a frit (G4). The filter cake washed with DME (0.5 mL). ^{1}H NMR spectroscopy on the combined filtrates revealed that Li_4[**3**] had been formed (approx. 18%). Upon storage of the filtrates at –30 °C, a solid precipitated, which contained at least eight different compounds; embedded in this solid, we found single crystals of $[Li(dme)]_4$[**3**]. According to ^{1}H NMR spectroscopy, Li_4[**3**] accounted for approx. 50% of the solid material. The single crystals of $[Li(dme)]_4$[**3**] were manually selected and analyzed by X-ray diffraction and NMR spectroscopy (cf. Figures S33−S35).

Li_4[**3**]:

^{1}H NMR (500.2 MHz, [D$_8$]THF): δ = 8.10 (d, ^4J(H,H) = 2.0 Hz, 4H; H-a), 7.95 (d, ^3J(H,H) = 8.5 Hz, 4H; H-d), 6.38 (dd, ^3J(H,H) = 8.5 Hz, ^4J(H,H) = 2.0 Hz, 4H; H-c), 1.35 ppm (s, 36H, C(CH_3)$_3$).

^{11}B NMR (160.5 MHz, [D$_8$]THF): δ = 12.6 ppm ($h_{1/2}$ ≈ 450 Hz).

^{13}C{^{1}H} NMR (125.8 MHz, [D$_8$]THF): δ = 136.3* (C-f), 132.6 (C-b), 127.1 (C-a), 120.7 (C-d), 118.4 (C-e), 108.2 (C-c), 35.1 (*C*(CH$_3$)$_3$), 32.7 ppm (C(*C*H$_3$)$_3$).

* This resonance was only detectable in an ^{1}H-^{13}C-HMBC NMR experiment.

1.2.2 Reductions of 2,7-di-*tert*-butyl-9-bromo-9-borafluorene with Li under various conditions

In a series of experiments, 2,7-di-*tert*-butyl-9-bromo-9-borafluorene was treated with Li granules in different solvents (THF, 1,4-dioxane, DME, C_6H_6/DME, toluene/THF, toluene) and at different temperatures (range between –78 °C and room temperature). In none of these cases did the proportion of Li_4[**3**] exceed approx. 30%. *Note:* 2,7-di-*tert*-butyl-9-bromo-9-borafluorene, dissolved in [D_8]THF or [D_8]THF/DME, forms a stable B–O adduct 2,7-di-*tert*-butyl-9-bromo-9-borafluorene·thf; we observed no evidence of ether cleavage (see the X-ray crystallographically determined solid-state structure of the pristine 9-bromo-9-borafluorene·thf analogue without *t*Bu substituents in Figure S95).[S7]

The reaction of 2,7-di-*tert*-butyl-9-bromo-9-borafluorene with Li metal in DME at room temperature furnished Li_4[**7**] as one of the products, which is most likely formed by solvent activation: 2,7-di-*tert*-butyl-9-bromo-9-borafluorene (299 mg, 0.842 mmol) was dissolved in DME (6 mL). Li granules (128 mg, 18.4 mmol, 22 equiv) were added and the mixture was stirred overnight. The solution was filtered by using a frit (G4) and the filter cake was washed with DME (0.5 mL). ^{1}H NMR spectroscopy on the combined filtrates revealed that Li_4[**3**] (approx. 29%), Li_4[**7**] (approx. 27%), and Li_2[**2**] (approx. 5%) had been formed. Storage of the solution at –30 °C led to the formation of a black precipitate, which was recrystallized from DME at –30 °C to obtain single crystals of $[Li(dme)]_2[Li(dme)_{1.5}]_2$[**7**].

Note: An authentic sample of Li_4[**7**], which gave identical NMR spectra, was obtained by stirring the neutral ethylene-bridged bisborafluorene **7** with excess Li granules in [D_8]THF.

Li_4[**7**]:

^{1}H NMR (500.2 MHz, [D_8]THF): δ = 7.95 (d, ^4J(H,H) = 1.9 Hz, 4H; H-a), 7.86 (d, ^3J(H,H) = 8.7 Hz, 4H; H-d), 6.26 (dd, ^3J(H,H) = 8.7 Hz, ^4J(H,H) = 1.9 Hz, 4H; H-c), 2.25 (4H; C_2H_4) 1.34 ppm (s, 36H, $C(CH_3)_3$).

^{11}B NMR (160.5 MHz, [D_8]THF): δ = 17.4 ppm ($h_{1/2}$ ≈ 350 Hz).

^{13}C{^{1}H} NMR (125.8 MHz, [D_8]THF): δ = 131.4 (C-b), 125.6 (C-a), 124.4 (br; C-f), 120.9 (C-d), 110.3 (C-e), 108.2 (C-c), 34.9 ($C(CH_3)_3$), 32.4 ($C(CH_3)_3$), 21.0 ppm (br; C_2H_4).

1.2.3 Reductions of 4 with Li

4 was treated with Li granules in different solvents (THF, DME, DME/hexane) and at different temperatures (range between –78 °C and room temperature). The highest selectivity regarding the formation of Li_4[**3**] was observed when the reaction was carried out in DME at –64 °C ($CHCl_3$/dry ice bath) and when the reaction mixture was stirred at this temperature overnight. After warming to room temperature, Li_4[**3**] accounted for approx. 73% and Li_2[**2**] for approx. 15% of the reaction solution (according to ^{1}H NMR spectroscopy). Despite multiple recrystallizations from DME or THF the two main products could not be separated well enough to obtain Li_4[**3**] in satisfactory purity of > 90%. *Note:* The use of 9-*iso*propoxy-9-borafluorene instead of **4** led to a less selective reduction reaction.

1.2.4 *In situ* NMR spectroscopic investigations of reduction reactions of Li[5] or Na_2[3] with alkali metals

CAUTION: In all NMR experiments described below (1.2.4.1 − 1.2.4.6), the sealed samples still contained substantial amounts of elemental alkali metal during NMR measurements. We never encountered any safety issues such as induction-induced overheating of the sample. Nevertheless, we explicitly do not encourage repeating these experiments. Their sole purpose was to obtain information about the reaction sequence. It is not necessary to perform these investigations for the actual synthesis of the products described herein.

1.2.4.1 Reduction of Li[5] with Li metal

A solution of [Li(dme)$_{3.5}$][**5**] (15 mg, 17 μmol) in [D_8]THF (0.5 mL) was placed in an NMR tube and Li granules (10 mg, 1.4 mmol, 82 equiv) were added. The tube was flame-sealed under vacuum and the sample thereafter monitored by ^{1}H NMR spectroscopy at room temperature (cf. Figure S39). At first, the formation of Li_2[**3**] (*vide infra*) and Li_2[**2**] was observed. An NMR spectrum recorded 23 h after addition of the Li metal exhibited broadened signals of Li_4[**3**], Li_2[**3**], and Li_2[**2**]. An NMR spectrum recorded 4 h later exhibited sharp signals of Li_4[**3**] and Li_2[**2**]. After a reaction time of 49 h, the solution consisted mainly of Li_4[**3**] (approx. 77%) and Li_2[**2**] (approx. 13%). Additional signals belong to unknown side products.

1.2.4.2 Reduction of Li[5] with Na metal

A solution of $[Li(dme)_{3.5}][\mathbf{5}]$ (15 mg, 17 μmol) in $[D_8]$THF (0.5 mL) was placed in an NMR tube and Na metal (19 mg, 0.83 mmol, 49 equiv) was added. The tube was flame-sealed under vacuum and the sample thereafter monitored by ^{1}H NMR spectroscopy at room temperature (cf. Figure S40). During a reaction time of 9 h, Li[**5**] was almost completely consumed and essentially quantitatively converted to Na_2[**3**]. After 38 h more, the solution consisted mainly of Na_4[**3**] (approx. 93%) and Na_2[**2**] (approx. 3%). Importantly, extremely broadened signals of low intensity were detectable in the regions where the protons of Na_2[**3**] resonate. After three weeks, the solution still consisted of Na_4[**3**] (approx. 93%) and Na_2[**2**] (approx. 6%), but the broadened signals were no longer observed. We attribute the broadened signals to a radical intermediate formed by one-electron reduction of Na_2[**2**] (cf. chapter 4).

1.2.4.3 Reduction of Li[5] with K metal

A solution of $[Li(dme)_{3.5}][\mathbf{5}]$ (15 mg, 17 μmol) in $[D_8]$THF (0.5 mL) was placed in an NMR tube and K metal (21 mg, 0.54 mmol, 32 equiv) was added. The tube was flame-sealed under vacuum and the sample thereafter monitored by ^{1}H NMR spectroscopy at room temperature (cf. Figure S41). After 50 min, most of the starting material was consumed (approx. 70%) and converted to K_2[**3**][S8] (approx. 64%) and K_2[**2**][S8] (approx. 4%). After 1 d, K_2[**3**] had undergone further reduction to K_4[**3**][S8] (broadened signals). Solutions of K_4[**3**] were not long-term stable under the applied conditions (room temperature, flame-sealed NMR tube, excess K metal present) and gave mainly K_2[**2**] and K_2[**1**][S6] in the course of several days.

K_2[**3**]:[S8]

^{1}H NMR (300.0 MHz, [D$_8$]THF): δ = 8.77 (br; 4H; H-a), 7.55 (d, ^3J(H,H) = 7.9 Hz, 4H; H-d), 6.85 (br d, ^3J(H,H) = 7.9 Hz, 4H; H-c), 1.44 ppm (s, 36H, C(CH_3)$_3$).

^{11}B NMR (96.3 MHz, [D$_8$]THF): δ = 36.9 ppm ($h_{1/2}$ ≈ 700 Hz).

K_4[**3**]:[S8]

^{1}H NMR (300.0 MHz, [D$_8$]THF): δ = 7.56 (br; 8H; H-a, H-d), 5.94 (br; 4H; H-d), 1.21 ppm (s, 36H, C(CH_3)$_3$).

^{11}B NMR (96.3 MHz, [D$_8$]THF): δ = 17.6 ppm ($h_{1/2}$ ≈ 950 Hz).

K_2[**2**]:[S8]

^{1}H NMR (300.0 MHz, [D$_8$]THF): δ = 9.07 (d, ^4J(H,H) = 2.1 Hz, 4H; H-a), 8.64 (d, ^3J(H,H) = 8.6 Hz, 4H; H-d), 7.04 (dd, ^3J(H,H) = 8.6 Hz, ^4J(H,H) = 2.1 Hz, 4H; H-c), 1.51 ppm (s, 36H, C(CH_3)$_3$).

^{11}B NMR (96.3 MHz, [D$_8$]THF): δ = 34.8 ppm ($h_{1/2}$ ≈ 700 Hz).

1.2.4.4 Reduction of Na_2[3] with Li metal

A solution of [Na_2(dme)$_{3.75}$][**3**] (10 mg, 11 μmol) in [D$_8$]THF (0.5 mL) was placed in an NMR tube and Li granules (10 mg, 1.4 mmol, 127 equiv) were added. The tube was flame-sealed under vacuum and the sample thereafter monitored by ^{1}H NMR spectroscopy at room temperature (cf. Figure S48). After 24 h, the solution consisted mainly of [**3**]$^{4-}$ (approx. 81%) while the amount of the [**2**]$^{2-}$ contaminant remained essentially unchanged (approx. 1% Li_2[**2**]). Additional signals belong to unknown side products.

1.2.4.5 Reduction of Na_2[3] with Na metal

A solution of [Na_2(dme)$_{3.75}$][**3**] (12 mg, 13 μmol) in [D$_8$]THF (0.5 mL) was placed in an NMR tube and Na metal (18 mg, 0.78 mmol, 56 equiv) was added. The tube was flame-sealed under vacuum and the sample thereafter monitored by ^{1}H NMR spectroscopy at room temperature (cf. Figure S49). After 1 h, the solution consisted of Na_4[**3**] (approx. 45%) and Na_2[**2**] (approx. 3%). Importantly, extremely broadened signals of low intensity were detectable in the regions where the protons of Na_2[**3**] resonate. The broad signals disappeared within the next 6 h, such that (after overall 7 h) the sample consisted almost exclusively of Na_4[**3**] (approx. 94%; Na_2[**2**] approx. 3%) After 18 d, the relative amount of Na_2[**2**] (approx. 6%) with respect to Na_4[**3**] (approx. 94%) had slightly increased.

1.2.4.6 Reduction of Na_2[3] with K metal

A solution of [Na_2(dme)$_{3.75}$][**3**] (11 mg, 12 μmol) in [D$_8$]THF (0.5 mL) was placed in an NMR tube and K metal (29 mg, 0.74 mmol, 62 equiv) was added. The tube was flame-sealed under

vacuum and the sample thereafter monitored by ^{1}H NMR spectroscopy at room temperature (cf. Figure S50). After 7 h, [**3**]$^{2-}$ was completely consumed and mainly [**3**]$^{4-}$ had formed. Solutions of (Na,K)$_4$[**3**] were not long-term stable under the applied conditions (room temperature, flame-sealed NMR tube, excess K metal present) and gave mainly [**2**]$^{2-}$ and [**1**]$^{2-}$ in the course of several days.

1.3 Reactivities of 4, Na_2[3], and M_4[3] (M = Li, Na)

1.3.1 Reaction of 4 with Li[2H]

A solid mixture of **4** (4 mg, 13 μmol) and [Li(thf)$_3$][**2**H] (10 mg, 13 μmol, 1 equiv) was dissolved in [D$_8$]THF (0.5 mL) and placed in an NMR tube, which was flame-sealed under vacuum. The sample was thereafter monitored by ^{1}H NMR spectroscopy at room temperature (cf. Figure S51). After 2 d, most of the Li[**2**H] was consumed and Li[**5**] as well as Li[**2**H·**1**] (the reaction product of Li[**2**H] and **1**[S9]) had been formed selectively in a 1:1 ratio; as a consequence, approx. half of the **4** remained in the solution. After two weeks, the previously reported isomerization of Li[**2**H·**1**] to Li[(**2**H·**1**)'] was observed.[S9]

1.3.2 Thermal rearrangement of Na_2[3] to Na_2[2]

A solution of [Na$_2$(dme)$_{3.75}$][**3**] (15 mg, 16 μmol) in [D$_8$]THF (0.5 mL) was placed in an NMR tube, which was flame-sealed under vacuum. The sample was heated to 130 °C in an oven for the following consecutive time periods: 1 d, 1 d, 1 d, 3 d, 3 weeks, 3 weeks, 2 weeks, 2 weeks, 1 week. (three months in total, cf. Figure S52). After each time interval, ^{1}H NMR spectra were recorded at room temperature. We found that Na_2[**3**] was continuously converted to Na_2[**2**] with an overall selectivity of approx. 66%. Na[**1**H][S6] (approx. 13%) was one among several other decomposition products.

A comparison sample of [Na$_2$(dme)$_{3.75}$][**3**] (15 mg, 16 μmol) in [D$_8$]THF (0.5 mL), which was not heated, remained unchanged over three months.

1.3.3 Reaction of Na_2[3] with Na_4[3]

[Na$_2$(dme)$_{3.75}$][**3**] (5 mg, 5 μmol) was dissolved in [D$_8$]THF (0.3 mL) and treated with Na metal (30 mg, 1.3 mmol, 260 equiv). The mixture was set to rest overnight to give a solution of Na_4[**3**] (cf. 1.2.8). The Na metal was removed manually and the remaining solution was mixed with a solution of [Na$_2$(dme)$_{3.75}$][**3**] (6 mg, 6 μmol, 1 equiv) in [D$_8$]THF (0.3 mL). The combined solutions were placed in an NMR tube, which was flame-sealed under vacuum. The sample was thereafter monitored by ^{1}H NMR spectroscopy at room temperature. During 11 weeks, Na_2[**3**] was completely consumed and essentially quantitatively converted to Na_2[**2**], while Na_4[**3**] remained largely unchanged (cf. Figures S53–S55).

Already 10 min after sample preparation, the ^{1}H NMR signals of Na_2[**3**] were severely broadened, the signals of Na_4[**3**] were broadened to a lesser extent, while the ^{1}H NMR signals

of Na_2[**2**] showed no broadening. We attribute the signal broadening to the presence of a radical intermediate formed by one-electron reduction of Na_2[**2**]. In agreement with that, a mixture of Na_4[**3**] and Na_2[**3**] in THF gave a signal in an EPR spectrum shortly after sample preparation (cf. chapter 4).

1.3.4 Reaction of Na_2[3] with catalytic amounts of HCl

A solution of [$Na_2(dme)_{3.75}$][**3**] (10 mg, 11 μmol) in [D_8]THF (0.5 mL) was treated with a substoichiometric amount of HCl in Et_2O (2 mol/L, 0.5 μL, 1 μmol, 0.09 equiv) and placed in an NMR tube, which was flame-sealed under vacuum. The sample was thereafter monitored by ^{1}H NMR spectroscopy at room temperature. The rearranged protonation product Na[**2**H] was formed immediately (approx. 10% relative to the remaining Na_2[**3**]). After 2 d, Na_2[**3**] had been quantitively converted to Na_2[**2**], while the Na[**2**H] remained unchanged (cf. Figure S56).

1.3.5 Titration of Li_4[3] with HCl

A sample (36 mg) containing [$Li(thf)_3$]$_4$[**3**] (approx. 80% according to ^{1}H NMR spectroscopy; approx. 20 μmol) was dissolved in [D_8]THF (0.6 mL). HCl in Et_2O (2 mol/L, 4 μL, 8 μmol, 0.4 equiv) was added with stirring at room temperature. The solution was placed in an NMR tube and the tube was flame-sealed under vacuum. After ^{1}H NMR spectroscopic investigation, the solution was recovered from the NMR tube and HCl in Et_2O (2 mol/L, 6 μL, 12 μmol, 0.6 equiv) was added with stirring at room temperature. The solution was placed back into an NMR tube, the tube was flame-sealed under vacuum, and an ^{1}H NMR spectrum was recorded. The latter step was repeated four more times so that an overall volume of 34 μL HCl in Et_2O was added (68 μmol, 3.4 equiv; cf. Figure S57).

1.3.5 Reactions of Na_2[3] with [*n*Bu_4N][PF_6]

*(A) Reaction of Na_2[**3**] with 1 equiv [nBu_4N][PF_6]*

An NMR tube was charged with [$Na_2(dme)_{3.75}$][**3**] (10 mg, 11 μmol) and [*n*Bu_4N][PF_6] (4 mg, 10 μmol, 1 equiv). [D_8]THF (0.5 mL) was added and the tube was flame-sealed under vacuum. The sample was thereafter monitored by ^{1}H NMR spectroscopy at room temperature. After three weeks, the solution contained mainly Na[**9**] as well as *n*Bu_3N (cf. Figures S58 and S59).

*(B) Reactions of Na_2[**3**] with 2 equiv [nBu_4N][PF_6]*

NMR-tube scale: An NMR tube was charged with [$Na_2(dme)_{3.75}$][**3**] (15 mg, 16 µmol) and [nBu$_4$N][PF_6] (12 mg, 31 µmol, 2 equiv). [D_8]THF (0.5 mL) was added and the tube was flame-sealed under vacuum. The sample was thereafter monitored by ^{1}H NMR spectroscopy at room temperature. After 4 d, the solution contained mainly [nBu$_4$N][**9**] as well as nBu$_3$N (cf. Figures S60 and S61).

Preparative scale: [$Na_2(dme)_{3.75}$][**3**] (150 mg, 161 µmol) and [nBu$_4$N][PF_6] (120 mg, 310 µmol, 1.9 equiv) were dissolved in THF (5 mL) and the solution was stirred overnight. A colorless microcrystalline precipitate of [nBu$_4$N][**9**] was obtained from a THF solution at −30 °C.

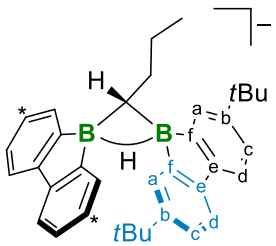

Figure S4. Structure and numbering for the NMR assignments of [**9**]$^-$. C atoms marked with asterisks bear *t*Bu substituents.

^{1}H NMR (500.2 MHz, [D_8]THF): δ = 8.18 (d, ^4J(H,H) = 1.8 Hz, 2H; H-a), 8.01 (d, ^4J(H,H) = 1.8 Hz 2H; H-a), 7.52 (d, ^3J(H,H) = 7.9 Hz, 2H; H-d), 7.49 (d, ^3J(H,H) = 7.9 Hz, 2H; H-d), 7.15 (dd, ^3J(H,H) = 7.9 Hz, ^4J(H,H) = 1.8 Hz, 2H; H-c), 7.13 (dd, ^3J(H,H) = 7.8 Hz, ^4J(H,H) = 1.8 Hz, 2H; H-c), 2.32* (br, 1H; B*H*B), 2.29 (m, 8H; NCH_2CH$_2$CH$_2$CH$_3$), 2.07 (vq, 2H; BCHCH_2CH$_2$CH$_3$), 1.44 (s, 18H; C(CH_3)$_3$), 1.42 (s, 18H; C(CH_3)$_3$), 1.13 (m, 1H; BC*H*CH$_2$CH$_2$CH$_3$) 1.09 (vquint, 2H; BCHCH$_2$CH_2CH$_3$), 0.78–0.69 (m, 28H; NCH$_2$CH_2CH_2CH_3), 0.65 ppm (t, ^3J(H,H) = 7.4 Hz, 3H; BCHCH$_2$CH$_2$CH_3).

* This signal gave a cross-peak in an ^{1}H-^{11}B-HSQC NMR experiment.

^{11}B NMR (160.5 MHz, [D_8]THF): δ = −13.9 ppm ($h_{1/2}$ ≈ 450 Hz).

^{13}C{^{1}H} NMR (125.8 MHz, [D_8]THF): δ = 159.0 (br; C-f), 156.5 (br; C-f), 148.1 (C-e), 147.3 (C-e), 147.2 (C-b), 146.8 (C-b), 130.1 (C-a), 128.1 (C-a), 122.5 (C-c), 122.3 (C-c), 118.3 (C-d), 118.2 (C-d), 57.5 (br, NCH_2CH$_2$CH$_2$CH$_3$), 35.3 (C(CH$_3$)$_3$) 35.2 (*C*(CH$_3$)$_3$), 33.0 (BCH*C*H$_2$CH$_2$CH$_3$), 32.6 (C(*C*H$_3$)$_3$), 32.6 (C(*C*H$_3$)$_3$), 28.2 (BCHCH$_2$*C*H$_2$CH$_3$), 23.8 (NCH$_2$*C*H$_2$CH$_2$CH$_3$) 20.6 (br; B*C*HCH$_2$CH$_2$CH$_3$), 19.7 (NCH$_2$CH$_2$*C*H$_2$CH$_3$), 14.8 (BCHCH$_2$CH$_2$*C*H$_3$), 13.9 ppm (NCH$_2$CH$_2$CH$_2$*C*H$_3$).

*(C) Reaction of Na_2[**3**] with 4 equiv [nBu_4N][PF_6]*

An NMR tube was charged with [$Na_2(dme)_{3.75}$][**3**] (10 mg, 11 μmol) and [nBu$_4$N][PF_6] (16 mg, 41 μmol, 3.7 equiv). [D_8]THF (0.5 mL) was added and the tube was flame-sealed under vacuum. The sample was thereafter monitored by ^{1}H NMR spectroscopy at room temperature. After a reaction time of 80 min, [**3**]$^{2-}$ had been quantitively converted to [**9**]$^-$.

1.3.6 Reaction of Na_2[3] with 1-chlorobutane as a mimic of [nBu$_4$N]$^+$

[$Na_2(dme)_{3.75}$][**3**] (90 mg, 96 μmol) was dissolved in THF (2.5 mL). Neat 1-chlorobutane (10 μL, 95 μmol, 1 equiv) was added and the solution was stirred overnight. After filtration (G4 frit), the filtrate was evaporated to dryness under reduced pressure to obtain a solid residue that consisted mainly of Na[**9**], which was recrystallized from THF at –30 °C to give single crystals of [Na(dme)(thf)$_4$][**9**].

^{1}H NMR (500.2 MHz, [D$_8$]THF): δ = 8.19 (br, 2H; H-a), 8.02 (br, 2H; H-a), 7.44 (d, ^3J(H,H) = 7.8 Hz, 2H; H-d), 7.42 (d, ^3J(H,H) = 7.8 Hz, 2H; H-d), 7.08 (br d, ^3J(H,H) = 7.8 Hz, 2H; H-c), 7.06 (br d, ^3J(H,H) = 7.8 Hz, 2H; H-c), 2.05 (br, 1H; B*H*B), 2.03 (vq, ^3J(H,H) = 7.4 Hz, 2H; BCHC*H*$_2$CH$_2$CH$_3$), 1.45 (s, 18H; C(C*H*$_3$)$_3$), 1.43 (s, 18H; C(C*H*$_3$)$_3$), 1.05 (br t, ^3J(H,H) = 7.4 Hz, 1H; BC*H*CH$_2$CH$_2$CH$_3$), 1.04 (vqiunt, ^3J(H,H) = 7.4 Hz, 2H; BCHCH$_2$C*H*$_2$CH$_3$) 0.63 ppm (t, ^3J(H,H) = 7.4 Hz, 3H; BCHCH$_2$CH$_2$C*H*$_3$).

^{11}B NMR (160.5 MHz, [D$_8$]THF): δ = –12.4 ppm ($h_{1/2}$ ≈ 450 Hz).

^{13}C{^{1}H} NMR (125.8 MHz, [D$_8$]THF): δ = 159.6 (br; C-f), 156.9 (br; C-f), 148.2 (C-e), 147.4 (C-e), 146.3 (C-b), 145.9 (C-b), 130.0 (C-a), 127.9 (C-a), 121.6 (C-c), 121.5 (C-c), 117.7 (C-d), 117.6 (C-d), 35.2 (*C*(CH$_3$)$_3$), 35.2 (*C*(CH$_3$)$_3$), 33.3 (BCH*C*H$_2$CH$_2$CH$_3$), 32.7 (C(*C*H$_3$)$_3$), 32.6 (C(*C*H$_3$)$_3$), 28.2 (BCHCH$_2$*C*H$_2$CH$_3$), 20.8 (br; B*C*HCH$_2$CH$_2$CH$_3$), 15.0 ppm (BCHCH$_2$CH$_2$*C*H$_3$).

1.3.7 Reaction of Na[9] with [nBu$_4$N][PF$_6$]

The purpose of this experiment was to assess the influence of the cation on the ^{1}H NMR shift values of the anion.

[Na(dme)(thf)$_4$][**9**] (13 mg, 13 μmol) and [nBu$_4$N][PF_6] (5 mg, 13 μmol, 1 equiv) were dissolved in [D_8]THF (0.5 mL) and placed in an NMR tube, which was flame-sealed under vacuum. ^{1}H

NMR spectroscopy at room temperature revealed small but significant changes in the chemical shift values compared to those of the pure Na^+ salt (cf. 1.3.6 and Figures S71–S73).

^{1}H NMR (500.2 MHz, [D$_8$]THF): δ = 8.15 (d, ^4J(H,H) = 1.8 Hz, 2H; H-a), 7.97 (d, ^4J(H,H) = 1.8 Hz 2H; H-a), 7.48 (d, ^3J(H,H) = 7.9 Hz, 2H; H-d), 7.45 (d, ^3J(H,H) = 7.9 Hz, 2H; H-d), 7.12 (dd, ^3J(H,H) = 7.9 Hz, ^4J(H,H) = 1.8 Hz, 2H; H-c), 7.09 (dd, ^3J(H,H) = 7.8 Hz, ^4J(H,H) = 1.8 Hz, 2H; H-c) 2.13 (br, 1H; B*H*B), 2.12 (br t, ^3J(H,H) = 7.6 Hz; NC*H*$_2$CH$_2$CH$_2$CH$_3$), 2.04 (vq, ^3J(H,H) = 7.4 Hz, 2H; BCHC*H*$_2$CH$_2$CH$_3$), 1.42 (s, 18H; C(C*H*$_3$)$_3$), 1.41 (s, 18H; C(C*H*$_3$)$_3$), 1.07 (br t, ^3J(H,H) = 7.4 Hz, 1H; BC*H*CH$_2$CH$_2$CH$_3$) 1.05 (vquint, ^3J(H,H) = 7.4 Hz, 2H; BCHCH$_2$C*H*$_2$CH$_3$), 0.67–0.65 (m; NCH$_2$C*H*$_2$C*H*$_2$C*H*$_3$), 0.63 ppm (t, ^3J(H,H) = 7.4 Hz, 3H; BCHCH$_2$CH$_2$C*H*$_3$) 0.62–0.57 (m; NCH$_2$C*H*$_2$C*H*$_2$C*H*$_3$).

^{11}B NMR (160.5 MHz, [D$_8$]THF): δ = –13.0 ppm ($h_{1/2}$ ≈ 600 Hz).

^{13}C{^{1}H} NMR (125.8 MHz, [D$_8$]THF): δ = 159.0 (br; C-f), 156.5 (br; C-f), 148.0 (C-e), 147.3 (C-e), 147.0 (C-b), 146.6 (C-b), 130.0 (C-a), 128.0 (C-a), 122.4 (C-c), 122.2 (C-c), 118.2 (C-d), 118.1 (C-d), 57.2 (br, NC*H*$_2$CH$_2$CH$_2$CH$_3$), 35.2 (*C*(CH$_3$)$_3$), 35.2 (*C*(CH$_3$)$_3$), 33.1 (BCH*C*H$_2$CH$_2$CH$_3$), 32.6 (C(*C*H$_3$)$_3$), 32.6 (C(*C*H$_3$)$_3$), 28.1 (BCHCH$_2$*C*H$_2$CH$_3$), 23.6 (NCH$_2$*C*H$_2$CH$_2$CH$_3$) 20.6 (br; B*C*HCH$_2$CH$_2$CH$_3$), 19.5 (NCH$_2$CH$_2$*C*H$_2$CH$_3$), 14.8 ppm (BCHCH$_2$CH$_2$*C*H$_3$), 14.0 (NCH$_2$CH$_2$CH$_2$*C*H$_3$).

1.3.8 Reactions of Na$_2$[3] with [Me$_4$N]Cl

The purpose of this experiment was to exclude that the activation of [*n*Bu$_4$N][PF$_6$] (cf. 1.3.6) proceeds *via* a Hofmann elimination, which could, in principle, account for the formation of *n*Bu$_3$N as well; the byproducts 1-butene and Na[**2**H] might give Na[**9**].

In a series of three experiments, NMR tubes were charged with [Na$_2$(dme)$_{3.75}$][**3**] (17 mg, 18 μmol) and [Me$_4$N]Cl ((i) 2 mg, 18 μmol, 1 equiv, or (ii) 4 mg, 37 μmol, 2 equiv, or (iii) 10 mg, 91 μmol, 5 equiv). [D$_8$]THF (0.5 mL) was added and the respective tube was flame-sealed under vacuum. The samples were thereafter monitored by ^{1}H NMR spectroscopy at room temperature. Presumably due to the poor solubility of [Me$_4$N]Cl in THF, the reaction times were longer compared to the case of the [*n*Bu$_4$N][PF$_6$] salt. Reaction (i) was not complete even after three weeks. In all cases, the methylene-bridged bisborafluorene (see Figure S5)[S10] was formed as the major product.

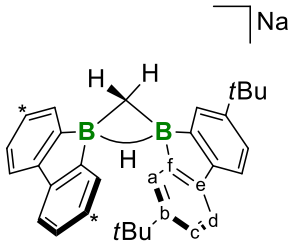

Figure S5 The methylene-bridged bisborafluorene formed by the reaction of Na_2[**3**] with [Me_4N]Cl. C atoms marked with asterisks bear *t*Bu substituents.

^{1}H NMR (500.2 MHz, [D$_8$]THF): δ = 7.99 (d, ^4J(H,H) = 1.9 Hz, 4H; H-a), 7.43 (d, ^3J(H,H) = 7.9 Hz, 4H; H-d), 7.07 (dd, ^3J(H,H) = 7.9 Hz, ^4J(H,H) = 1.9 Hz, 4H; H-c), 1.96* (br, 1H; B*H*B), 1.42 (s, 36H; C(CH_3)$_3$), 0.50 ppm (d, ^2J(H,H) = 4.8 Hz, 2H; BCH_2B).

* This signal sharpened up in a ^{1}H{^{11}B} NMR experiment.

^{11}B NMR (160.5 MHz, [D$_8$]THF): δ = –13.7 ppm ($h_{1/2}$ ≈ 450).

^{13}C{^{1}H} NMR (125.8 MHz, [D$_8$]THF): δ = 158.7 (br; C-f), 147.8 (C-e), 146.4 (C-b), 127.9 (C-a), 122.0 (C-c), 117.8 (C-d), 35.2 (*C*(CH$_3$)$_3$), 32.6 (C(*C*H$_3$)$_3$), 5.1 ppm (br; B*C*H$_2$B).

1.3.9 Chemiluminescence of M$_4$[3] upon contact with air

When solutions of M_4[**3**] (M = Li, Na) in THF or DME come into contact with air, an intense blue chemiluminescence is observed (cf. the video supplied as supporting information and Figures S101–S105 for the electronic spectra). The following further information regarding this phenomenon is noteworthy:

- Li_4[**3**] gave a more intense chemiluminescence than Na_4[**3**] (judged by naked eye inspection).
- Samples containing only M_2[**3**], M_2[**2**], or M_2[**1**] (M = Li, Na), as well as mixtures of these compounds, did not show any chemiluminescence upon admission of air.
- Carefully dried air (P_2O_5 overnight) gave the same result as ambient air (judged by naked eye inspection). By the same token, when M_4[**3**] (M = Li, Na) was treated with proton sources (*i*PrOH or H_2O), no chemiluminescence occurred.
- No chemiluminescence was observed upon reaction of Li_4[**3**] with *t*BuO–O*t*Bu.
- To investigate the products of the reaction underlying the chemiluminescence, samples of Li_4[**3**] in [D$_8$]THF were treated with dry air. After the blue

chemiluminescence had ceased, ^{1}H NMR spectra were recorded, which, however, showed a large number of poorly resolved resonances. Apparently, a complex mixture of several as yet unidentified products had formed (cf. Figure S77).

2. Plots of the NMR spectra

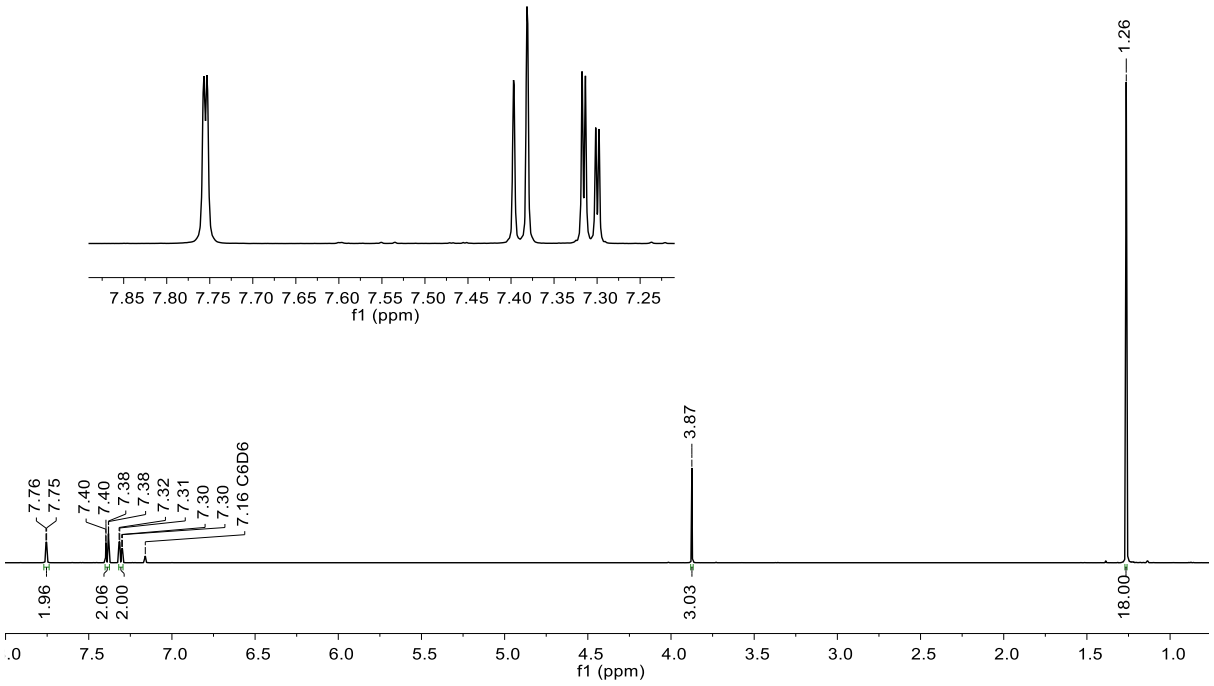

Figure S6: ^{1}H NMR spectrum of **4** (500.2 MHz, C_6D_6).

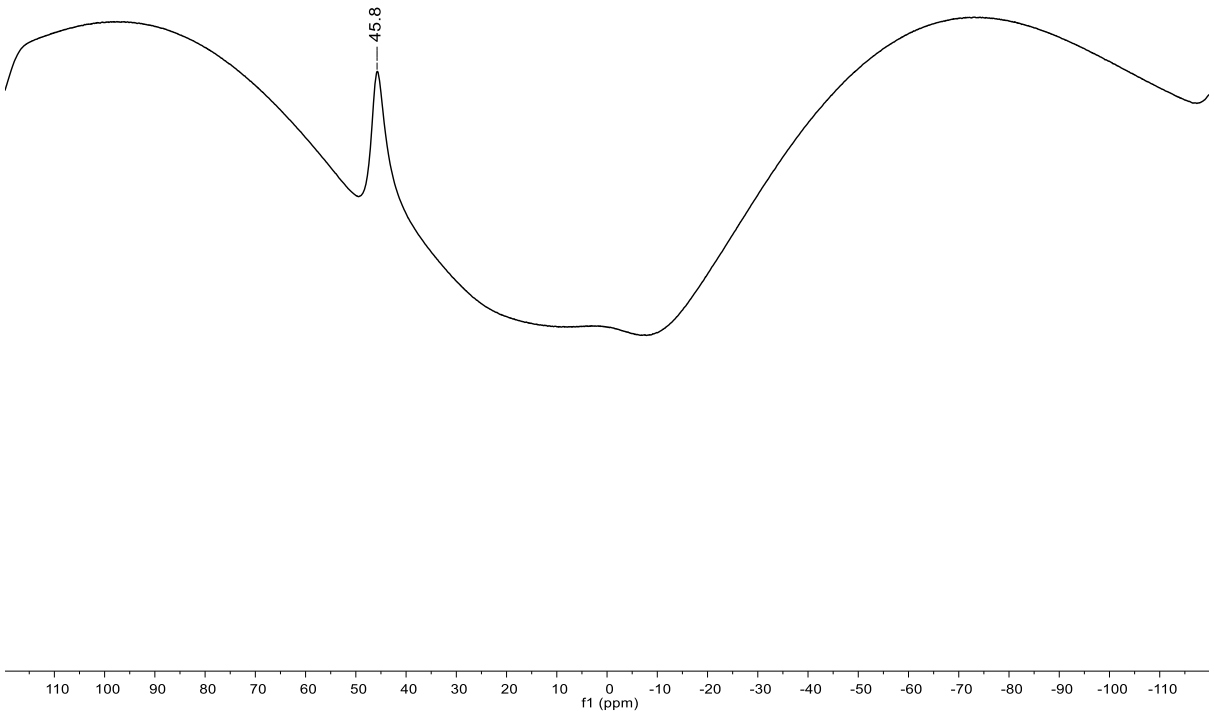

Figure S7: ^{11}B NMR spectrum of **4** (160.5 MHz, C_6D_6).

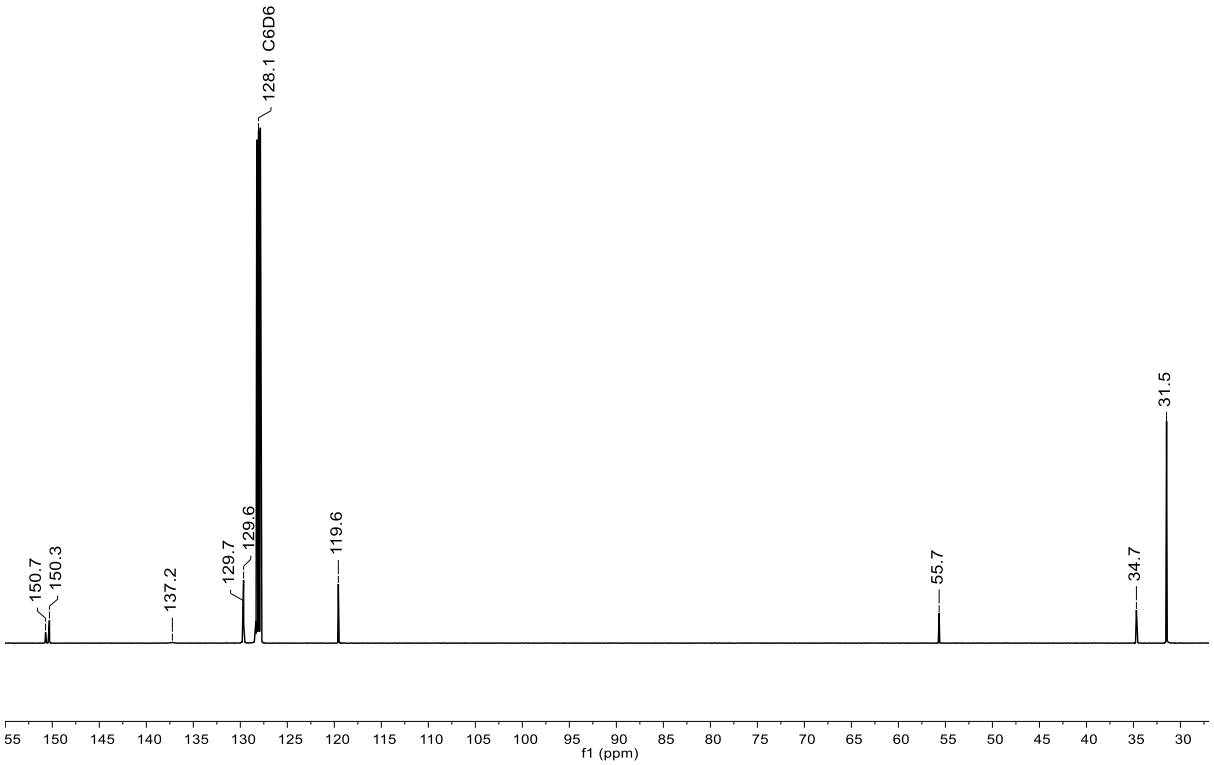

Figure S8: ^{13}C NMR spectrum of **4** (125.8 MHz, C_6D_6).

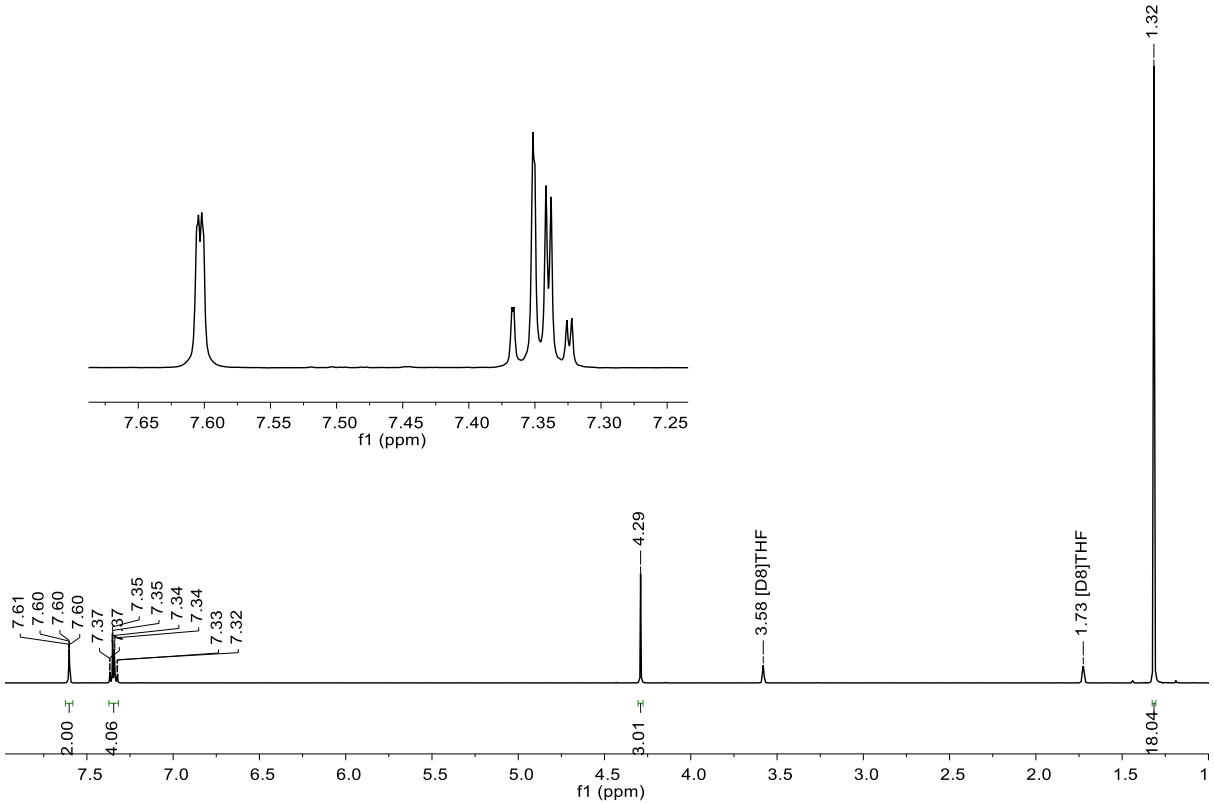

Figure S9: ^{1}H NMR spectrum of **4** (500.2 MHz, $[D_8]THF$).

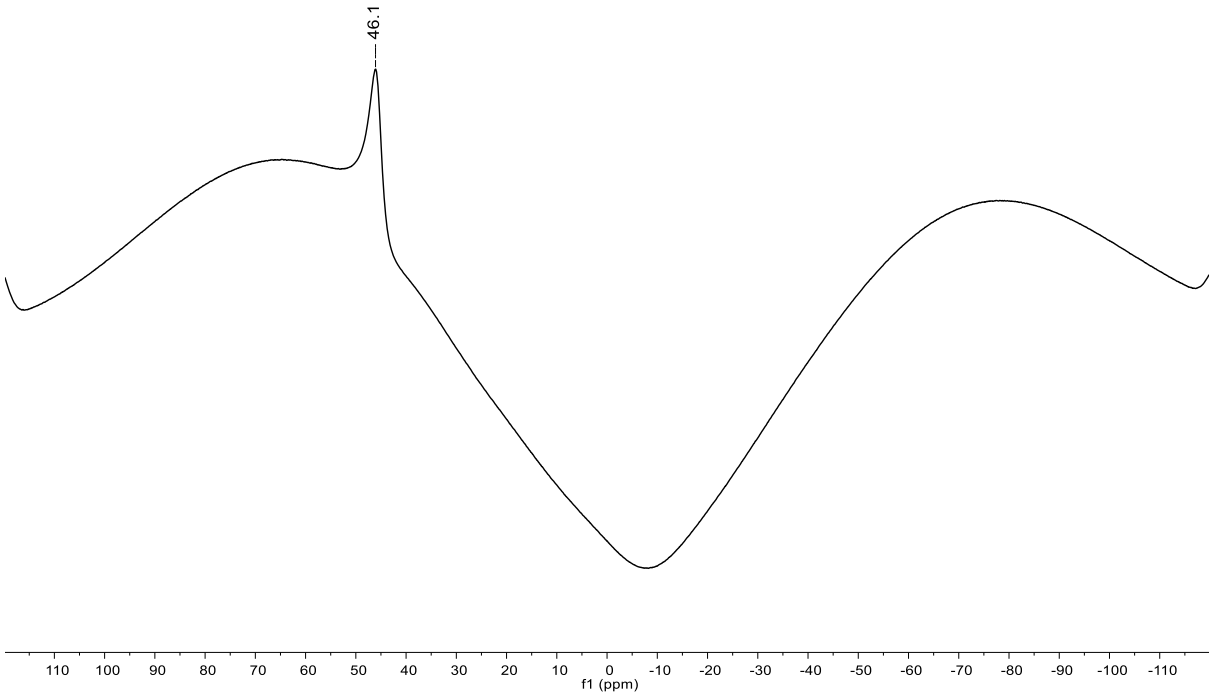

Figure S10: ^{11}B NMR spectrum of **4** (160.5 MHz, [D$_8$]THF).

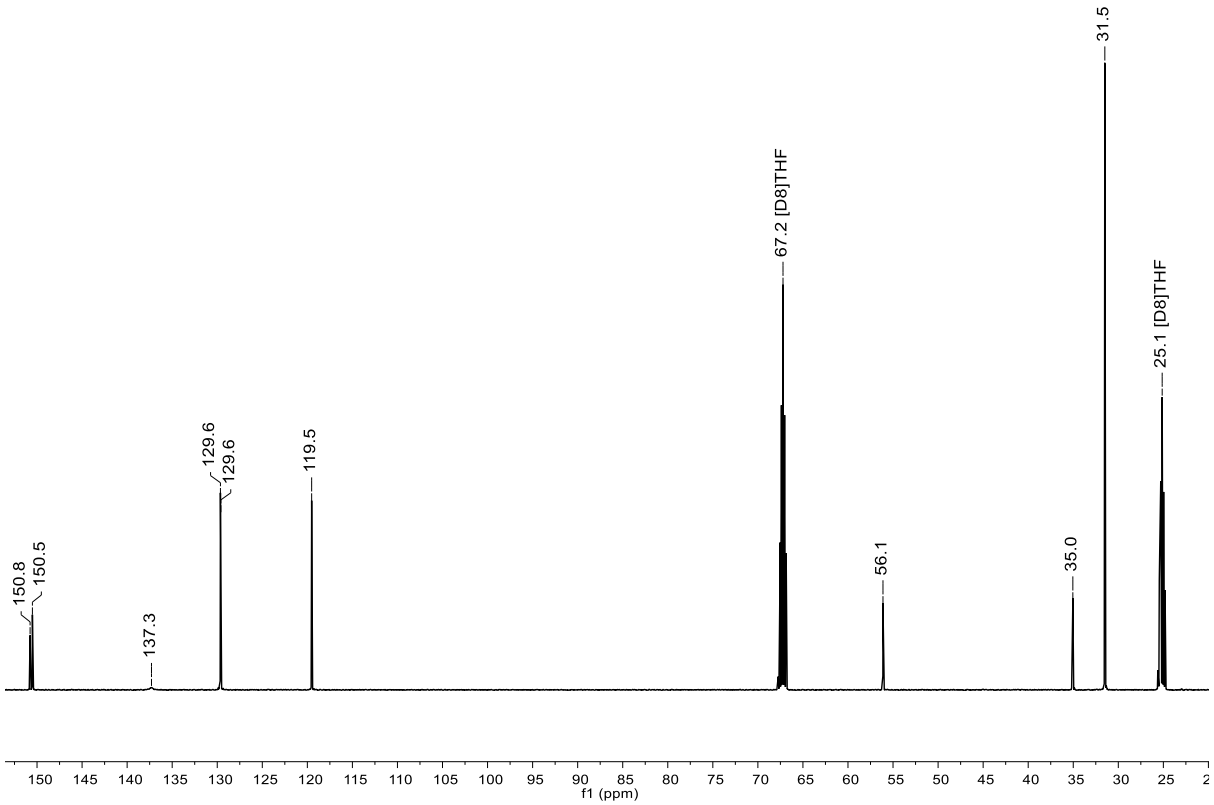

Figure S11: ^{13}C NMR spectrum of **4** (125.8 MHz, [D$_8$]THF).

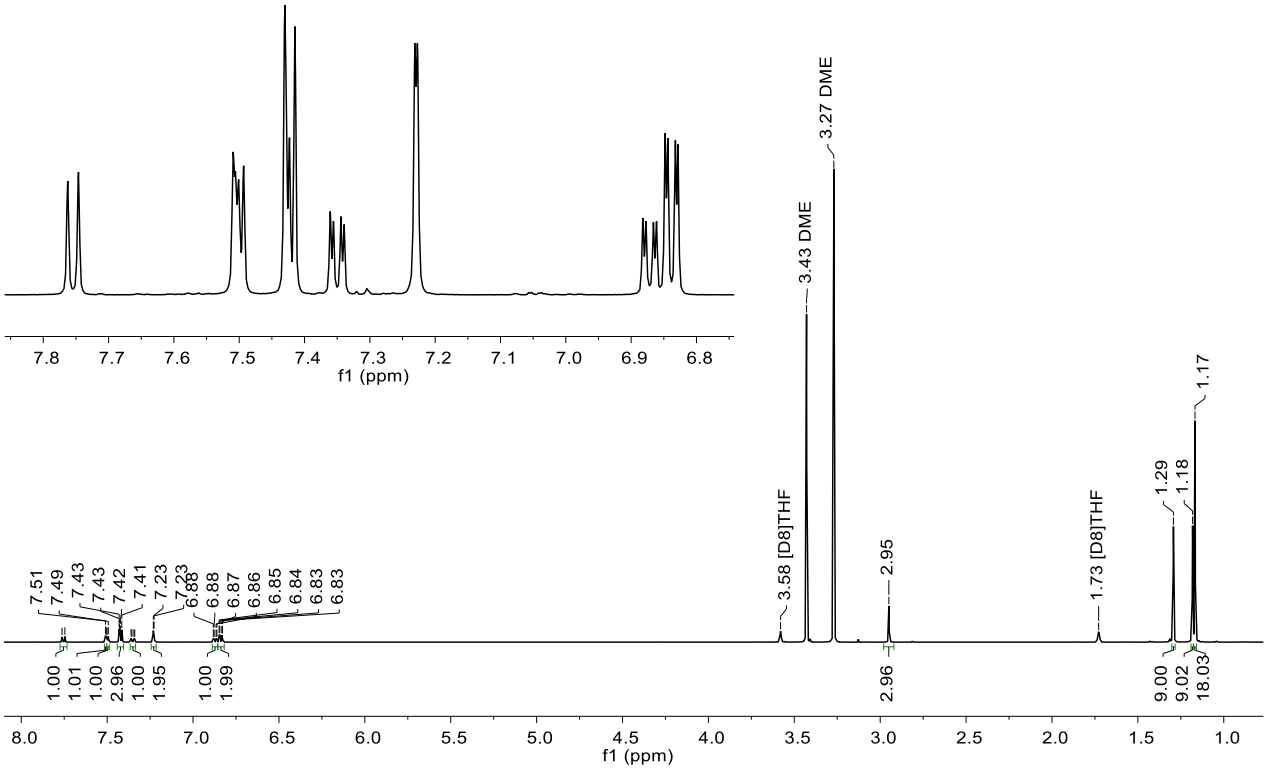

Figure S12: ^{1}H NMR spectrum of Li[**5**] (500.2 MHz, [D_8]THF).

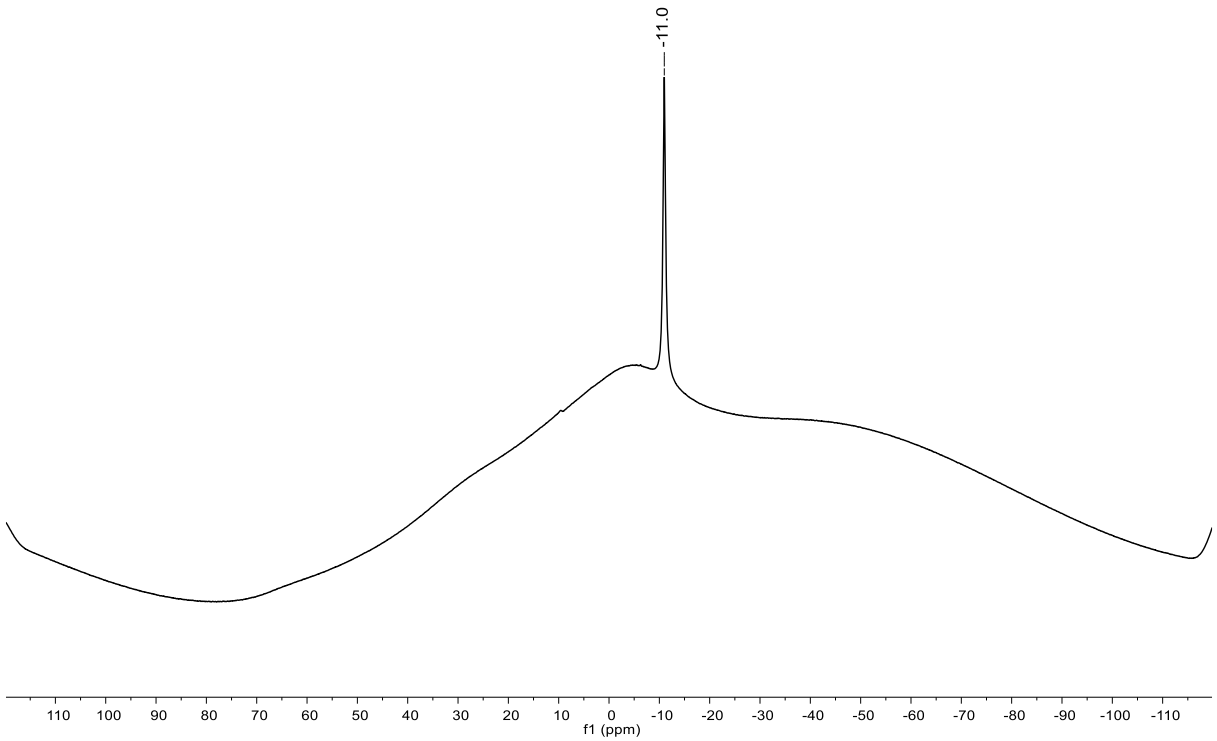

Figure S13: ^{11}B NMR spectrum of Li[**5**] (160.5 MHz, [D_8]THF).

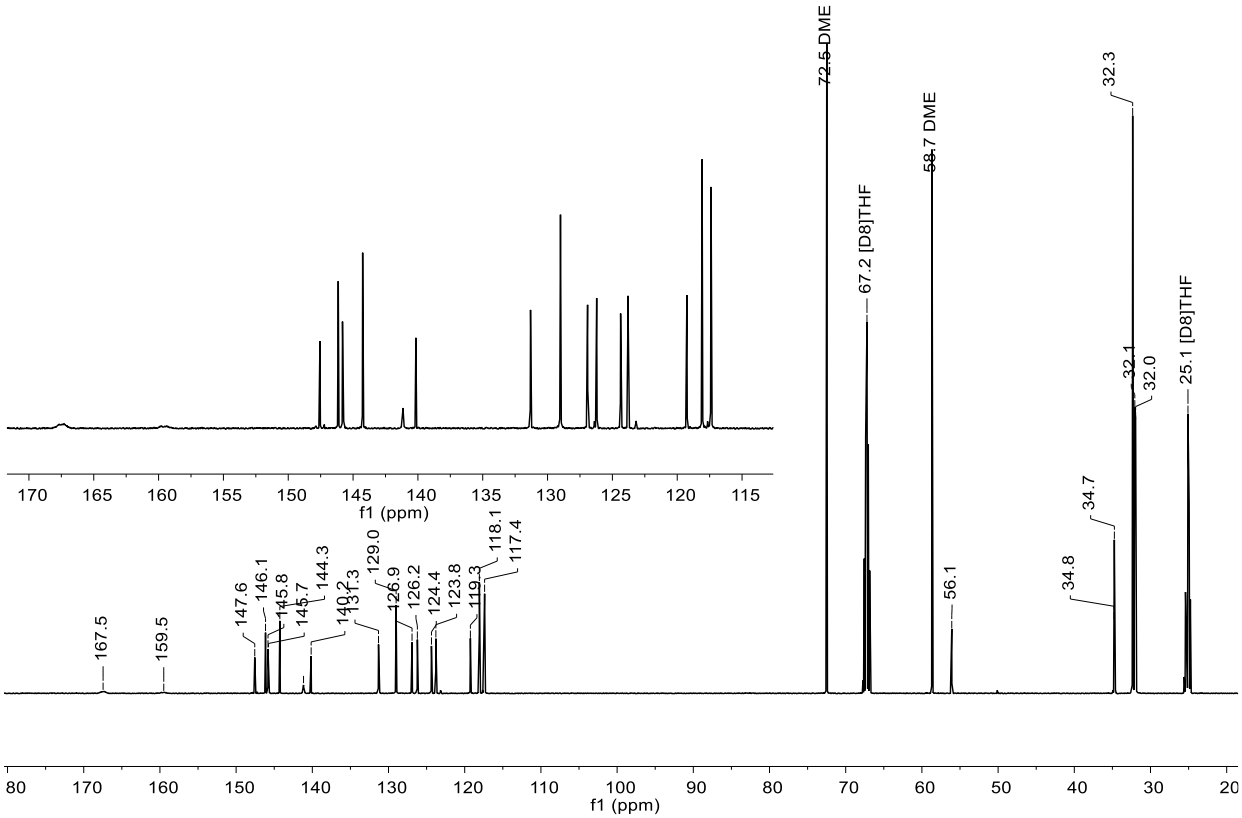

Figure S14: ^{13}C NMR spectrum of Li[**5**] (125.8 MHz, [D_8]THF).

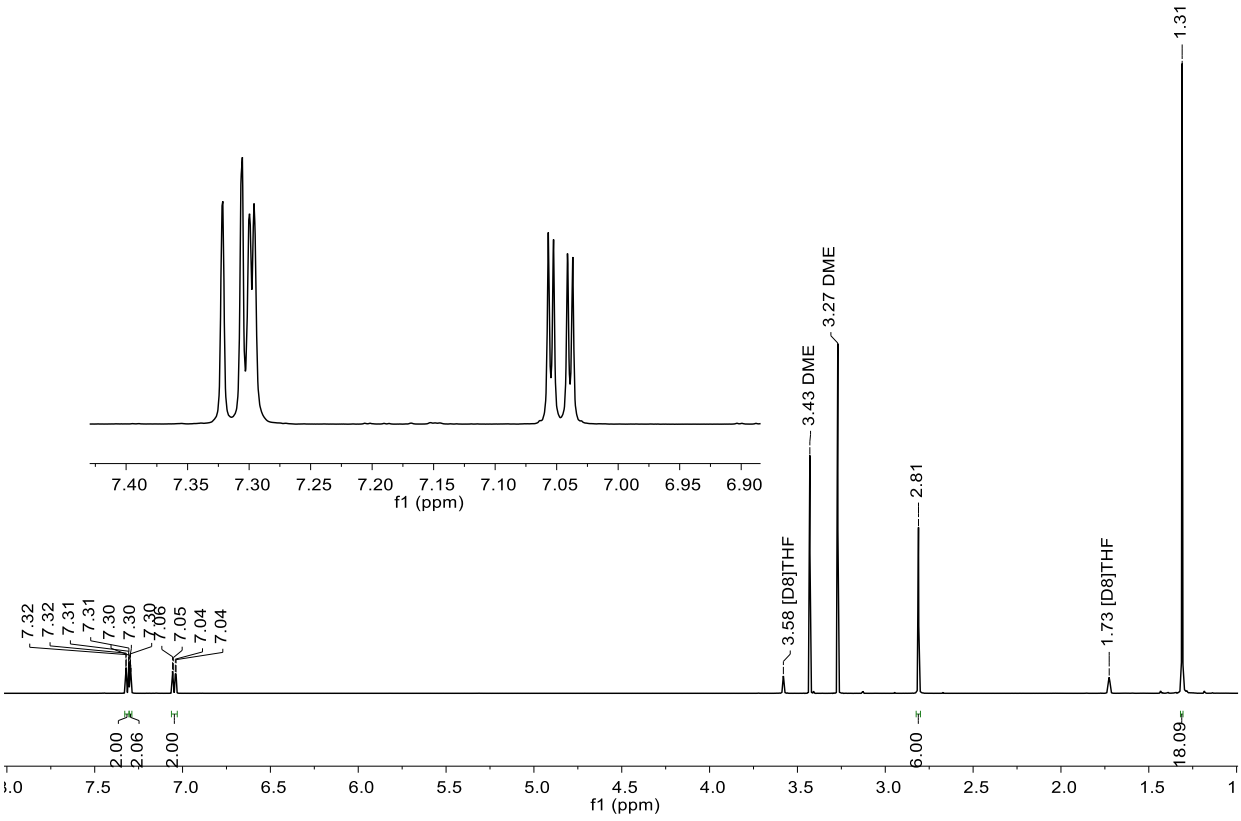

Figure S15: ^{1}H NMR spectrum of Li[**4**OMe] (500.2 MHz, [D_8]THF).

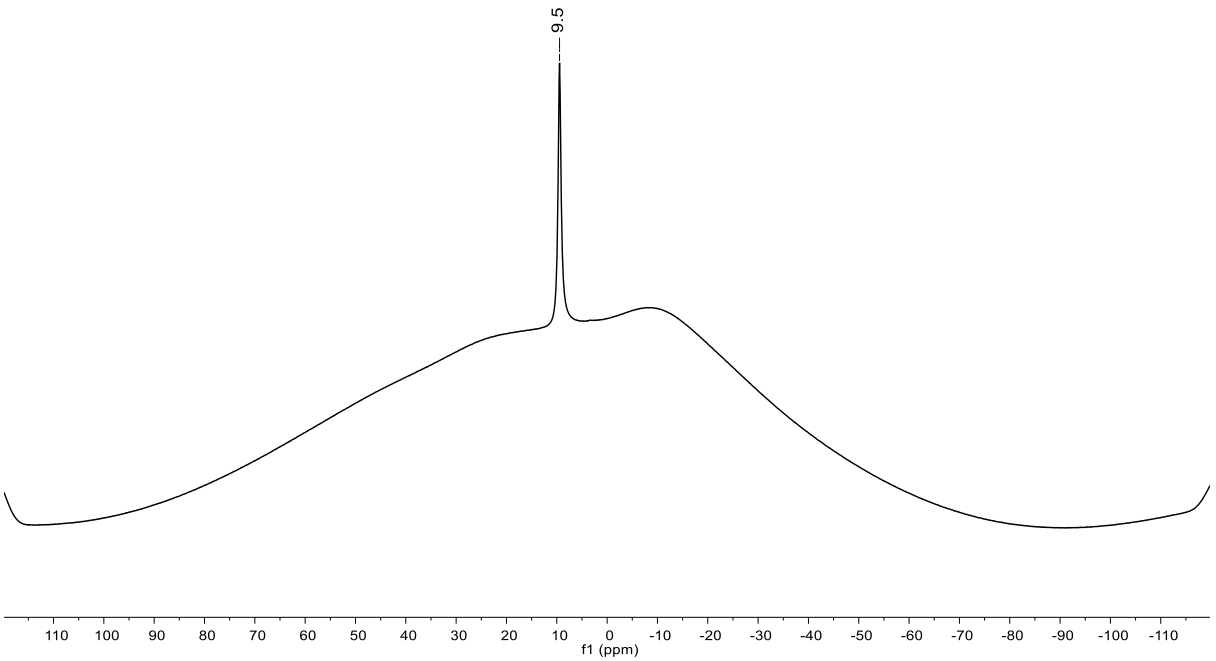

Figure S16: ^{11}B NMR spectrum of Li[**4**OMe] (160.5 MHz, [D_8]THF).

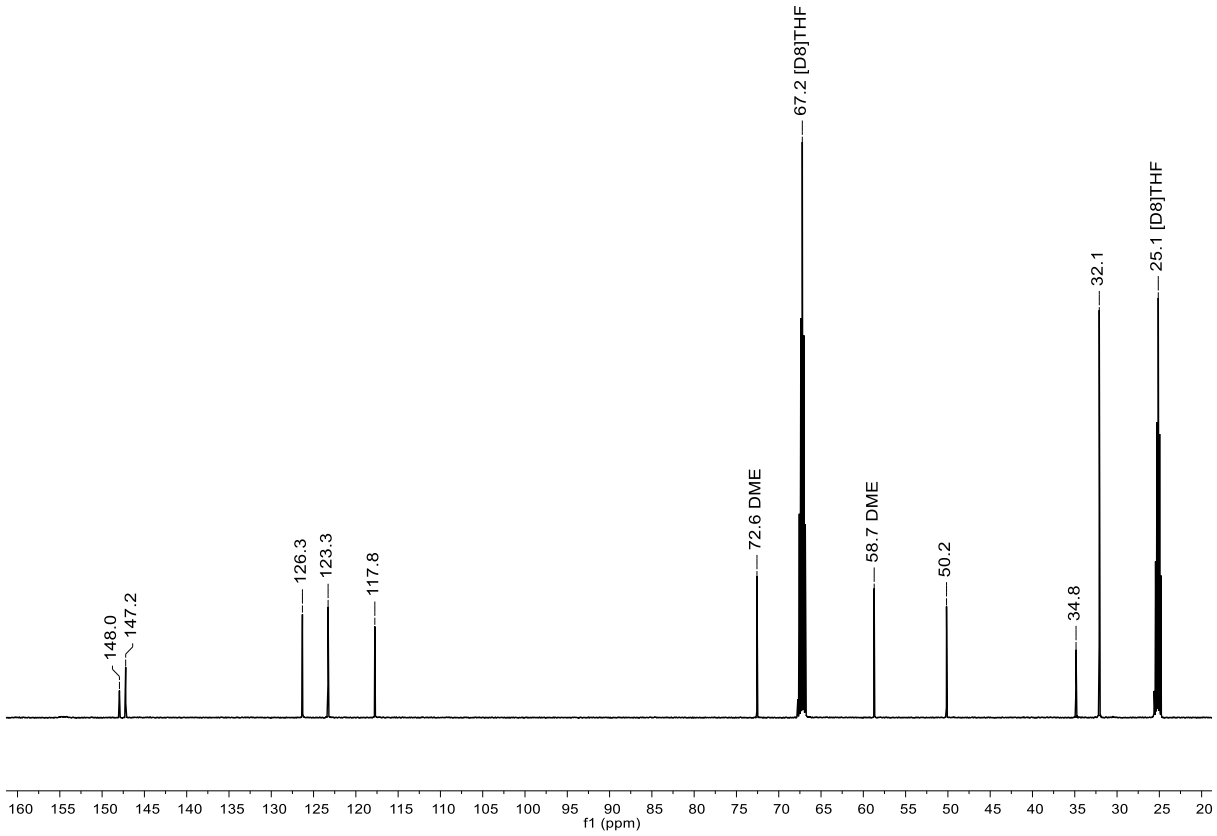

Figure S17: ^{13}C NMR spectrum of Li[**4**OMe] (125.8 MHz, [D_8]THF).

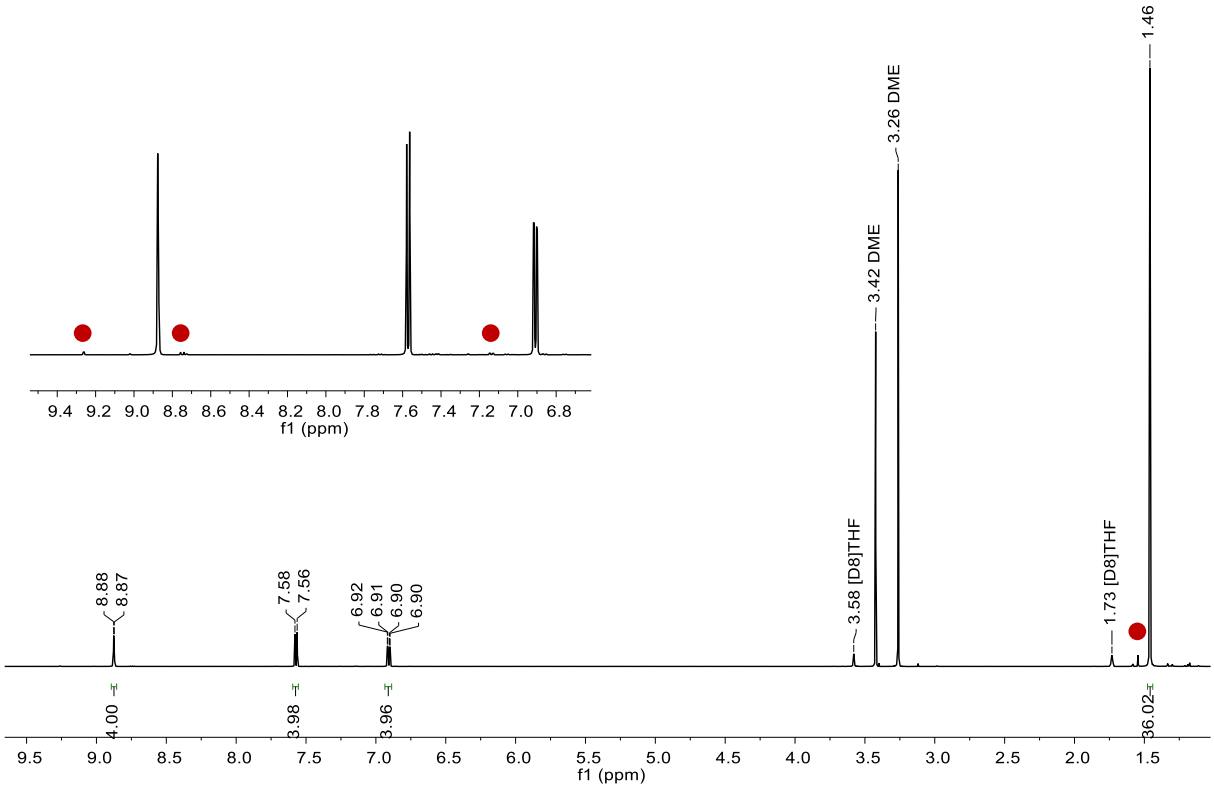

Figure S18: ^{1}H NMR spectrum of Na_2[**3**] (500.2 MHz, [D_8]THF). Marked contaminant: Na_2[**2**] (●).

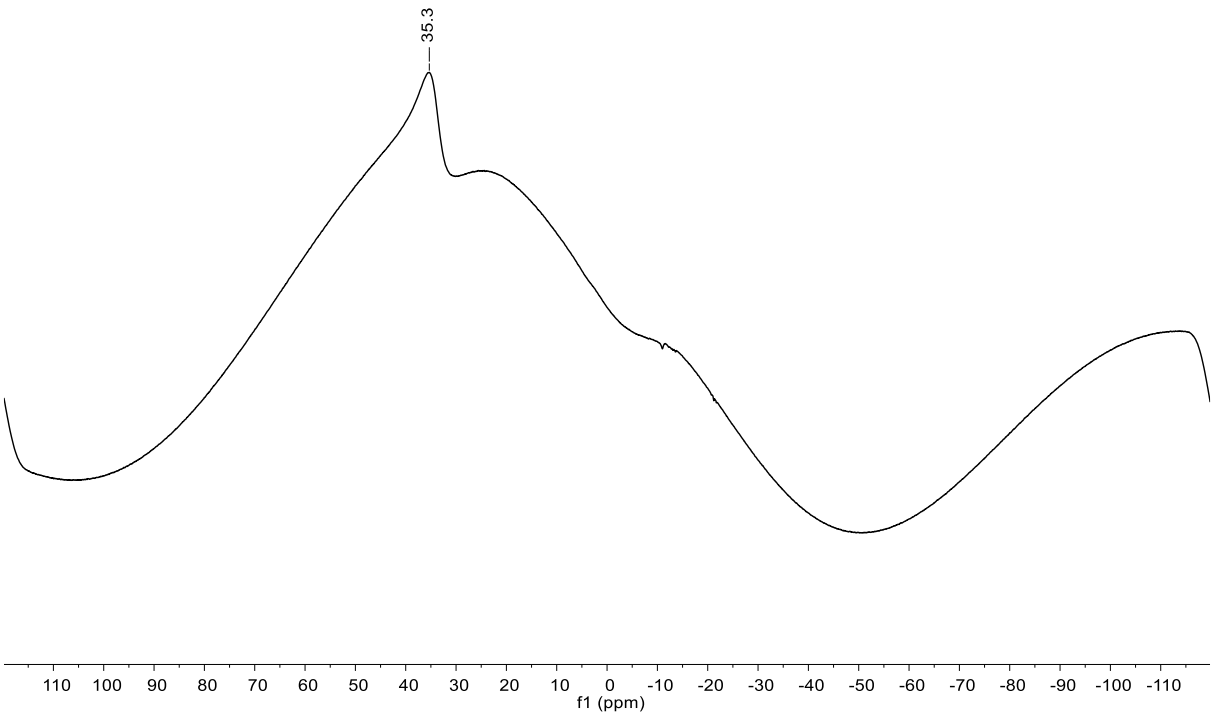

Figure S19: ^{11}B NMR spectrum of Na_2[**3**] (160.5 MHz, [D_8]THF).

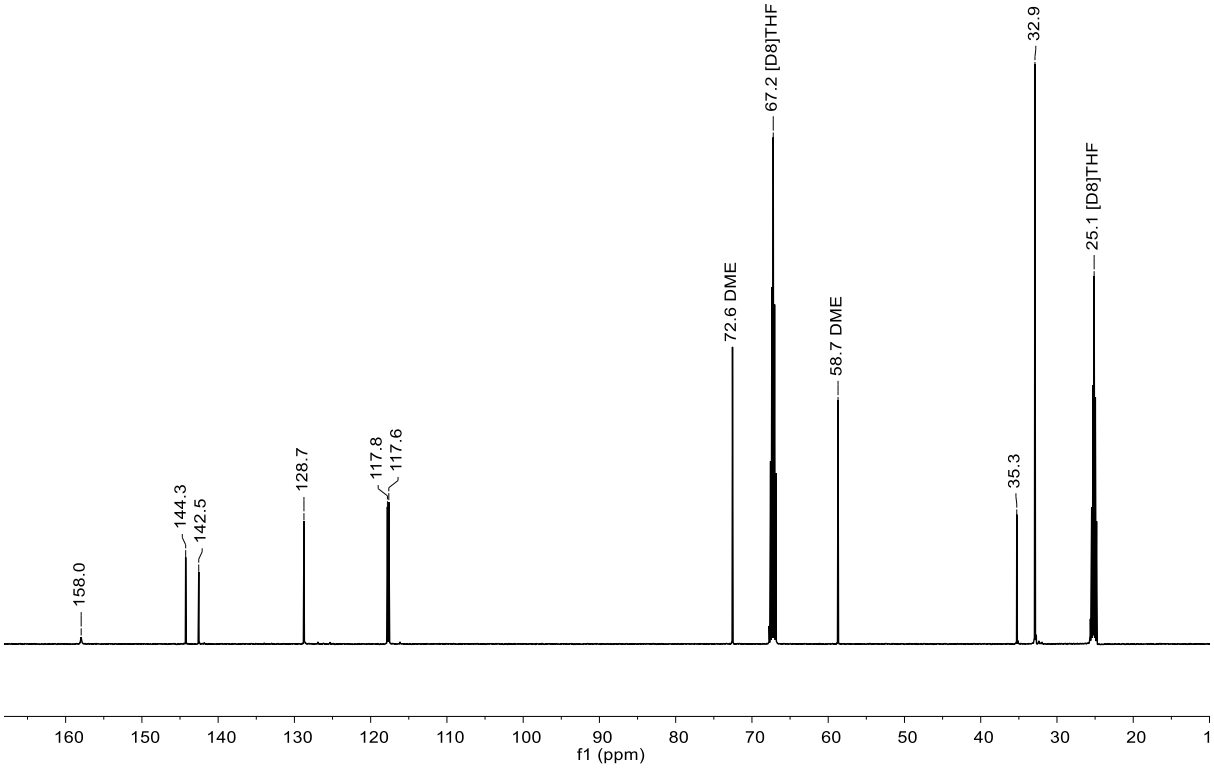

Figure S20: ^{13}C NMR spectrum of Na_2[**3**] (125.8 MHz, [D_8]THF).

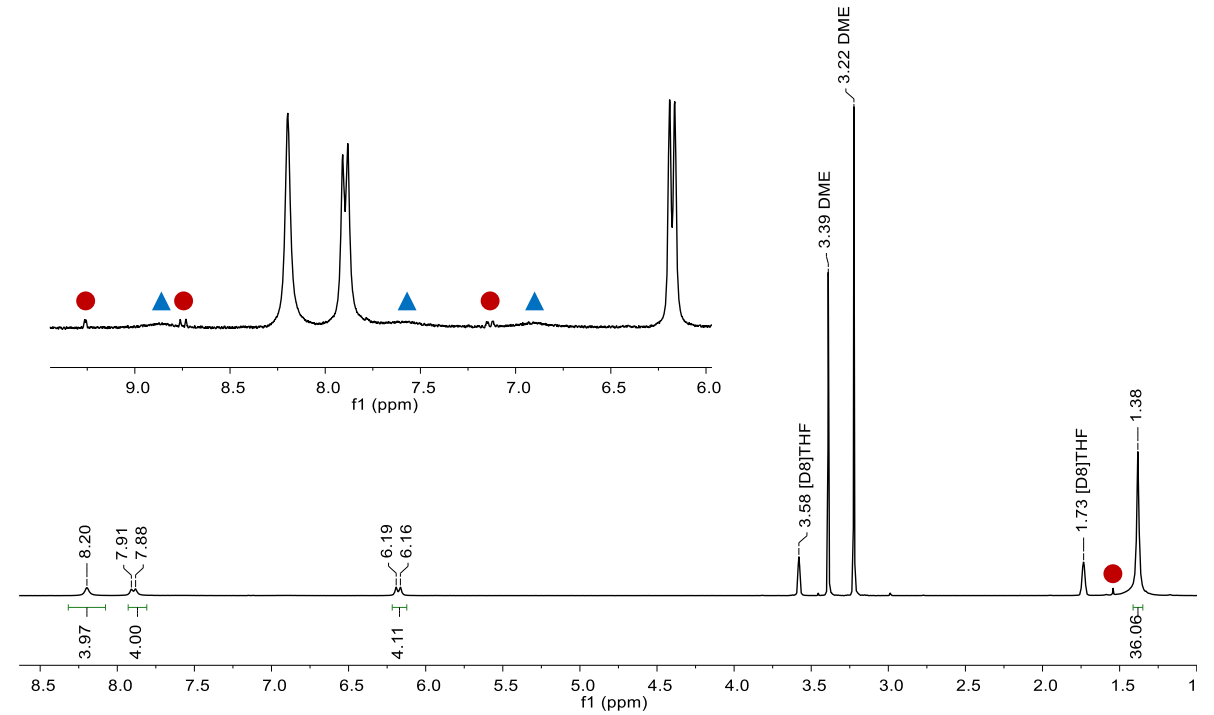

Figure S21: ^{1}H NMR spectrum of Na_4[**3**] prepared by *method A* (300.0 MHz, [D_8]THF). Marked contaminants: Na_2[**2**] (●), Na_2[**3**] (▲).

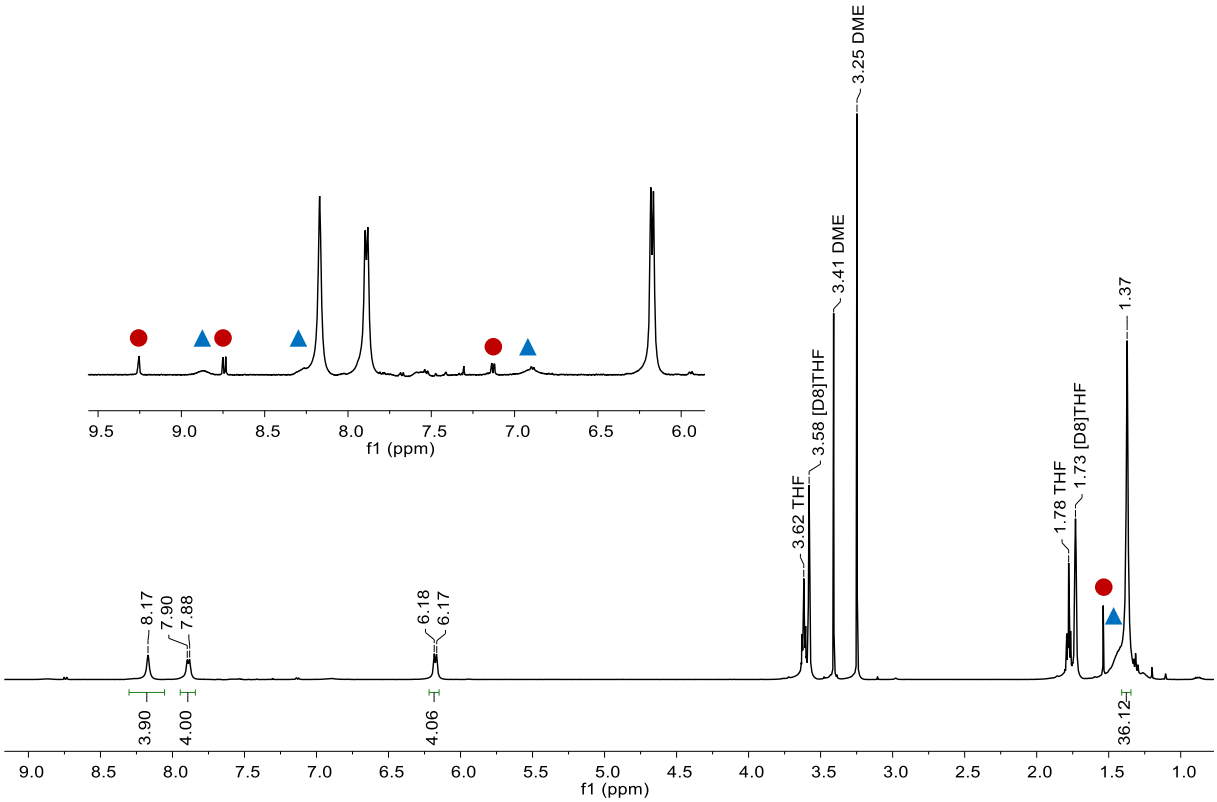

Figure S22: ^{1}H NMR spectrum of Na_4[**3**] prepared by *method B* (500.2 MHz, [D_8]THF). Marked contaminants: Na_2[**2**] (●), Na_2[**3**] (▲).

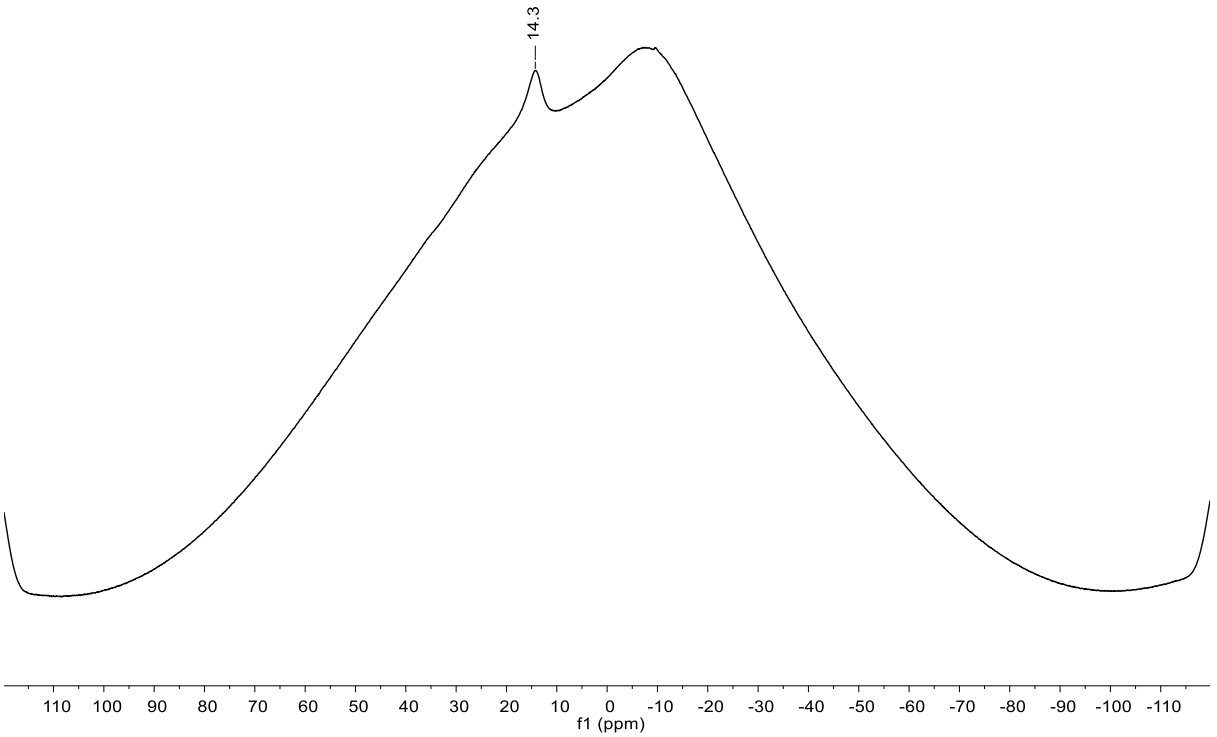

Figure S23: ^{11}B NMR spectrum of Na_4[**3**] (160.5 MHz, [D_8]THF).

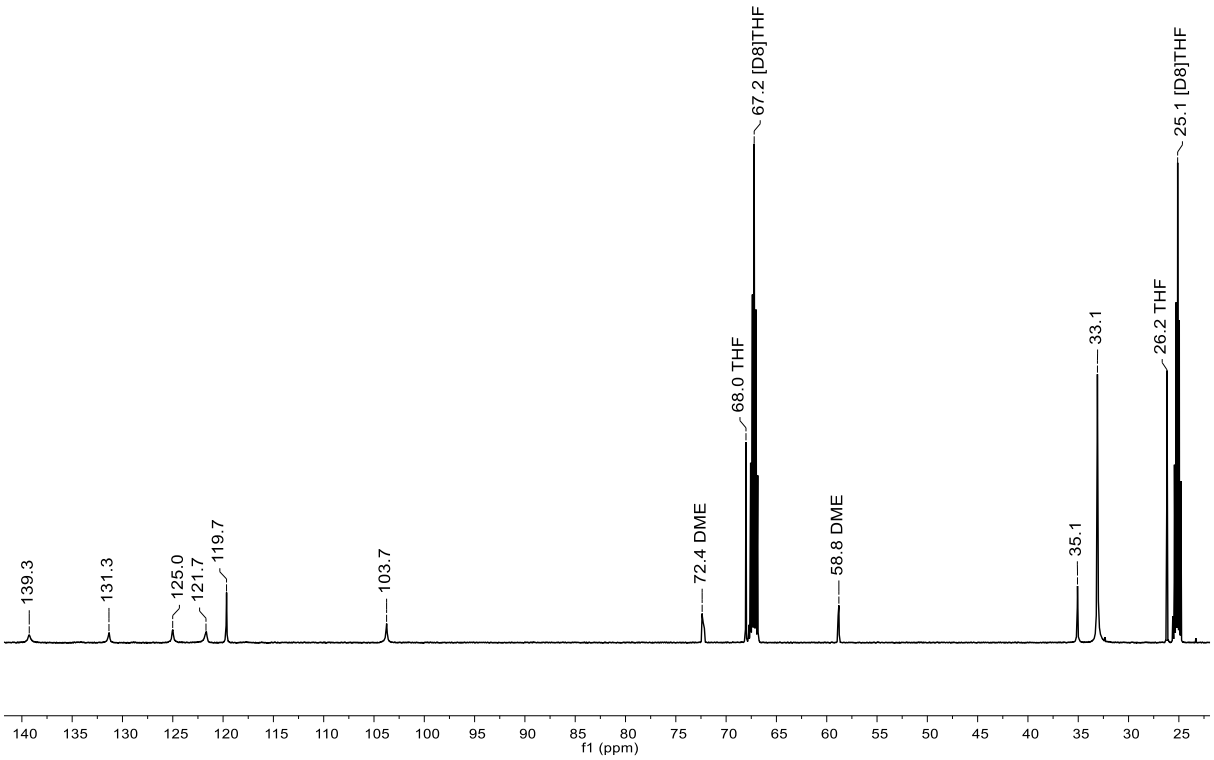

Figure S24: ^{13}C NMR spectrum of Na_4[**3**] recorded on a solution of single crystals of $[Na(thf)(dme)_{0.5}]_2[Na(thf)]_{0.5}[Na]_{1.5}$[**3**] (125.8 MHz, $[D_8]THF$).

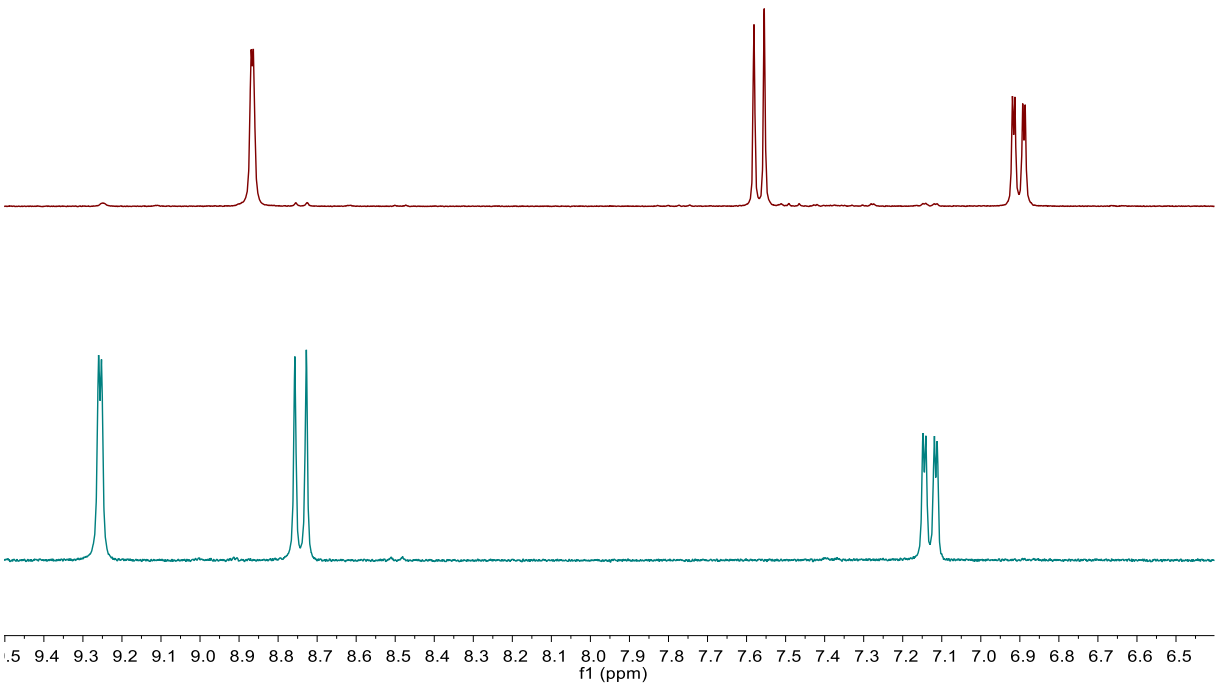

Figure S25: Aromatic regions of the ^1H NMR spectra (300.0 MHz, $[D_8]THF$) of Na_2[**3**] before the addition of HCl (top) and after stirring with 0.006 equiv of HCl overnight (bottom, cf. 1.1.6).

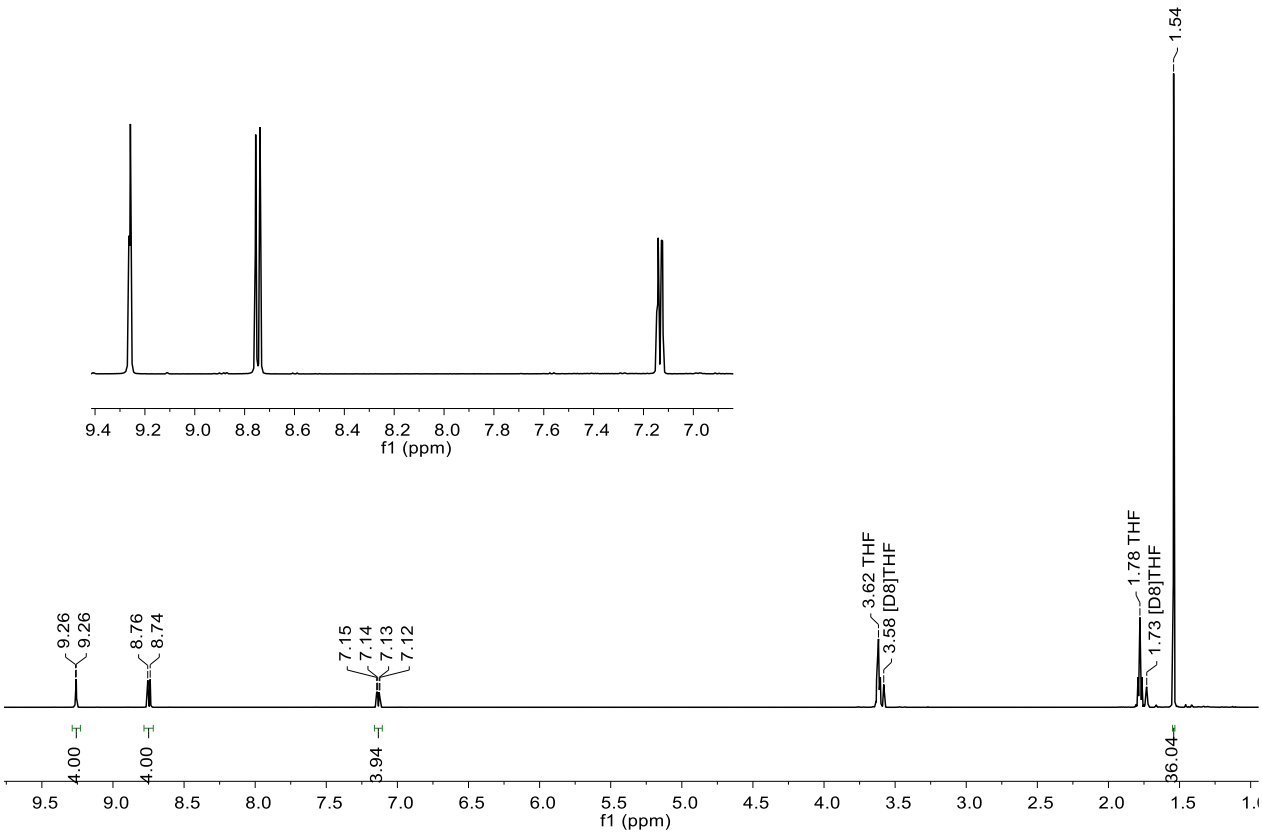

Figure S26: ^{1}H NMR spectrum of Na_2[**2**] (500.2 MHz, [D_8]THF).

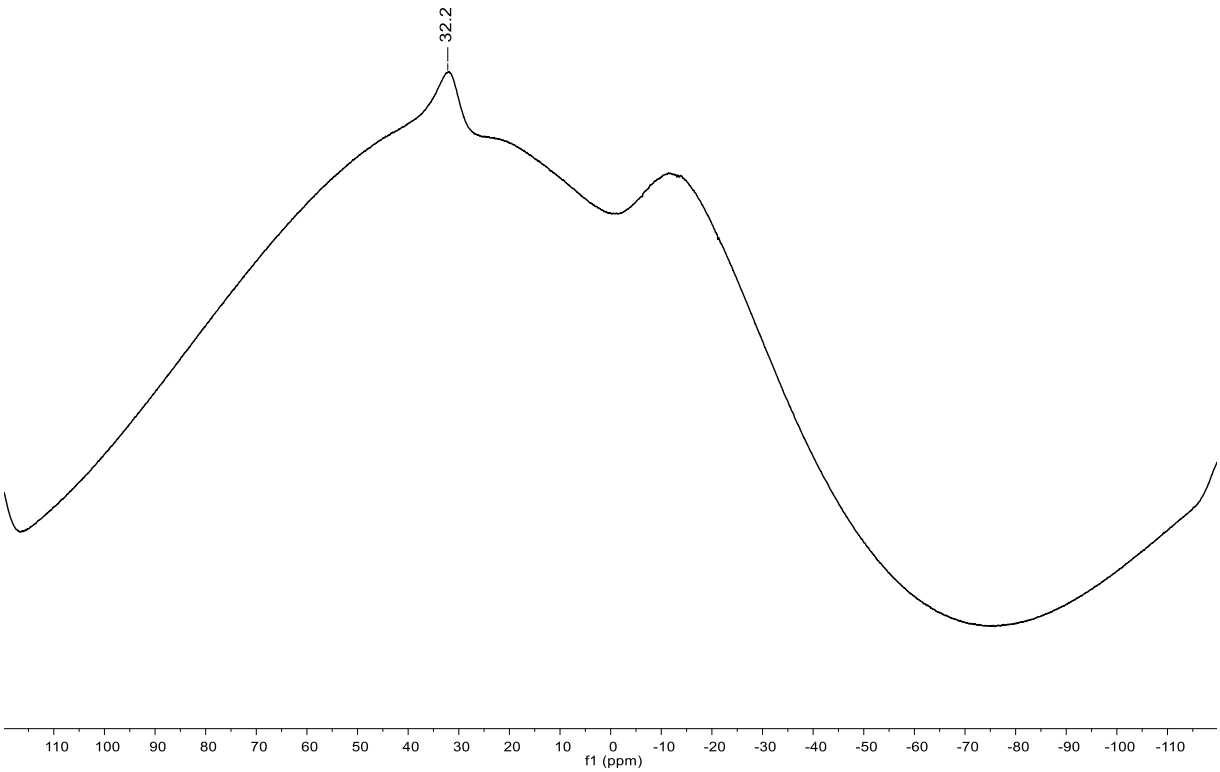

Figure S27: ^{11}B NMR spectrum of Na_2[**2**] (160.5 MHz, [D_8]THF).

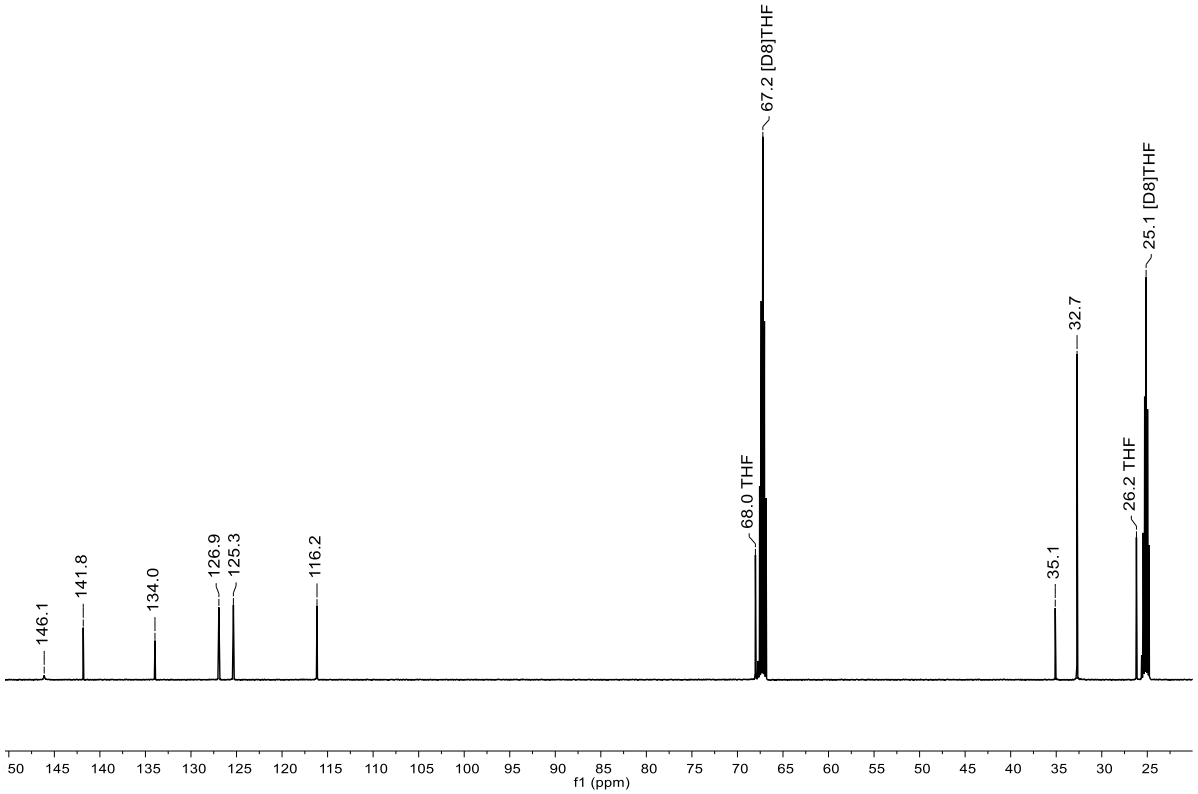

Figure S28: ^{13}C NMR spectrum of Na_2[**2**] (125.8 MHz, [D_8]THF).

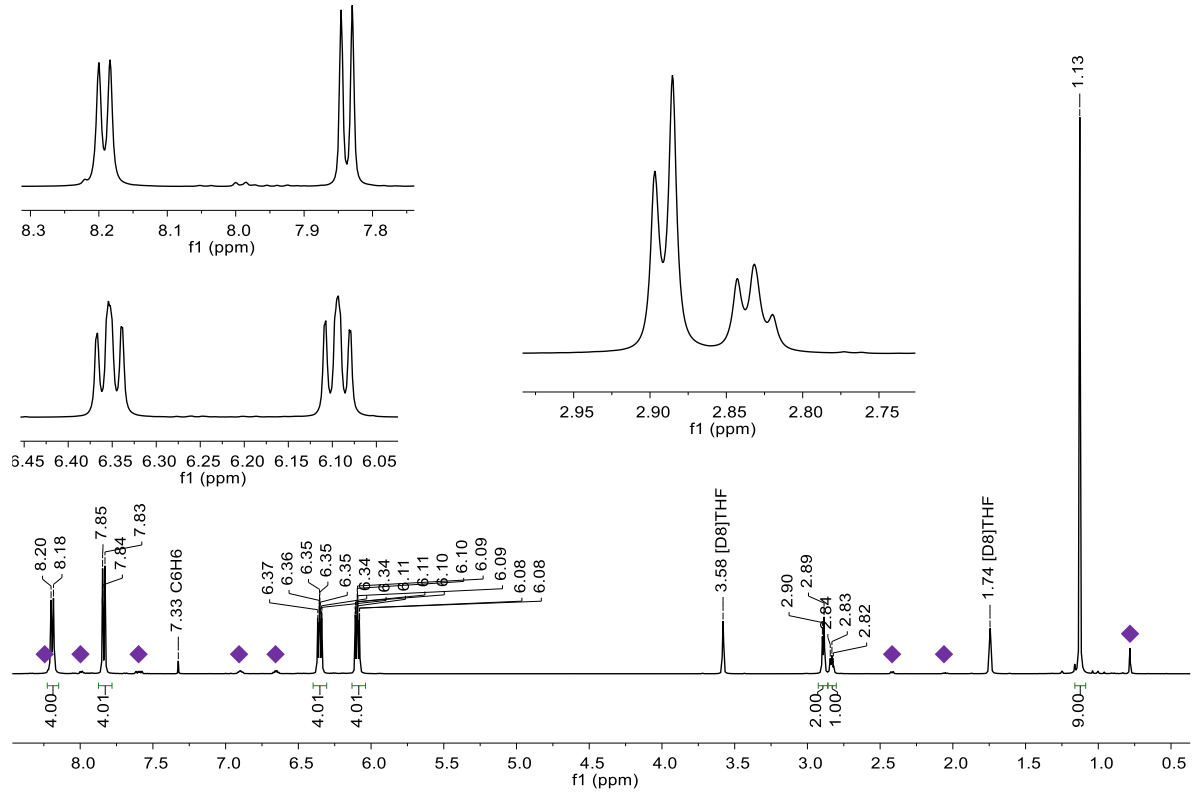

Figure S29: ^{1}H NMR spectrum of Li_4[**6**] (500.2 MHz, [D_8]THF). Marked contaminant: Li_2[**6**] (◆).

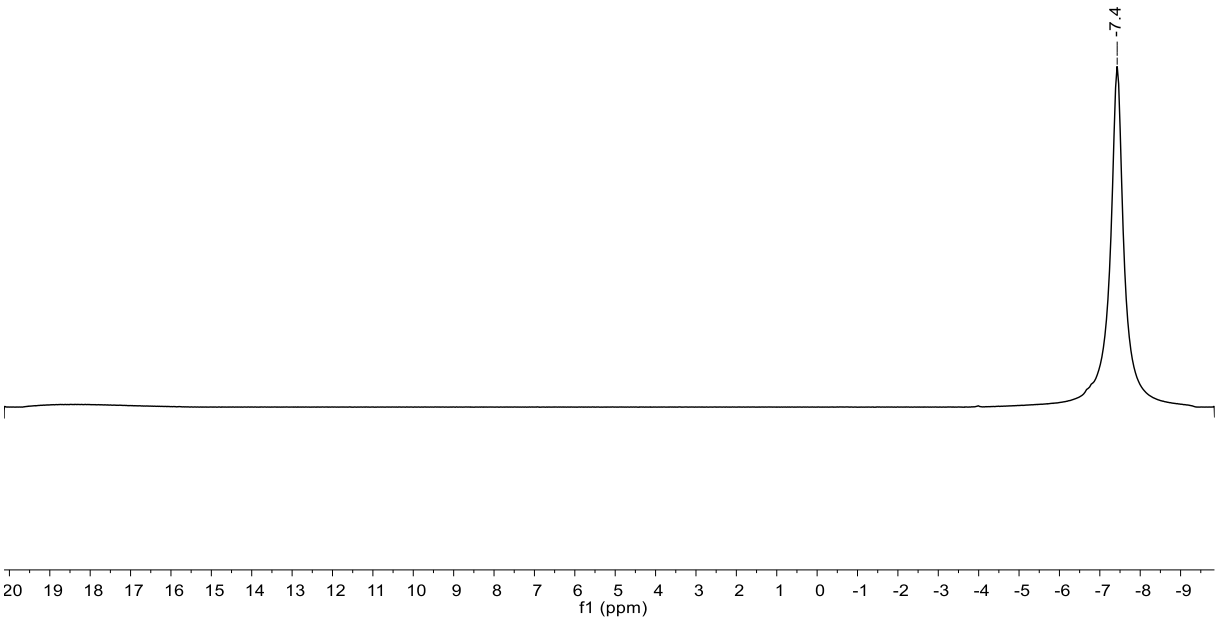

Figure S30: ^{7}H NMR spectrum of Li_4[**6**] (194.4 MHz, [D_8]THF).

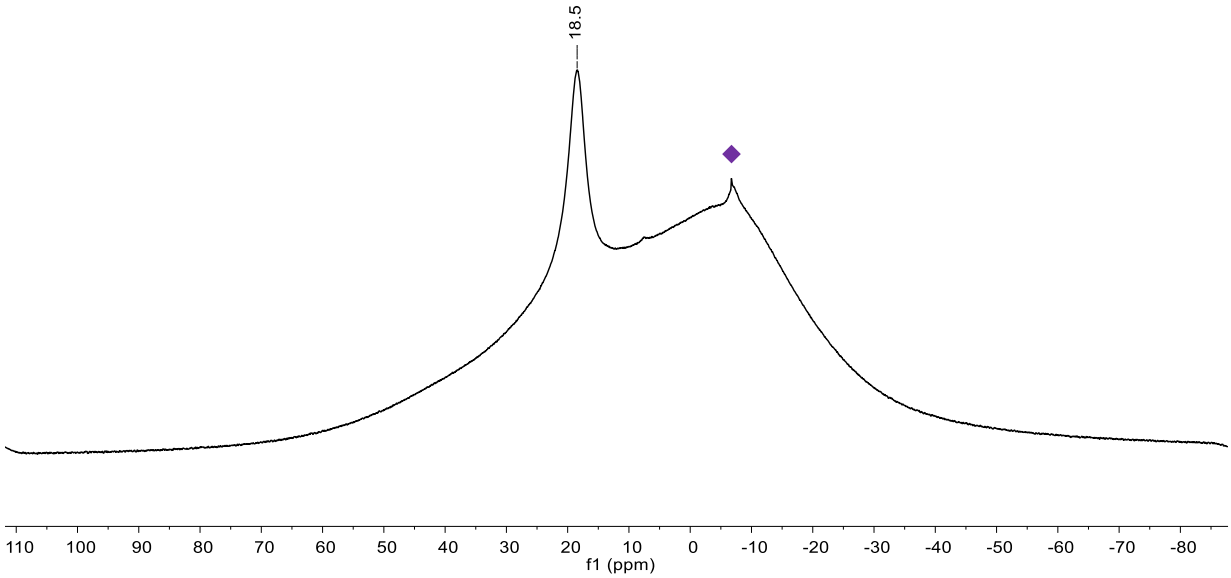

Figure S31: ^{11}B NMR spectrum of Li_4[**6**] (160.5 MHz, [D_8]THF). Marked component: Li_2[**6**] (◆).

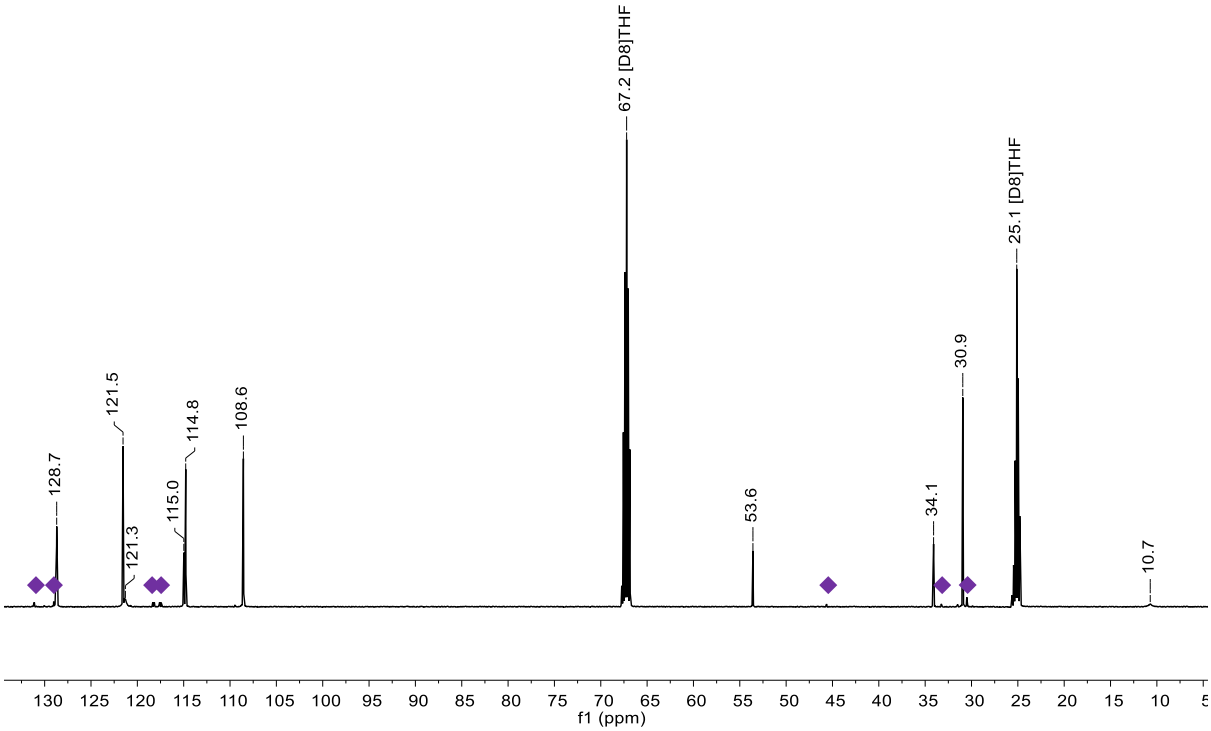

Figure S32: ^{13}C NMR spectrum of Li_4[**6**] (125.8 MHz, [D_8]THF). Marked contaminant: Li_2[**6**] (◆).

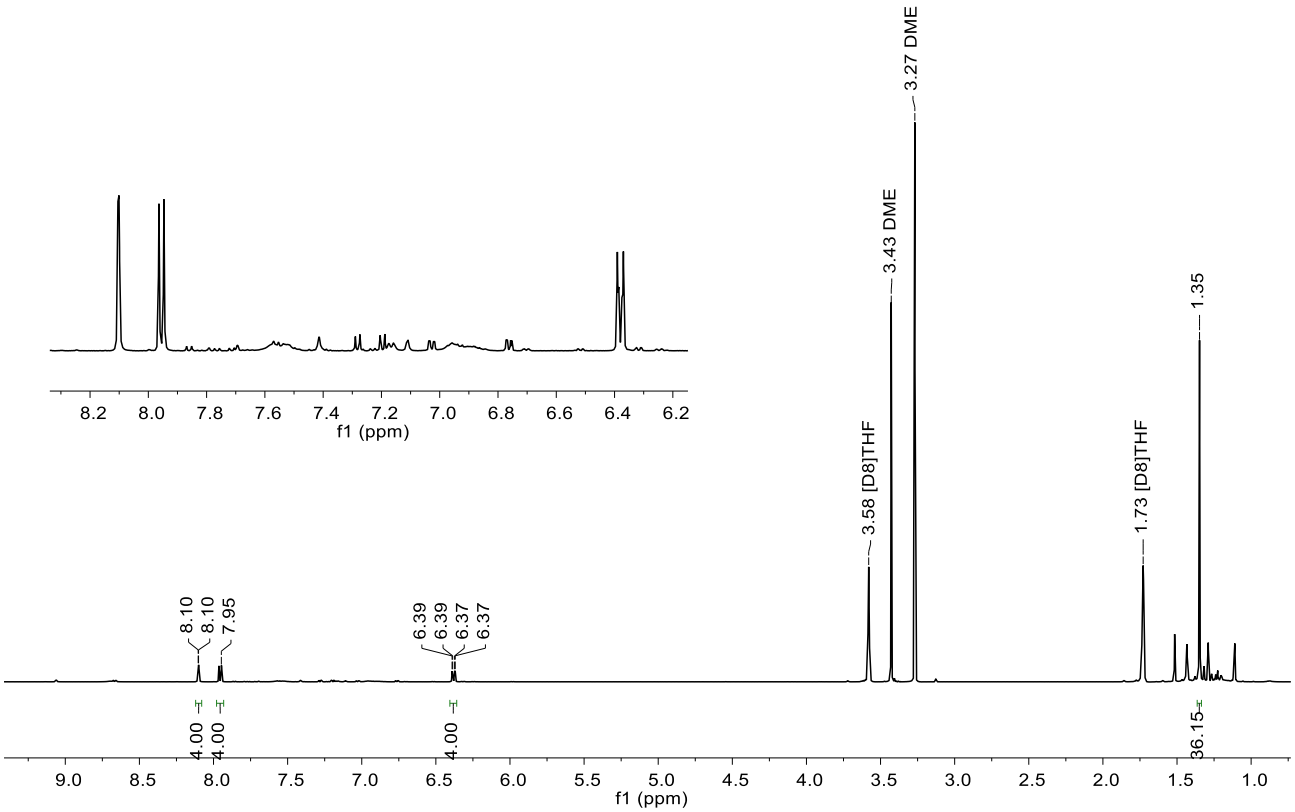

Figure S33: ^{1}H NMR spectrum of Li_4[**3**] (500.2 MHz, [D_8]THF).

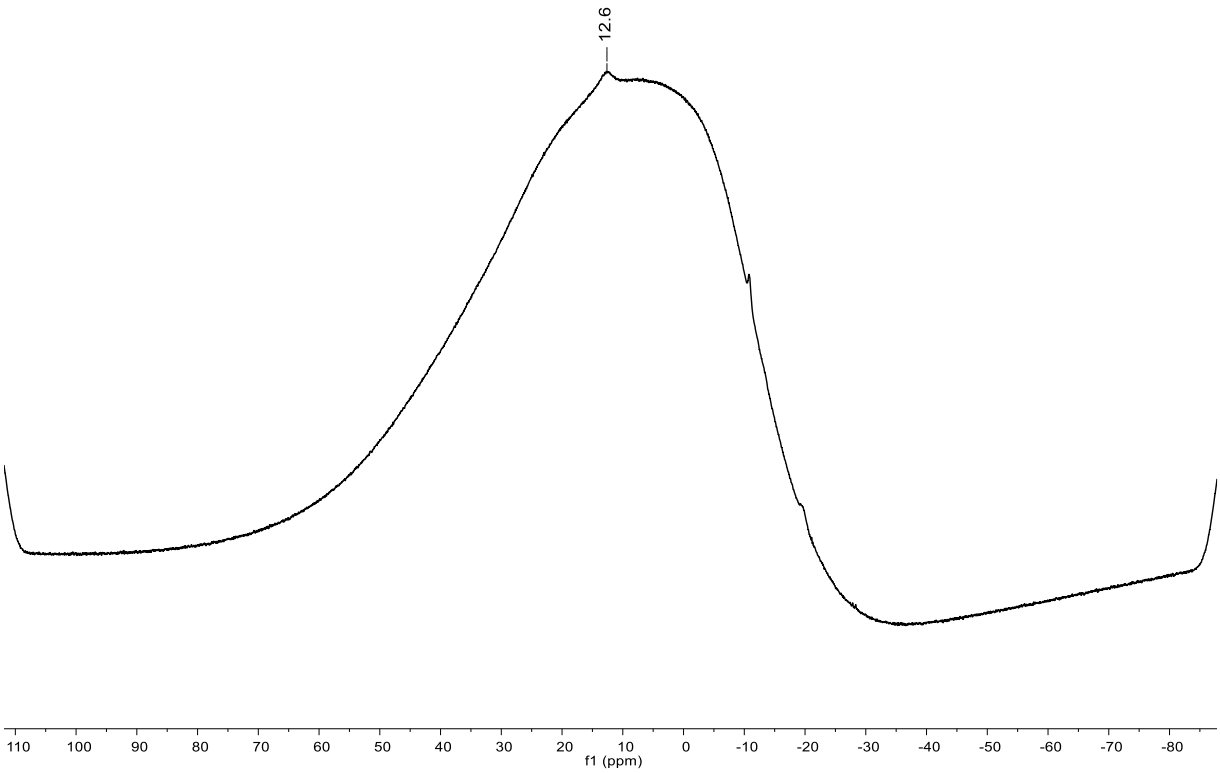

Figure S34: ^{11}B NMR spectrum of Li_4[**3**] (160.5 MHz, [D_8]THF).

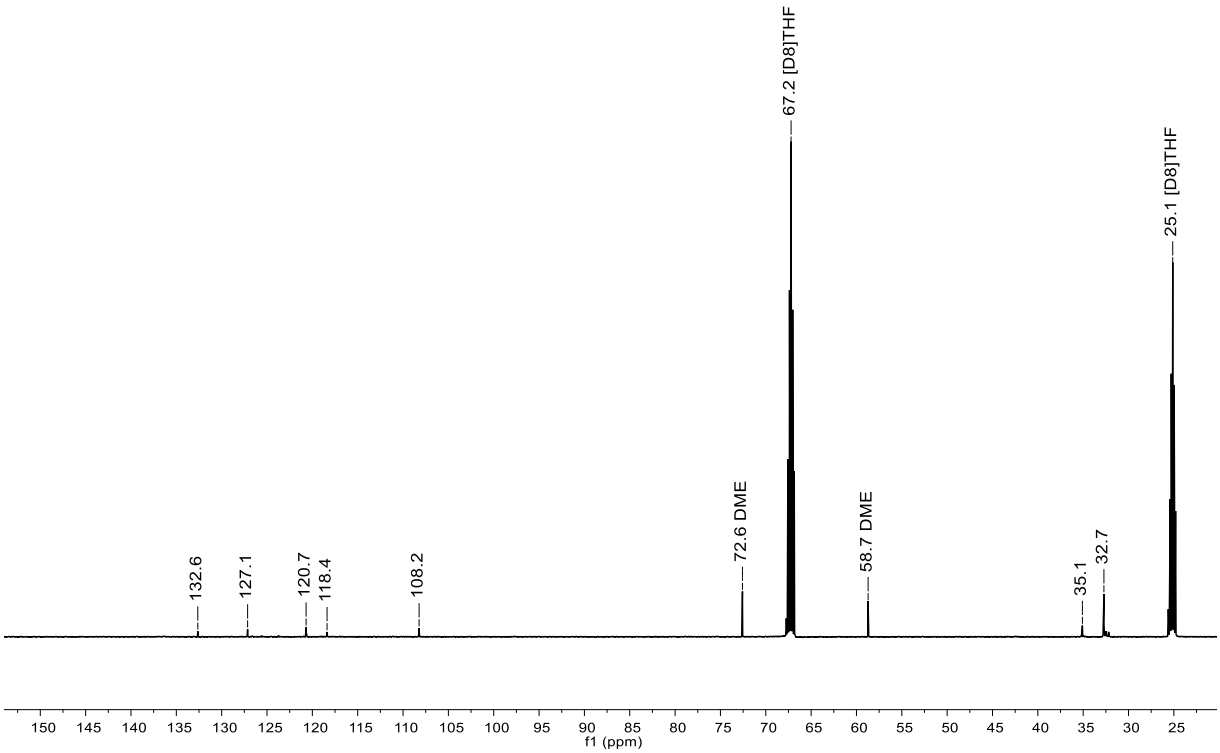

Figure S35: ^{13}C NMR spectrum of Li_4[**3**] (125.8 MHz, [D_8]THF).

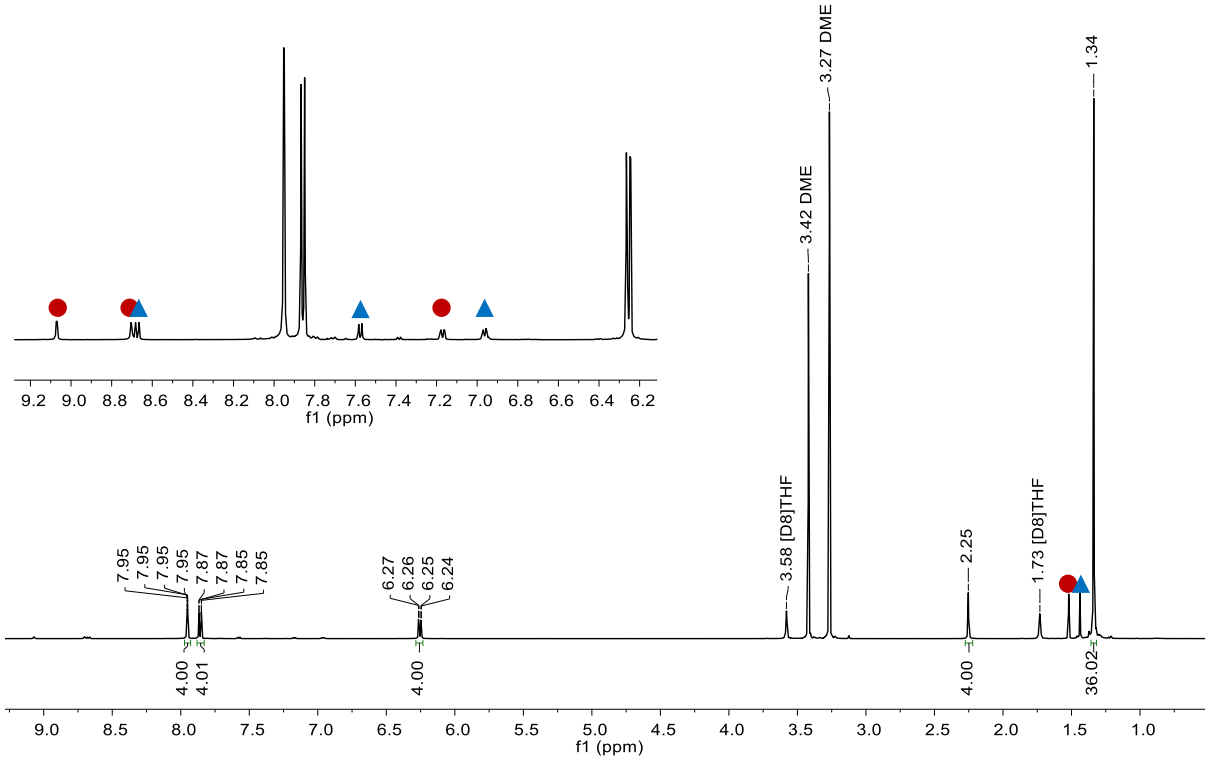

Figure S36: ^{1}H NMR spectrum of Li_4[**7**] (500.2 MHz, [D_8]THF). Marked contaminants: Li_2[**2**] (●), Li_2[**3**] (▲).

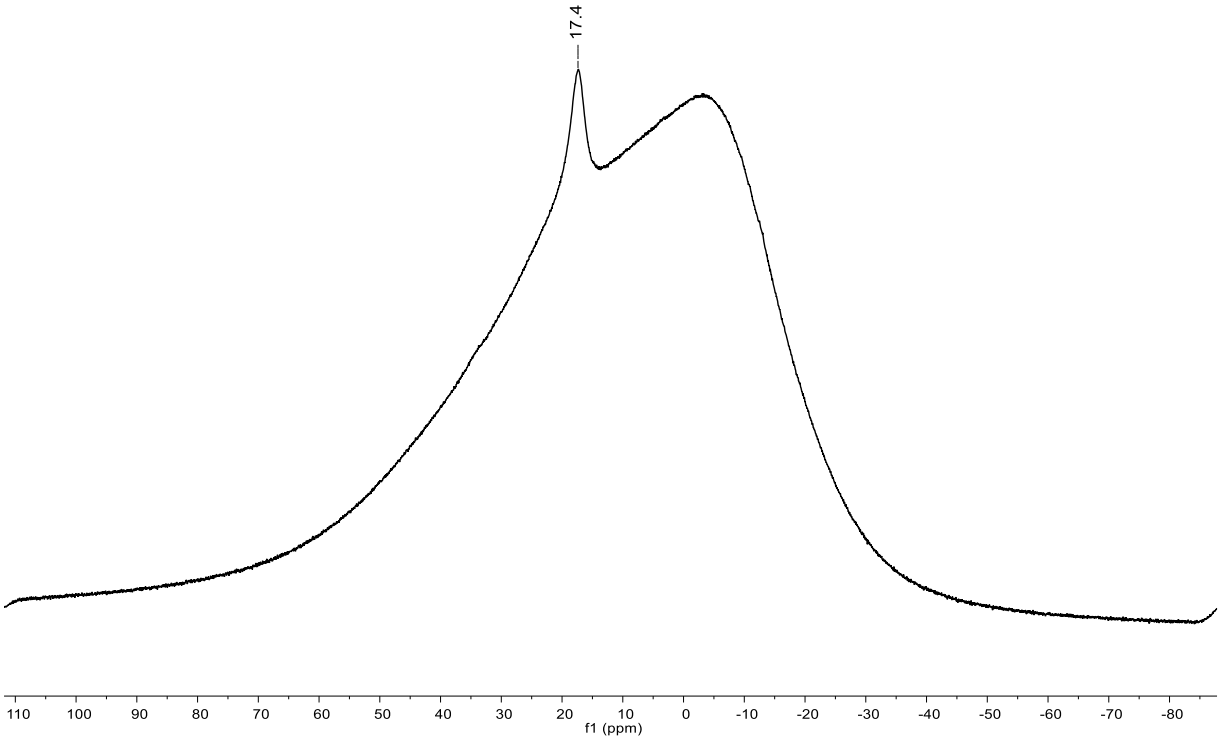

Figure S37: ^{11}B NMR spectrum of Li_4[**7**] (160.5 MHz, [D_8]THF).

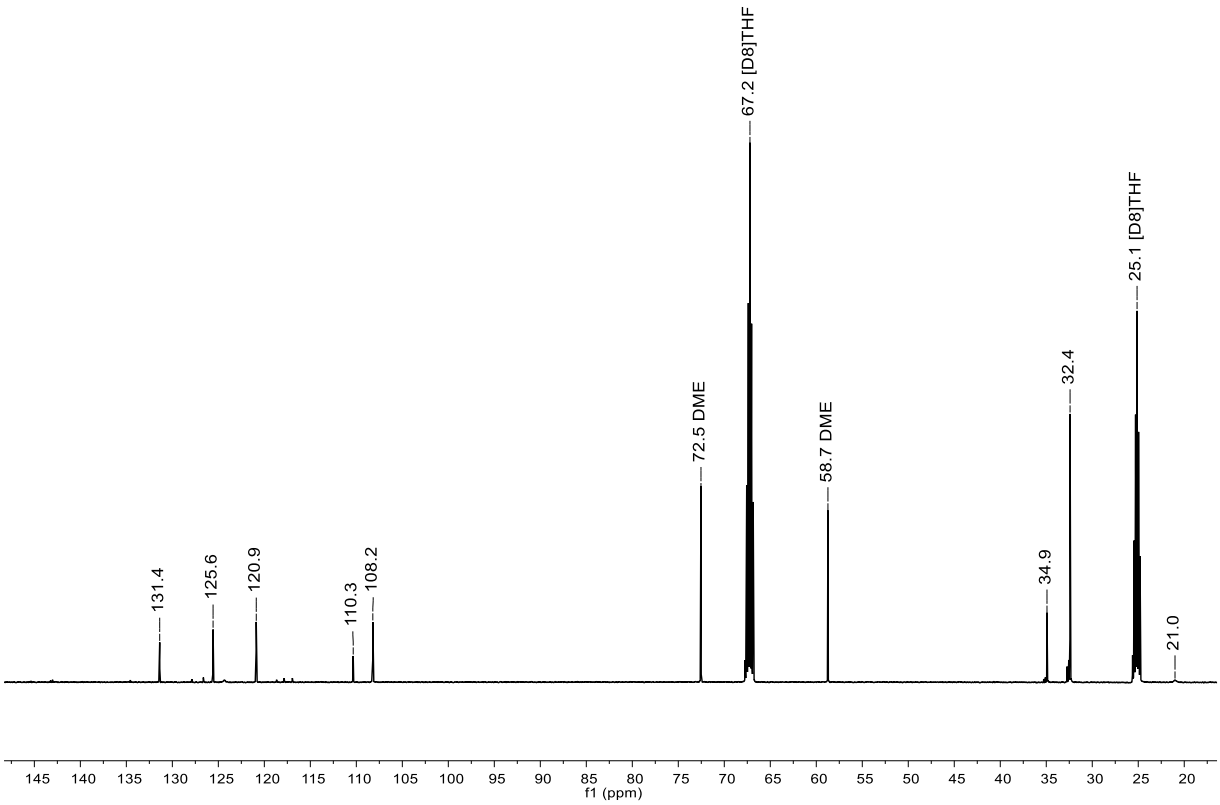

Figure S38: ^{13}C NMR spectrum of Li_4[**7**] (125.8 MHz, [D_8]THF).

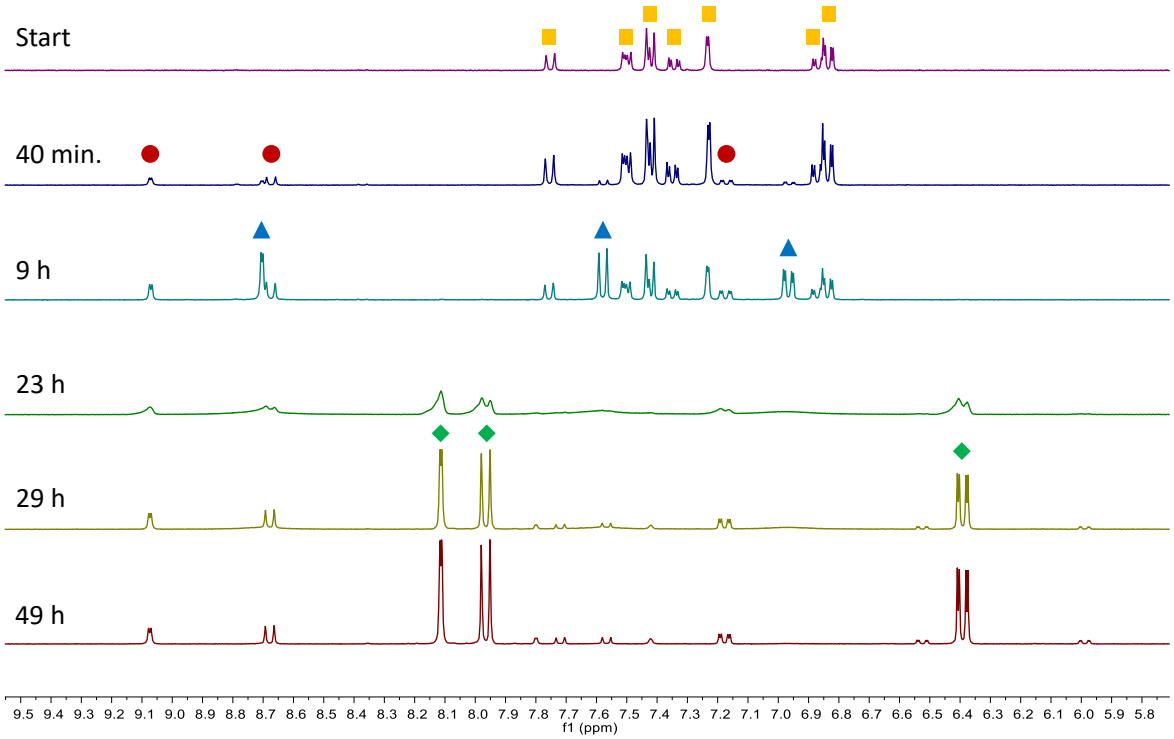

Figure S39: Aromatic regions of the ^{1}H NMR spectra (300.0 MHz, [D_8]THF) corresponding to different stages of the reaction of Li[**5**] with Li metal (cf. 1.2.4; Start: Li[**5**] before the addition of Li; the time stamps indicate the time that has passed since addition of the alkali metal). Marked components: Li[**5**] (■),Li_2[**2**] (●), Li_2[**3**] (▲), Li_4[**3**] (◆).

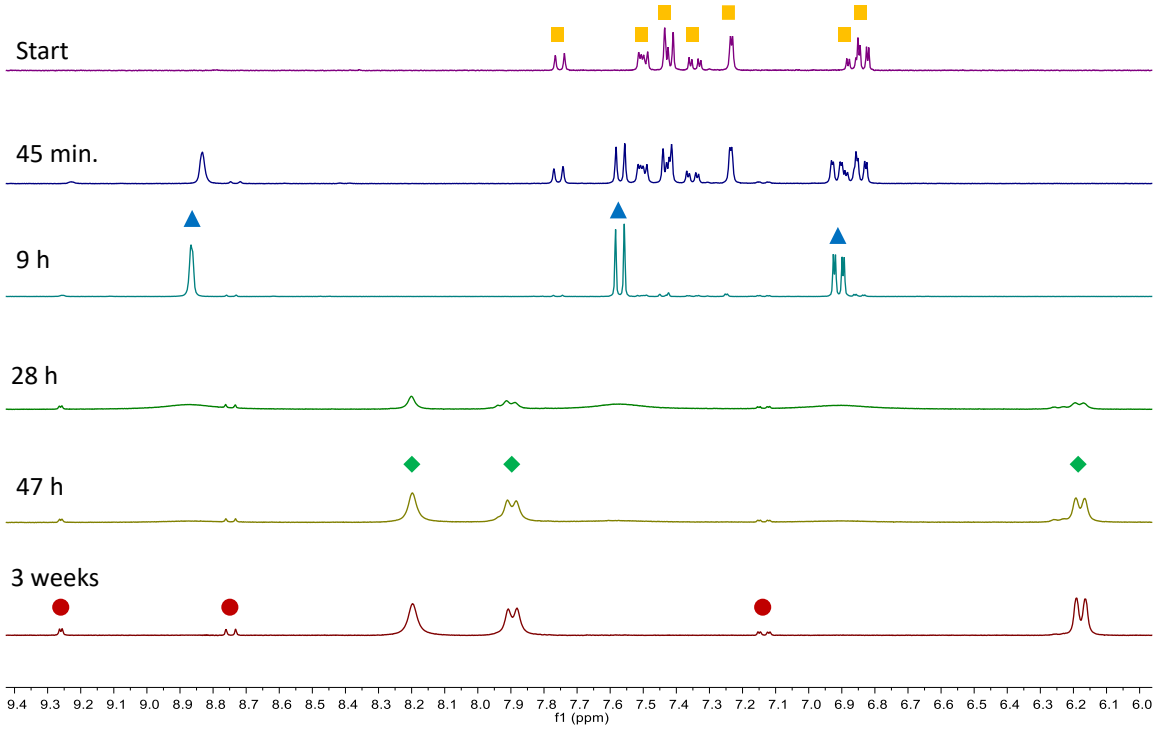

Figure S40: Aromatic regions of the ^{1}H NMR spectra (300.0 MHz, [D$_8$]THF) corresponding to different stages of the reaction of Li[**5**] with Na metal (cf. 1.2.5; Start: Li[**5**] before the addition of Na; the time stamps indicate the time that has passed since addition of the alkali metal). Marked components: Li[**5**] (■), Na_2[**3**] (▲), Na_4[**3**] (◆), Na_2[**2**] (●).

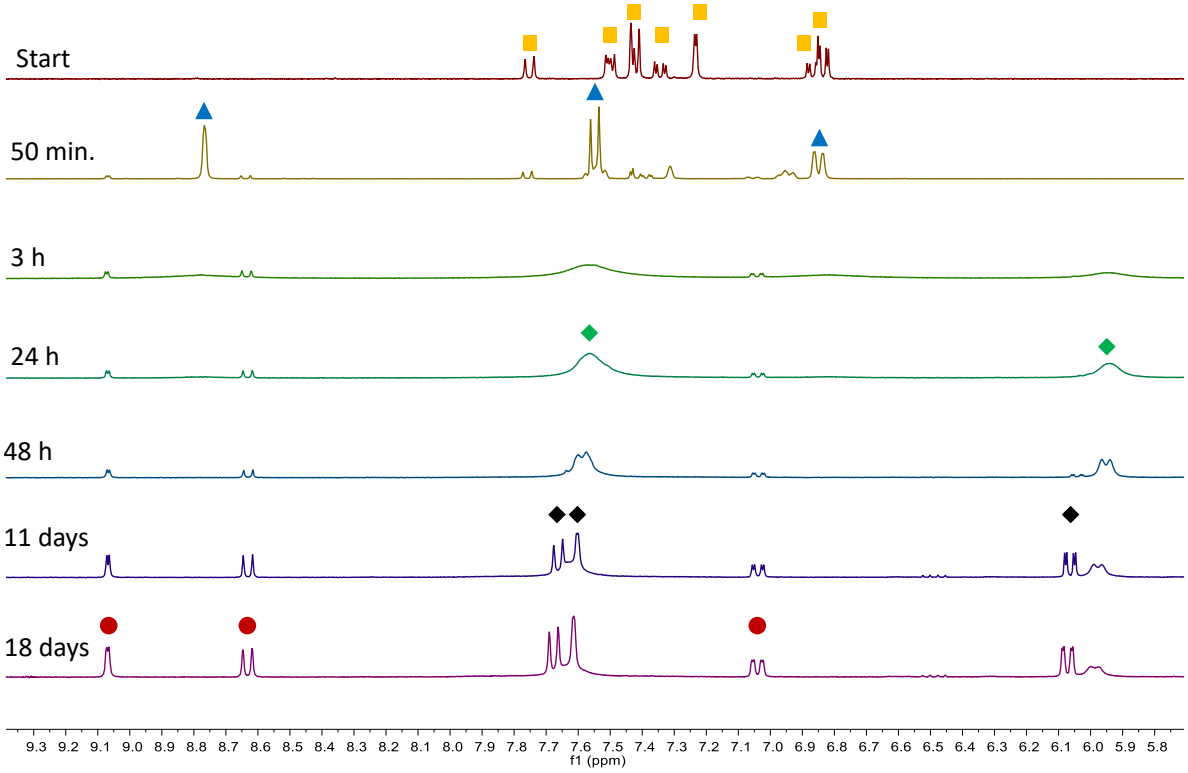

Figure S41: Aromatic regions of the ^{1}H NMR spectra (300.0 MHz, [D_8]THF) corresponding to different stages of the reaction of Li[**5**] with K metal (cf. 1.2.6; Start: Li[**5**] before the addition of K; the time stamps indicate the time that has passed since addition of the alkali metal). Marked components: Li[**5**] (■), K_2[**3**] (▲), K_4[**3**] (◆), K_2[**1**] (◆), K_2[**2**] (●).

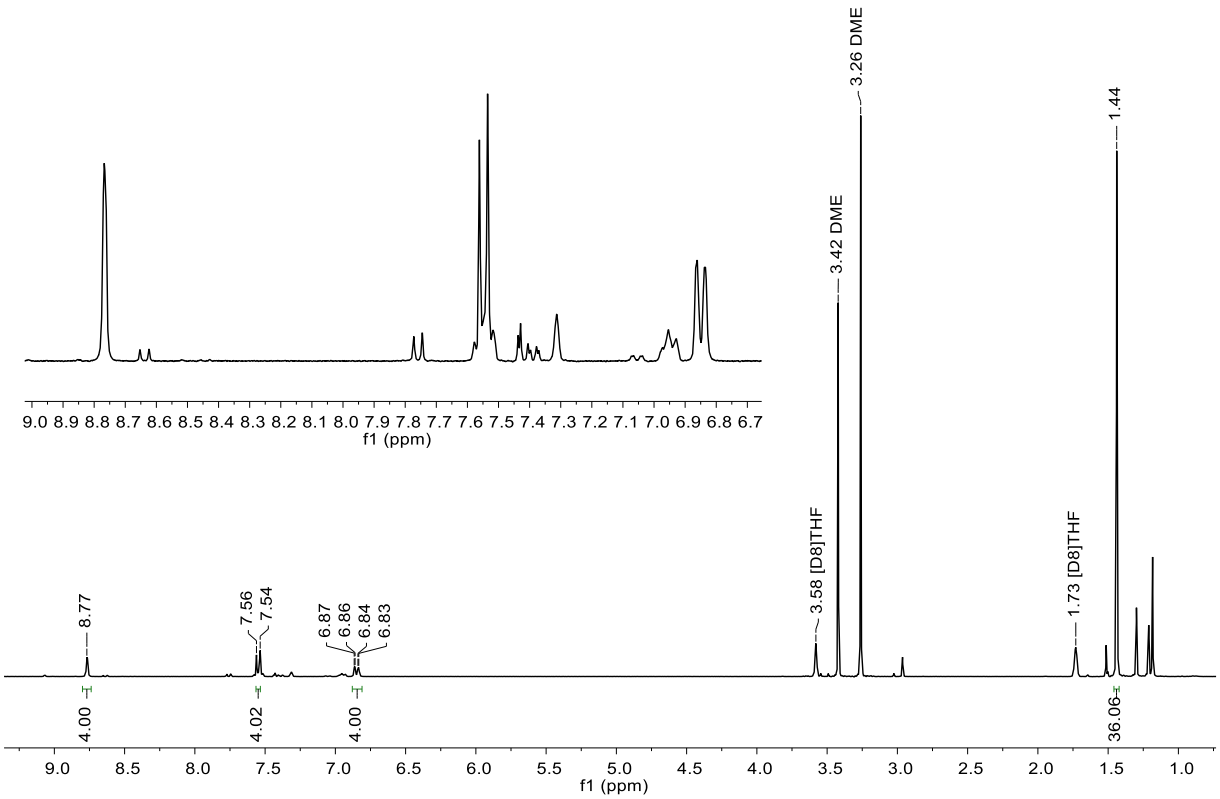

Figure S42: ^{1}H NMR spectrum of K_2[**3**] formed during the reaction of Li[**5**] with K metal (recorded 50 min. after addition of the alkali metal; 300.0 MHz, [D_8]THF; cf. Figure S41).

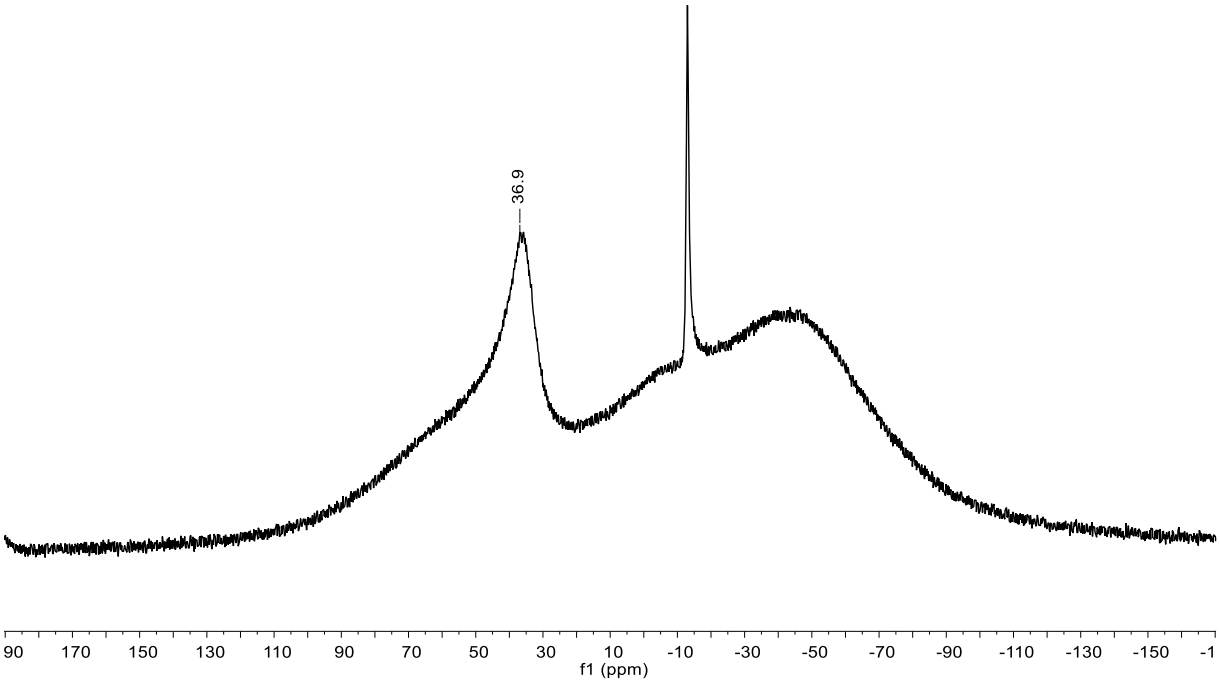

Figure S43: ^{11}B NMR spectrum of K_2[**3**] formed during the reaction of Li[**5**] with K metal (recorded 50 min. after addition of the alkali metal; 96.8 MHz, [D_8]THF).

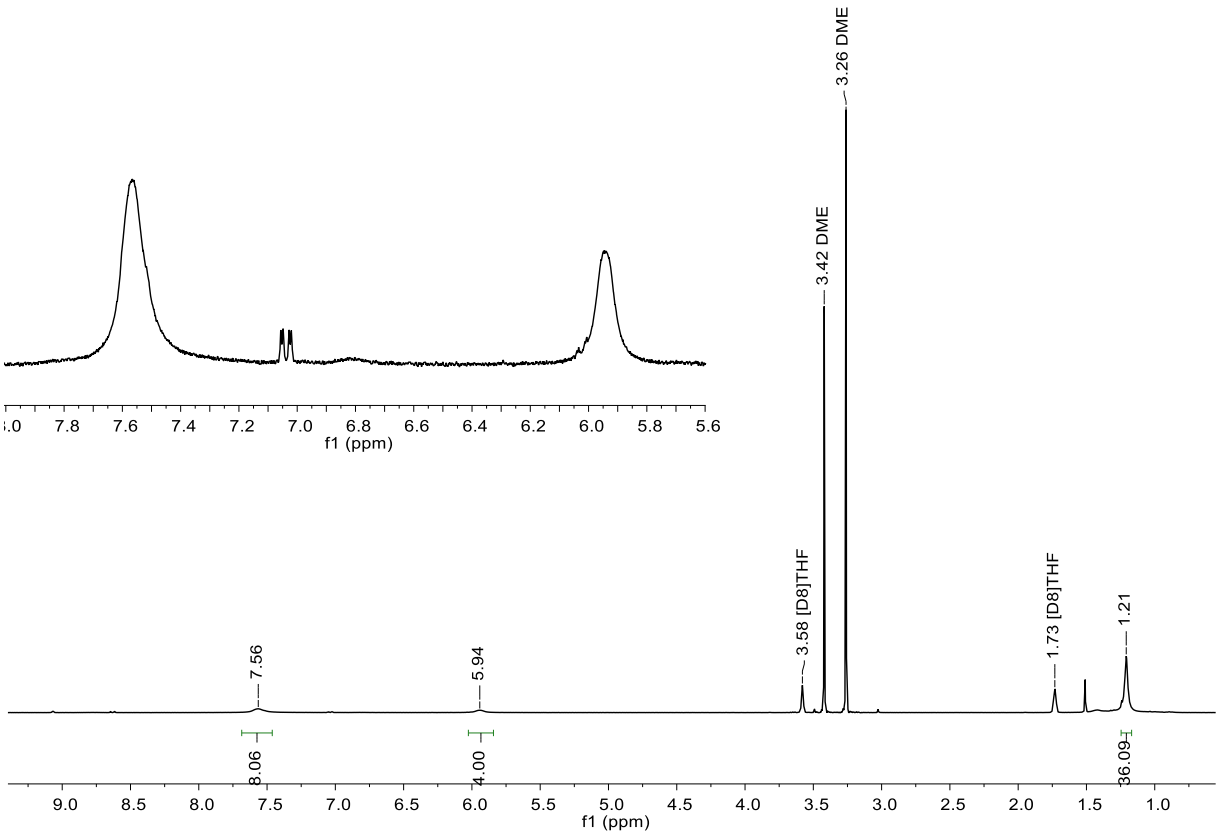

Figure S44: ^{1}H NMR spectrum of K_4[**3**] formed during the reaction of Li[**5**] with K metal (recorded 24 h after addition of the alkali metal; 300.0 MHz, [D_8]THF; cf. Figure S41).

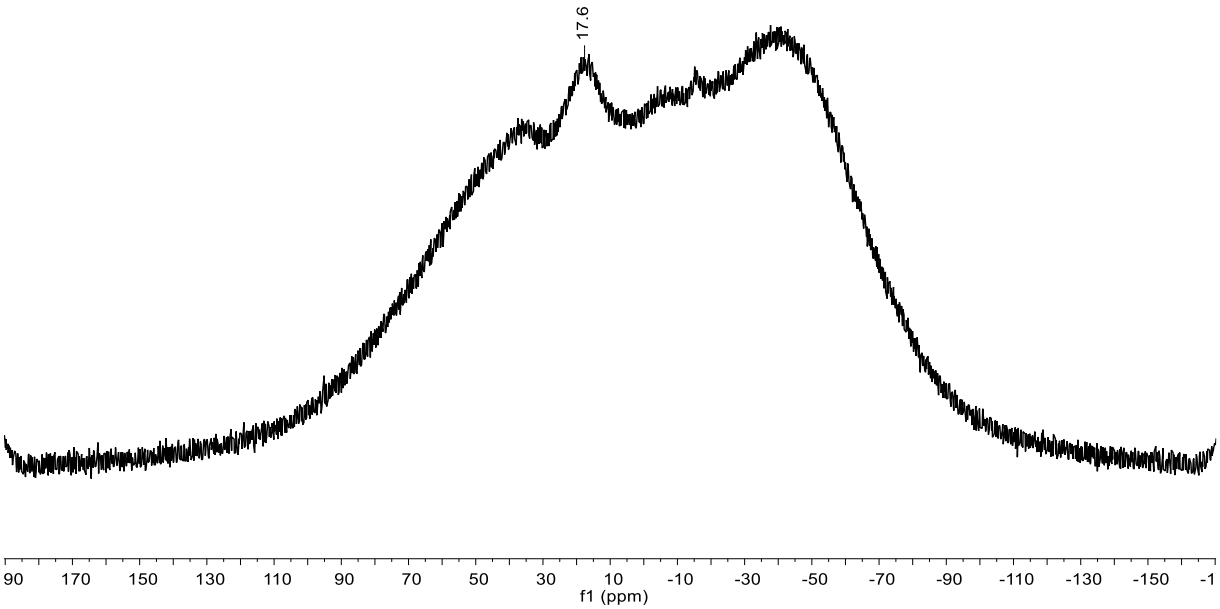

Figure S45: ^{11}B NMR spectrum of K_4[**3**] formed during the reaction of Li[**5**] with K metal (recorded 24 h after addition of the alkali metal; 96.8 MHz, [D_8]THF).

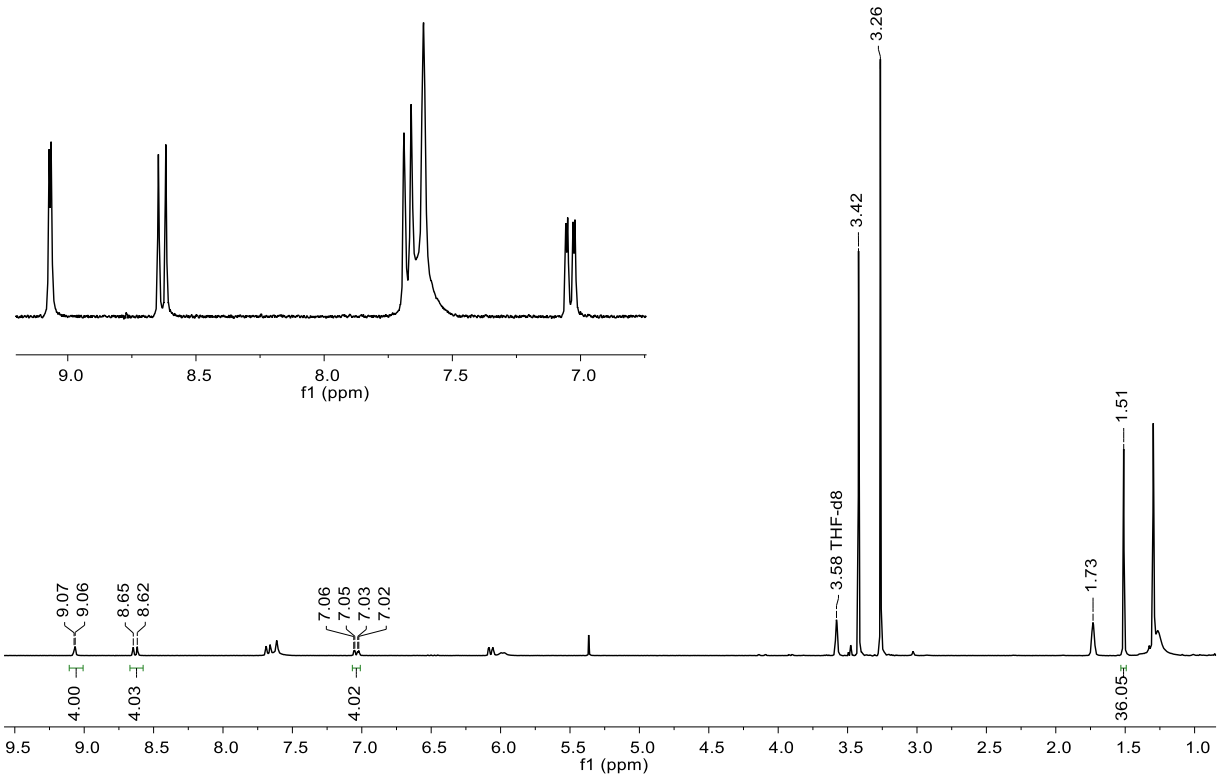

Figure S46: ^{1}H NMR spectrum of K_2[**2**] formed during the reaction of Li[**5**] with K metal (recorded 18 d after addition of the alkali metal; 300.0 MHz, [D_8]THF; cf. Figure S41).

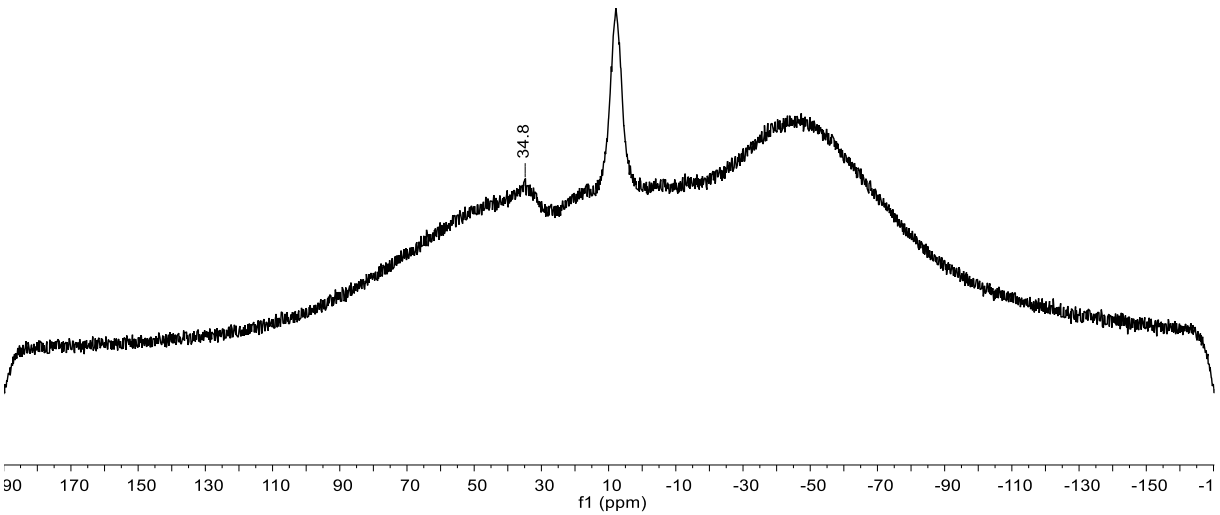

Figure S47: ^{11}B NMR spectrum of K_2[**2**] formed during the reaction of Li[**5**] with K metal (recorded 24 h after addition of the alkali metal; 96.8 MHz, [D_8]THF).

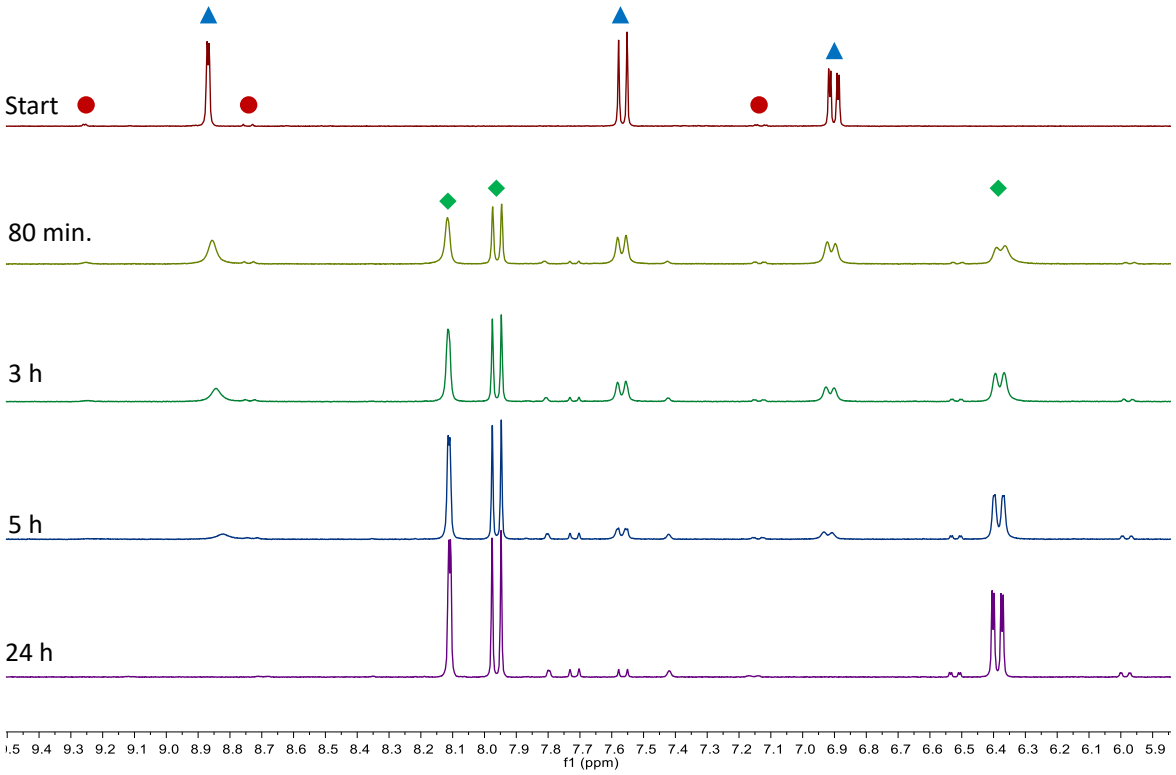

Figure S48: Aromatic regions of the ^{1}H NMR spectra (300.0 MHz, [D_8]THF) corresponding to different stages of the reaction of Na_2[**3**] with Li metal (cf. 1.2.7; Start: Na_2[**3**] before the addition of Li; the time stamps indicate the time that has passed since addition of the alkali metal). Marked components: Na_2[**3**] (▲), Na_2[**2**] (●), Li_4[**3**] (◆).

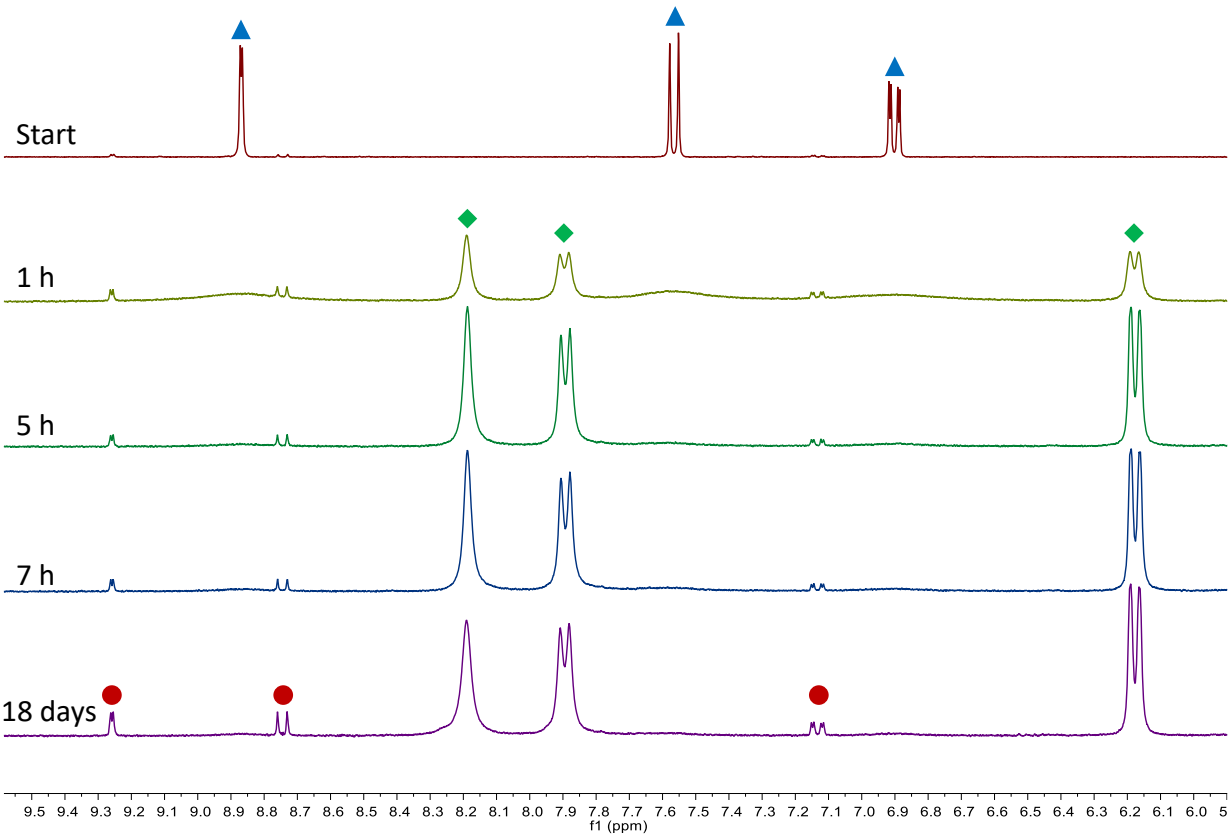

Figure S49: Aromatic regions of the ^{1}H NMR spectra (300.0 MHz, [D_8]THF) corresponding to different stages of the reaction of Na_2[**3**] with Na metal (cf. 1.2.8; Start: Na_2[**3**] before the addition of Na; the time stamps indicate the time that has passed since addition of the alkali metal). Marked components: Na_2[**3**] (▲), Na_4[**3**] (◆) Na_2[**2**] (●).

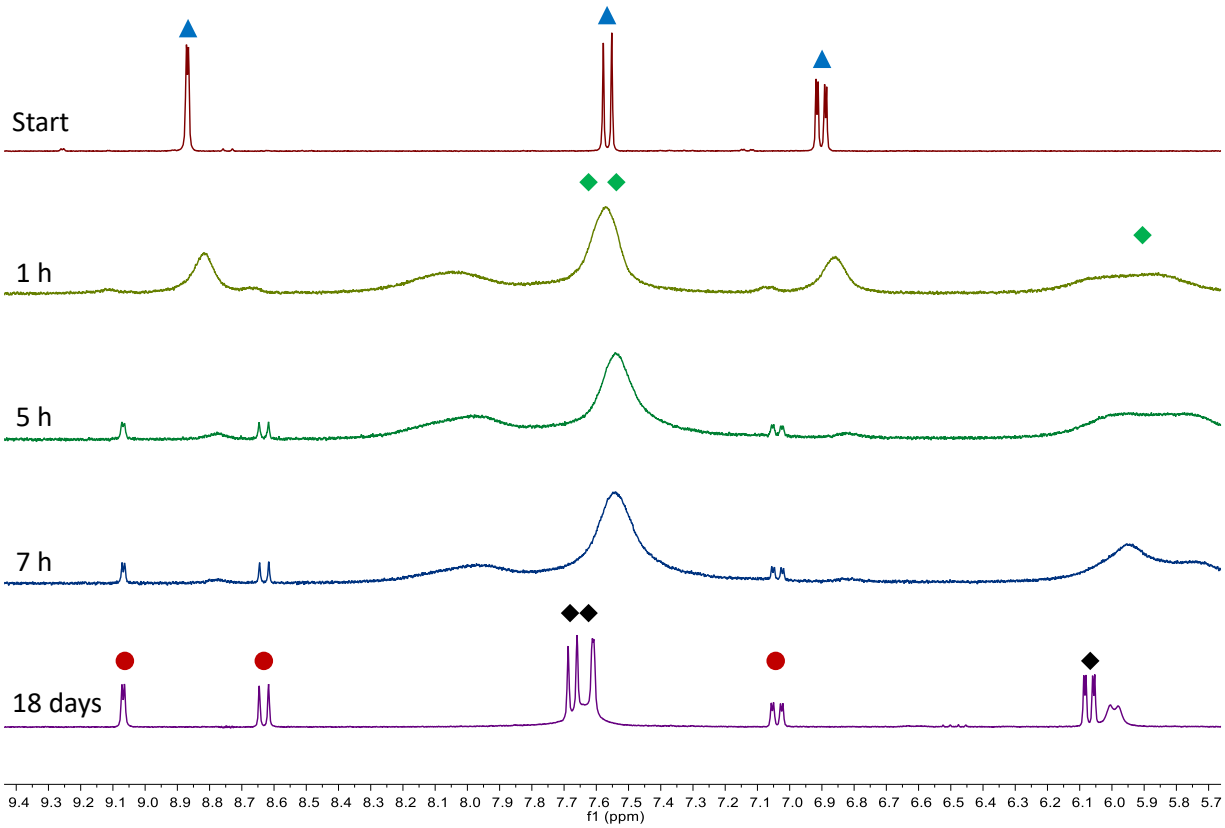

Figure S50: Aromatic regions of the ^{1}H NMR spectra (300.0 MHz, [D_8]THF) corresponding to different stages of the reaction of Na_2[**3**] with K metal (cf. 1.2.8; Start: Na_2[**3**] before the addition of K; the time stamps indicate the time that has passed since addition of the alkali metal). Marked components: Na_2[**3**] (▲), K_4[**3**] (◆) K_2[**2**] (●), K_2[**1**] (◆).

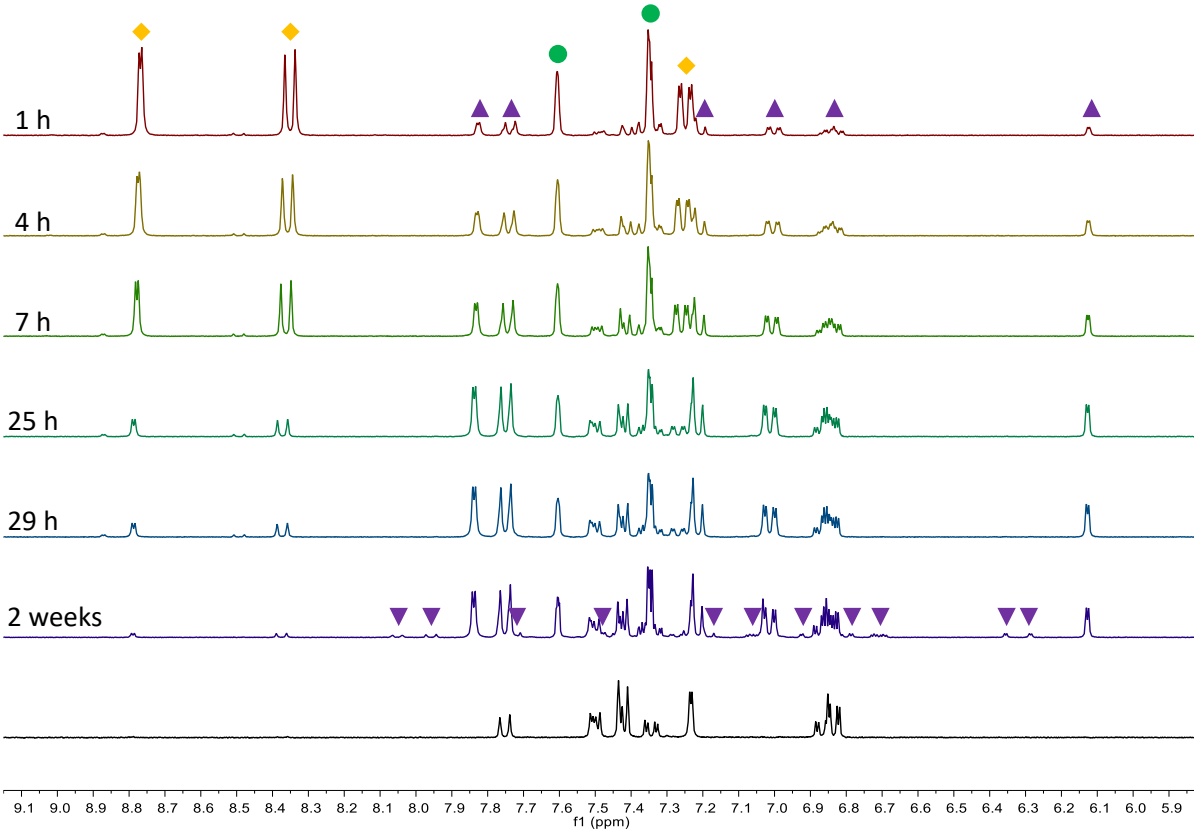

Figure S51: Aromatic region of the ^{1}H NMR spectrum (300.0 MHz, [D_8]THF) of Li[**5**] (black, bottom). Aromatic regions of the ^{1}H NMR spectra (300.0 MHz, [D_8]THF) corresponding to different stages of the reaction of **4** with Li[**2**H] (cf. 1.3.1; the time stamps indicate the time that has passed since the compounds were mixed). Marked components: Li[**2**H] (◆), **4** (●), Li[**2**H·**1**] (▲), Li[(**2**H·**1**)'] (▼).

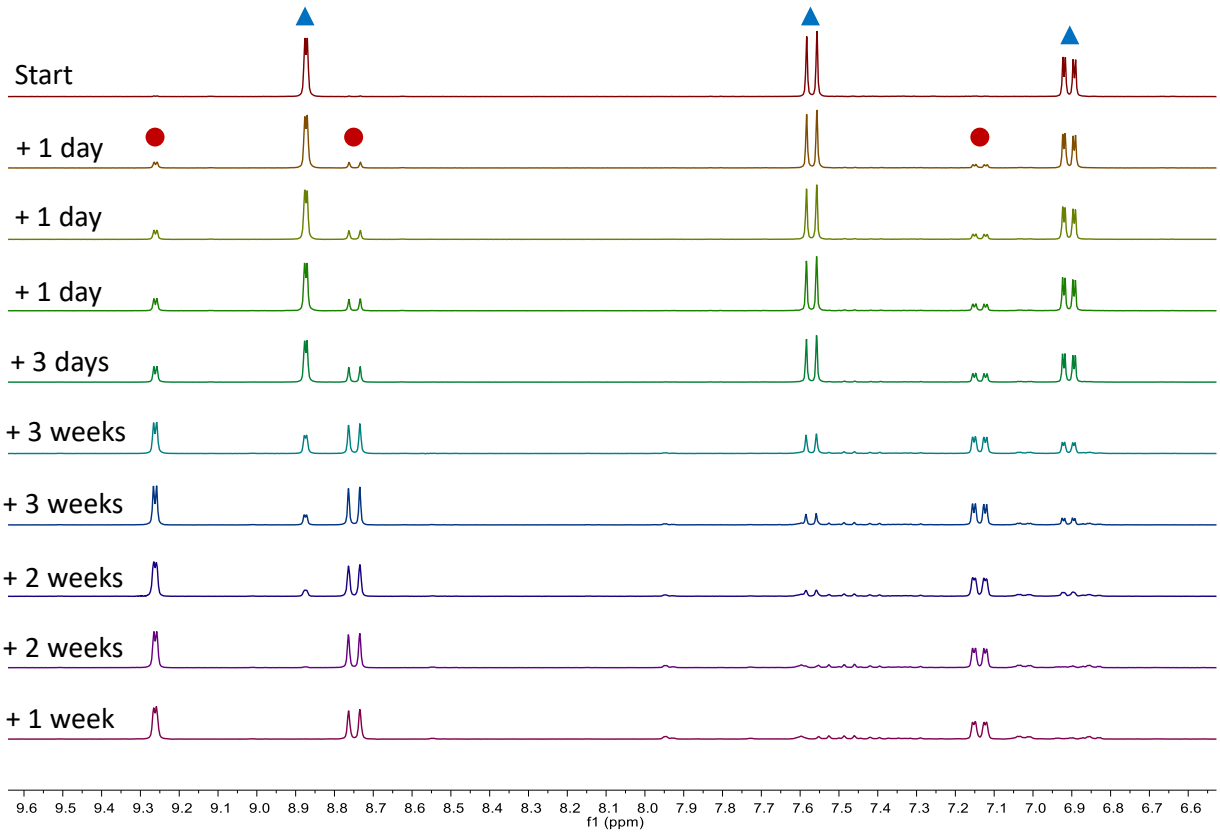

Figure S52: Aromatic regions of the ^{1}H NMR spectra (300.0 MHz, [D_8]THF) corresponding to different stages of the thermolysis of Na_2[**3**] (cf. 1.3.2; the time stamps indicate the time the sample has been heated at 130 °C since the last measurement). Marked components: Na_2[**3**] (▲), Na_2[**2**] (●).

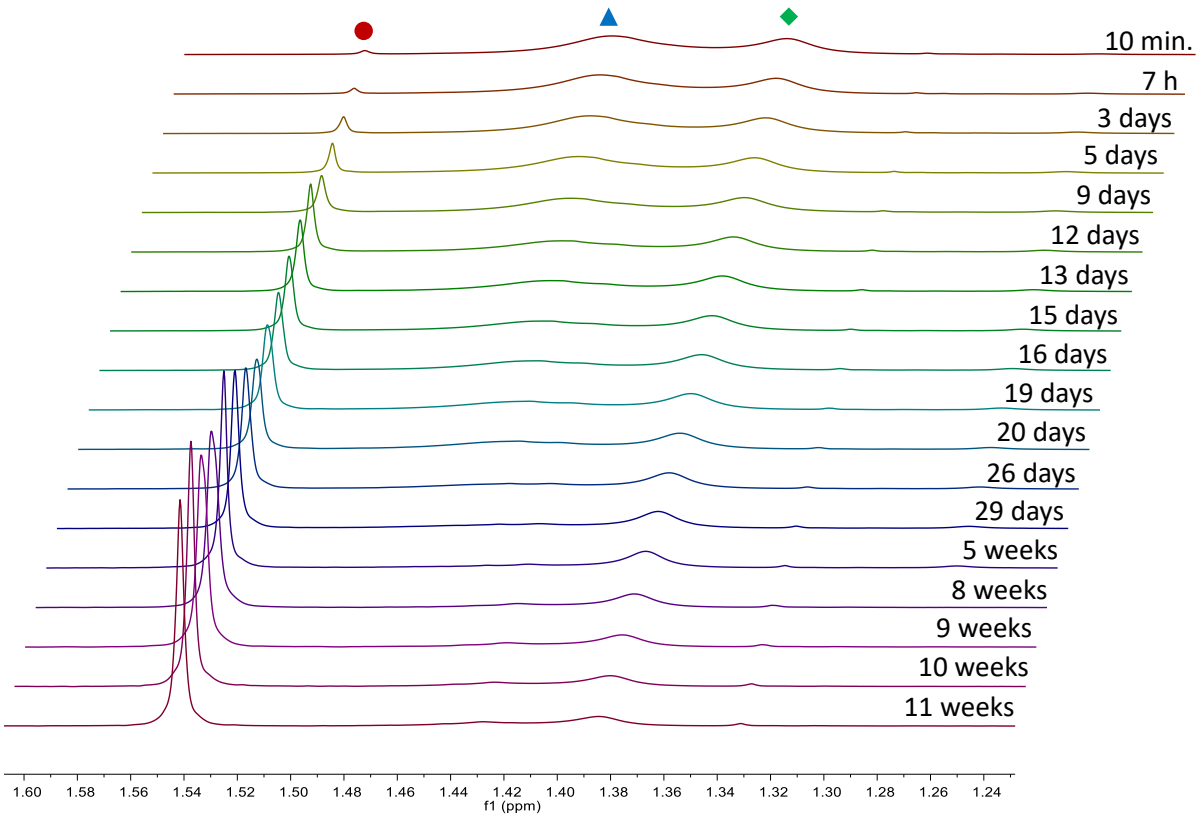

Figure S53: Alkyl regions of the ^{1}H NMR spectra (300.0 MHz, [D_8]THF) corresponding to different stages of the reaction of Na_4[**3**] with Na_2[**3**] (cf. 1.3.3; the time stamps indicate the time that has passed since the compounds were mixed). Marked components: Na_2[**2**] (●), Na_2[**3**] (▲), Na_4[**3**] (◆).

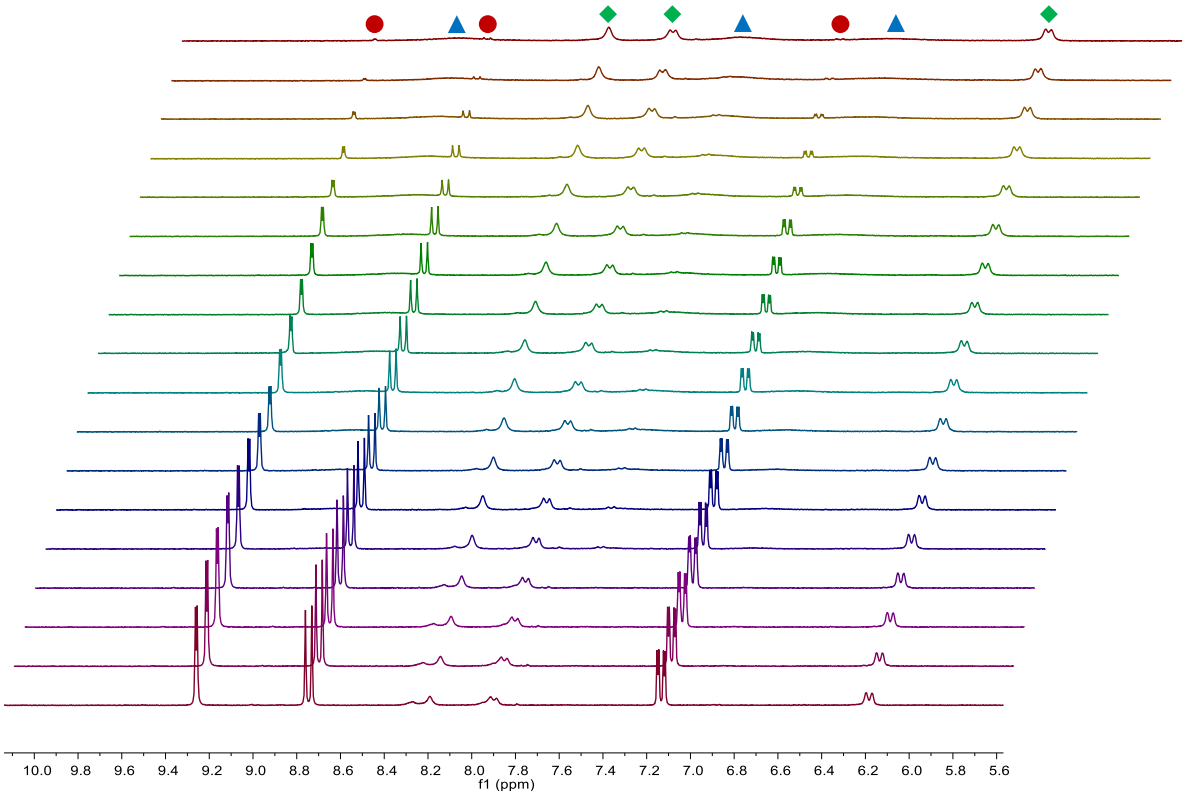

Figure S54: Aromatic regions of the ^{1}H NMR spectra (300.0 MHz, [D_8]THF) corresponding to different stages of the reaction of Na_4[**3**] with Na_2[**3**] (cf. 1.3.3; spectra are the same as those depicted in Figure S53). Marked components: Na_2[**2**] (●), Na_2[**3**] (▲), Na_4[**3**] (◆).

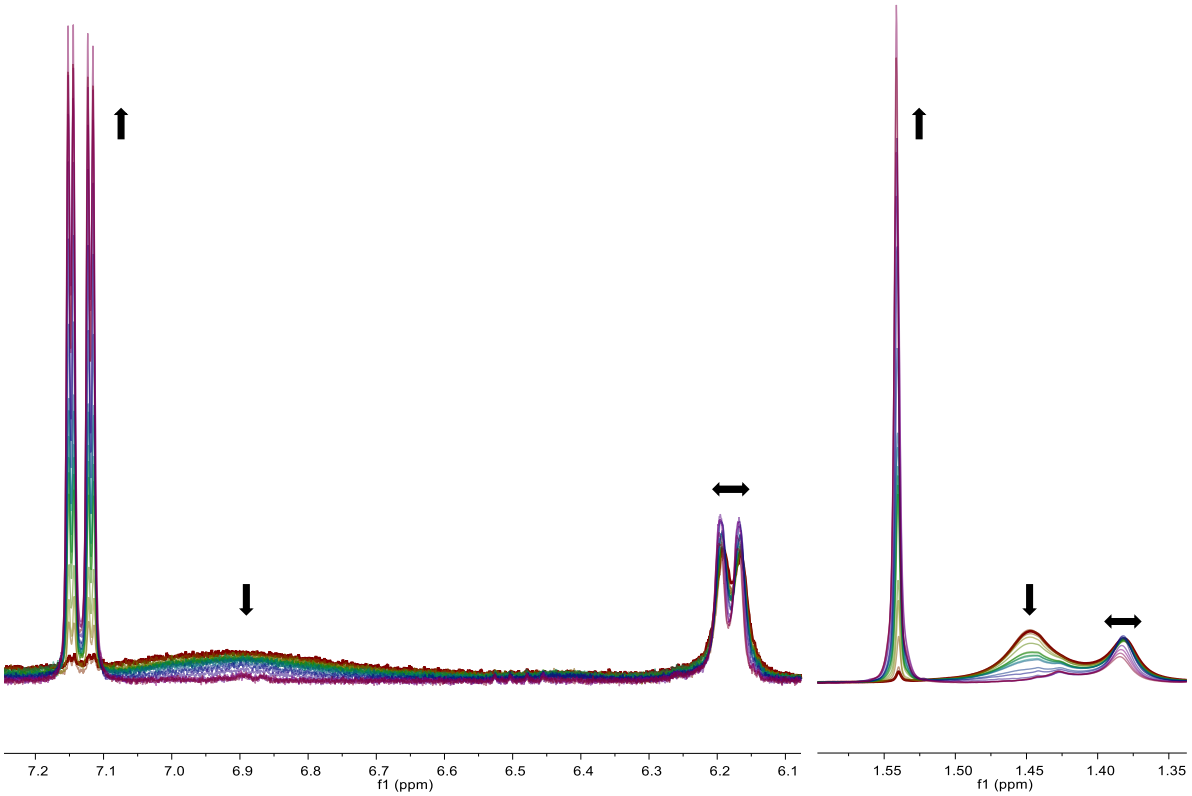

Figure S55: Superimposed aromatic (left) and alkyl (right) regions of the ^{1}H NMR spectra (300.0 MHz, [D_8]THF) corresponding to different stages of the reaction of Na_4[**3**] with Na_2[**3**] (cf. 1.3.3; the color schemes are the same as in Figure S53 and Figure S54). The aromatic and alkyl regions are scaled differently.

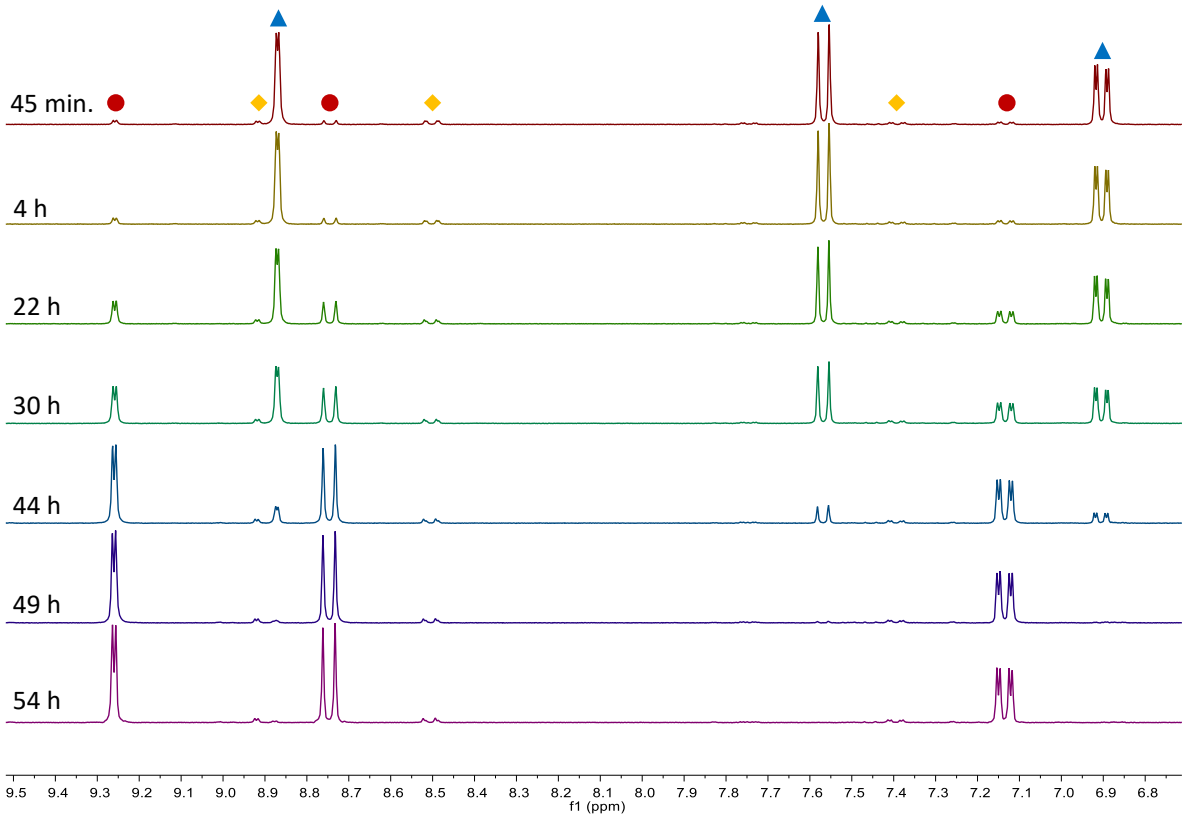

Figure S56: Aromatic regions of the ^{1}H NMR spectra (300.0 MHz, [D_8]THF) corresponding to different stages of the reaction of Na_2[**3**] with 0.09 equiv of HCl (cf. 1.3.4; the time stamps indicate the time that has passed since the compounds were mixed). Marked components: Na_2[**2**] (●),Na[**2**H] (◆), Na_2[**3**] (▲).

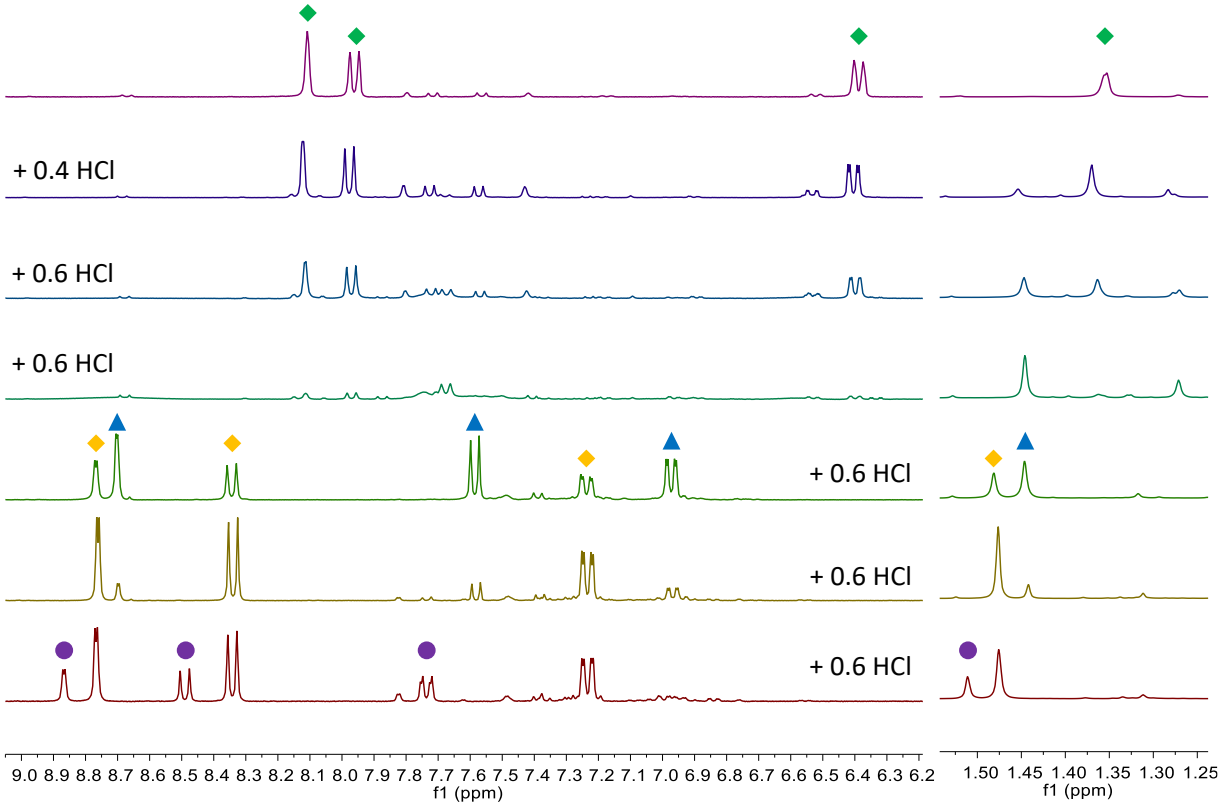

Figure S57: Alkyl and aromatic regions of the ^{1}H NMR spectra (300.0 MHz, [D_8]THF) corresponding to different stages of the titration of Li_4[**3**] with HCl (cf. 1.3.5). The aromatic and alkyl regions are scaled differently. Marked components: Li_4[**3**] (◆), Li_2[**3**] (▲), Li[**2**H] (◆), **2**H_2 (●)[S3].

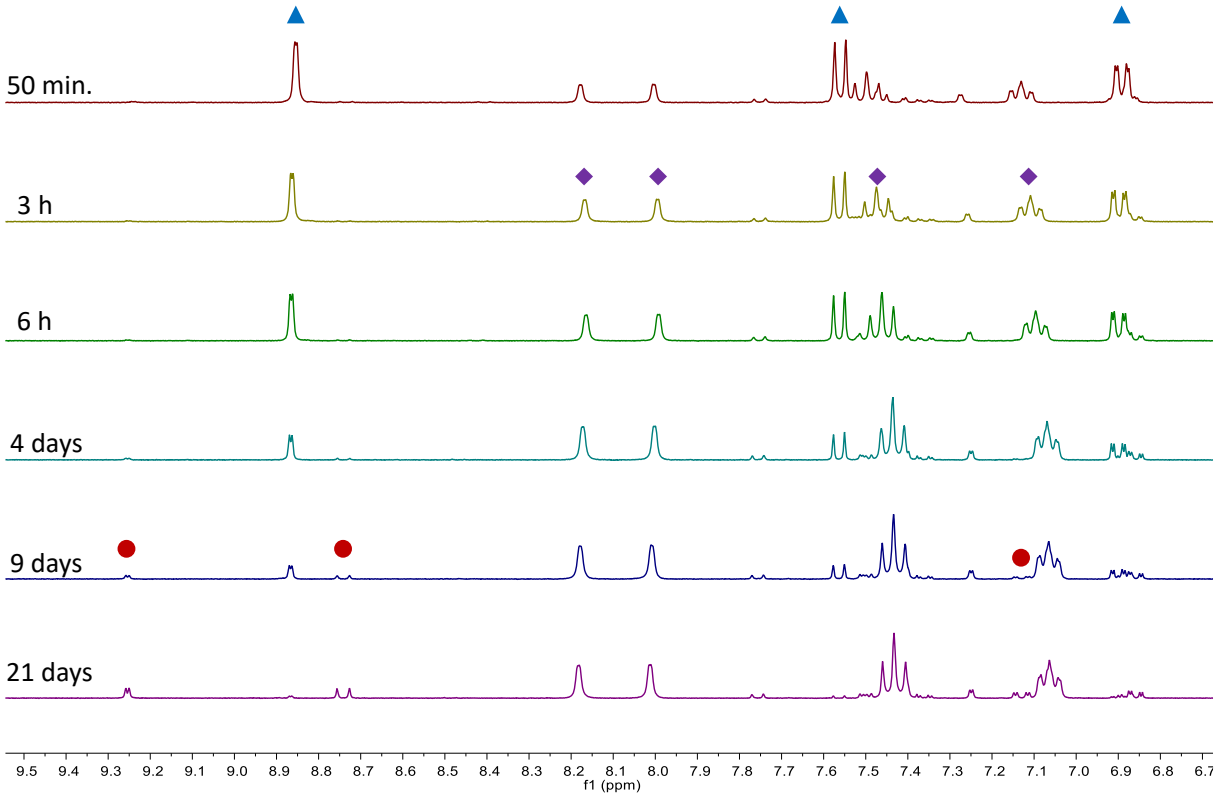

Figure S58: Aromatic regions of the ^{1}H NMR spectra (300.0 MHz, [D_8]THF) corresponding to different stages of the reaction of Na_2[**3**] with 1 equiv [*n*Bu_4N][PF_6] (cf. 1.3.6 (A); the time stamps indicate the time that has passed since the compounds were mixed). Marked components: Na_2[**3**] (▲), Na[**9**] (◆), Na_2[**2**] (●).

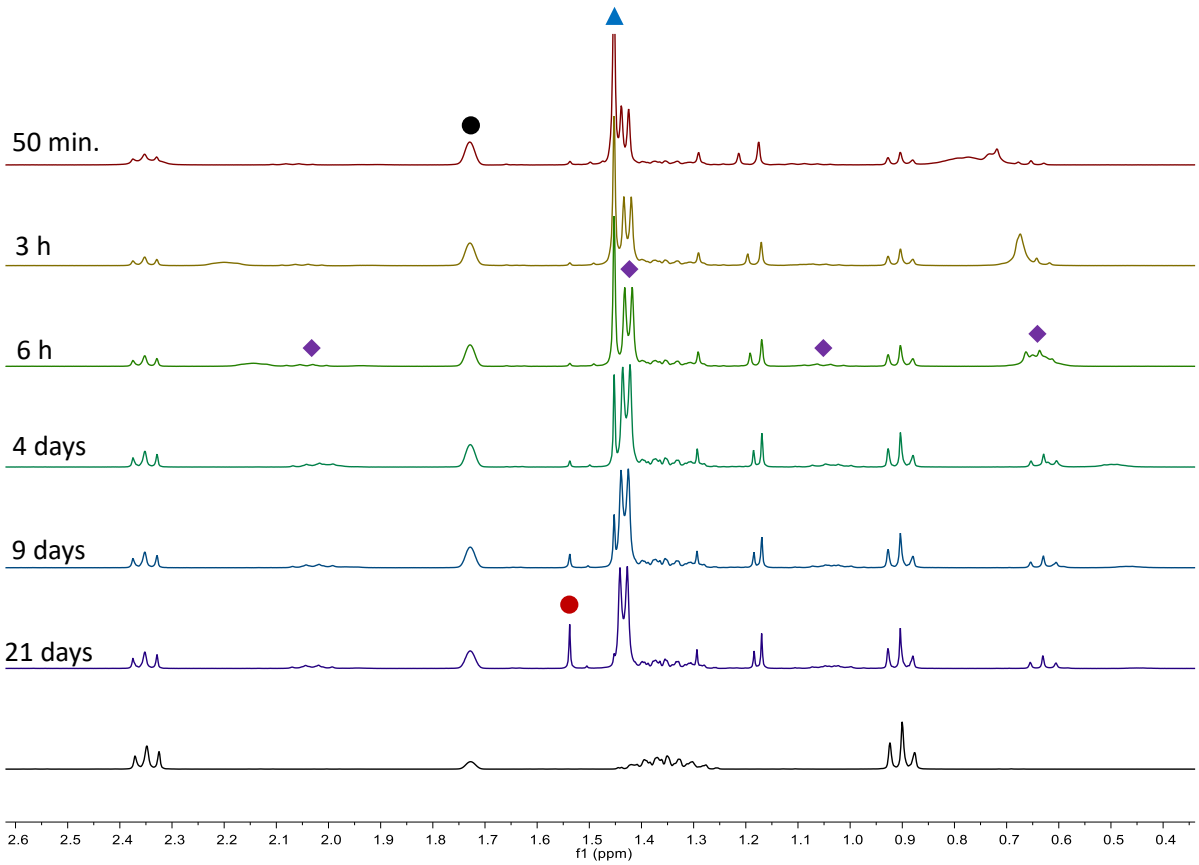

Figure S59: ^{1}H NMR spectrum (300.0 MHz, [D_8]THF) of nBu$_3$N (black, bottom). Alkyl regions of the ^{1}H NMR spectra (300.0 MHz, [D_8]THF) corresponding to different stages of the reaction of Na_2[**3**] with 1 equiv [nBu$_4$N][PF_6] (cf. 1.3.6 (A); the time stamps indicate the time that has passed since the compounds were mixed). Marked components: [D_8]THF (●), Na_2[**3**] (▲), Na[**9**] (◆), Na_2[**2**] (●).

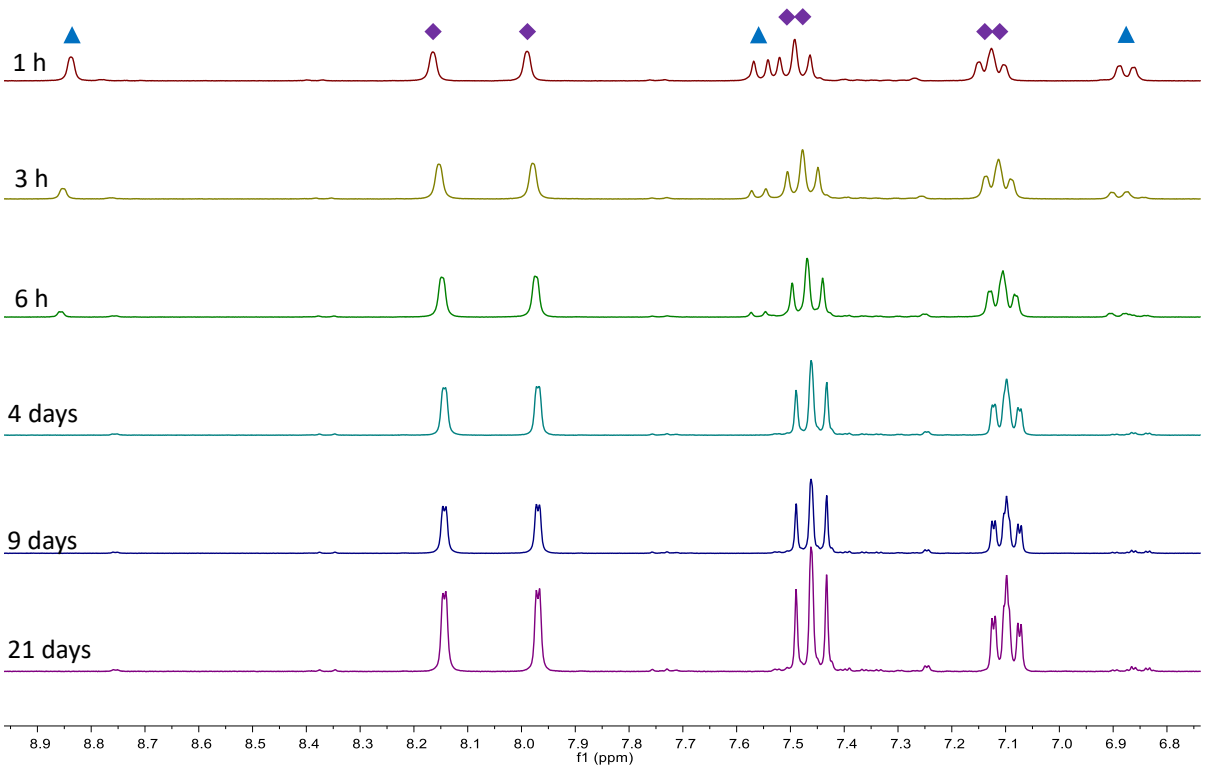

Figure S60: Aromatic regions of the ^{1}H NMR spectra (300.0 MHz, [D_8]THF) corresponding to different stages of the reaction of Na_2[**3**] with 2 equiv [*n*Bu_4N][PF_6] (cf. 1.3.6 (B); the time stamps indicate the time that has passed since the compounds were mixed). Marked components: Na_2[**3**] (▲), [*n*Bu_4N][**9**] (◆).

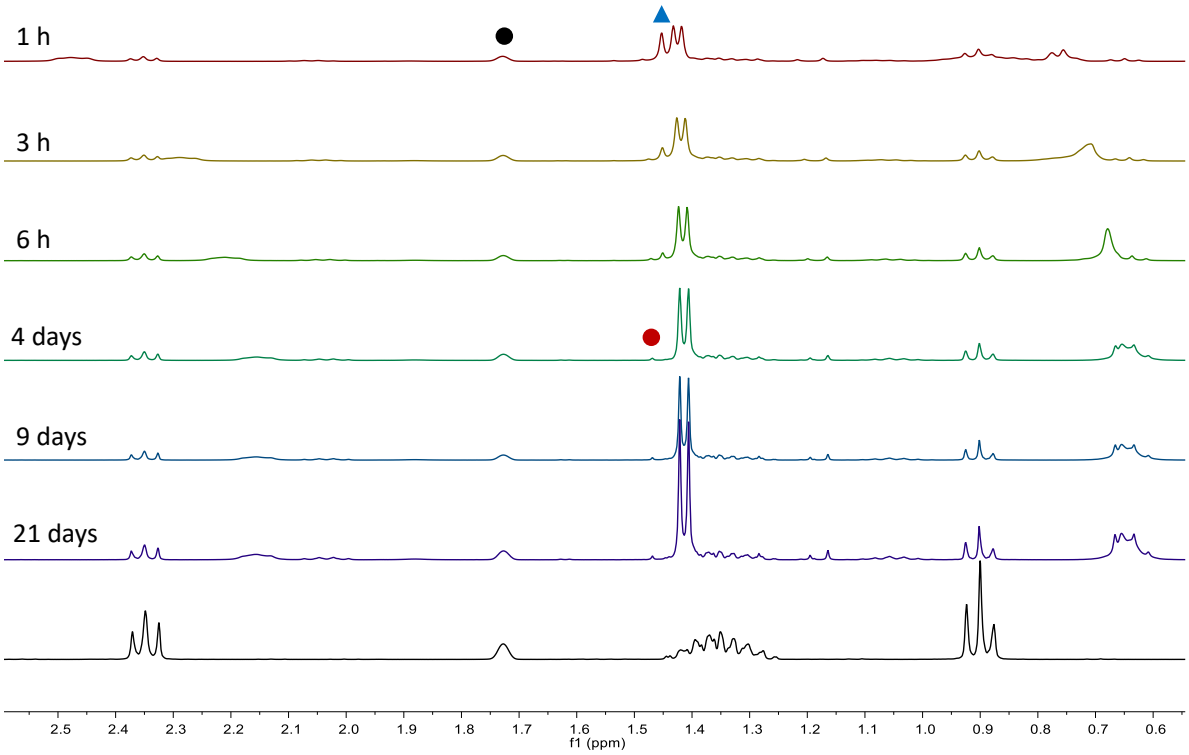

Figure S61: ^{1}H NMR spectrum (300.0 MHz, [D_8]THF) of *n*Bu_3N (black, bottom). Alkyl regions of the ^{1}H NMR spectra (300.0 MHz, [D_8]THF) corresponding to different stages of the reaction of Na_2[**3**] with 2 equiv [*n*Bu_4N][PF_6] (cf. 1.3.6 (B); the time stamps indicate the time that has passed since the compounds were mixed). Marked components: [D_8]THF (●), Na_2[**3**] (▲), Na_2[**2**] (●).

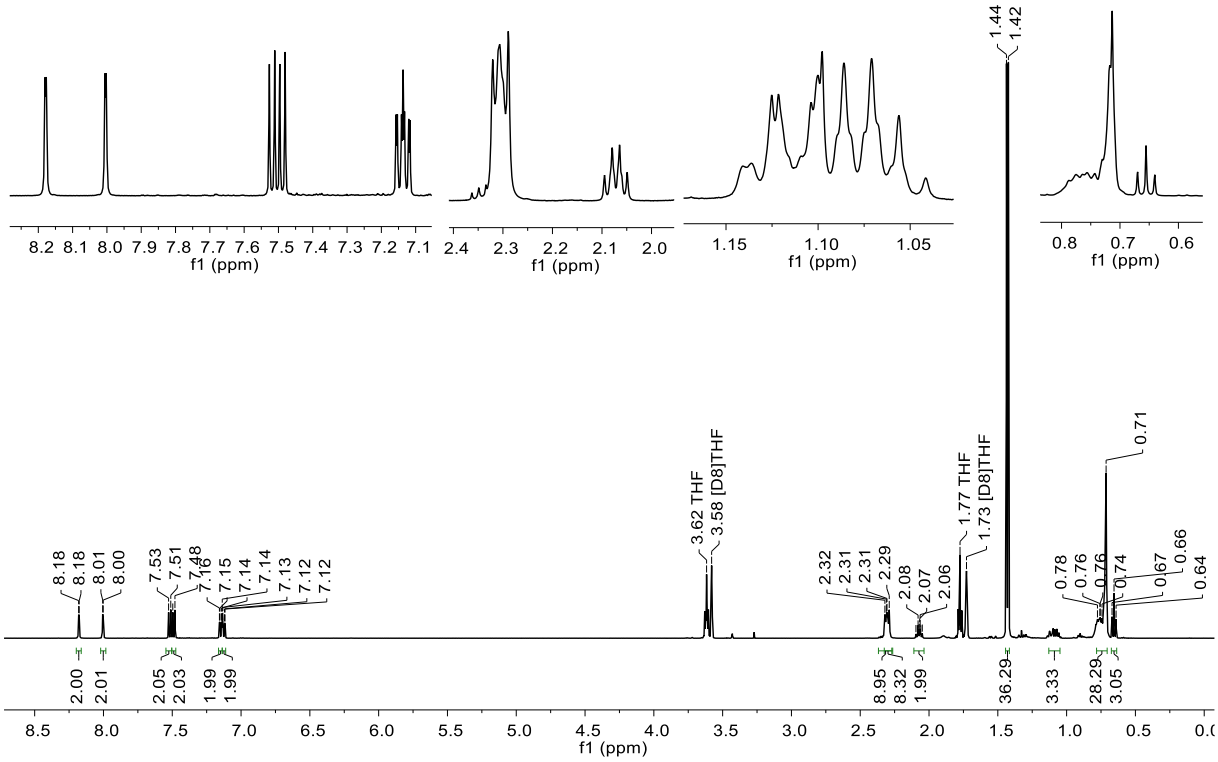

Figure S62: ^{1}H NMR spectrum of [*n*Bu$_4$N][**9**] (500.2 MHz, [D$_8$]THF).

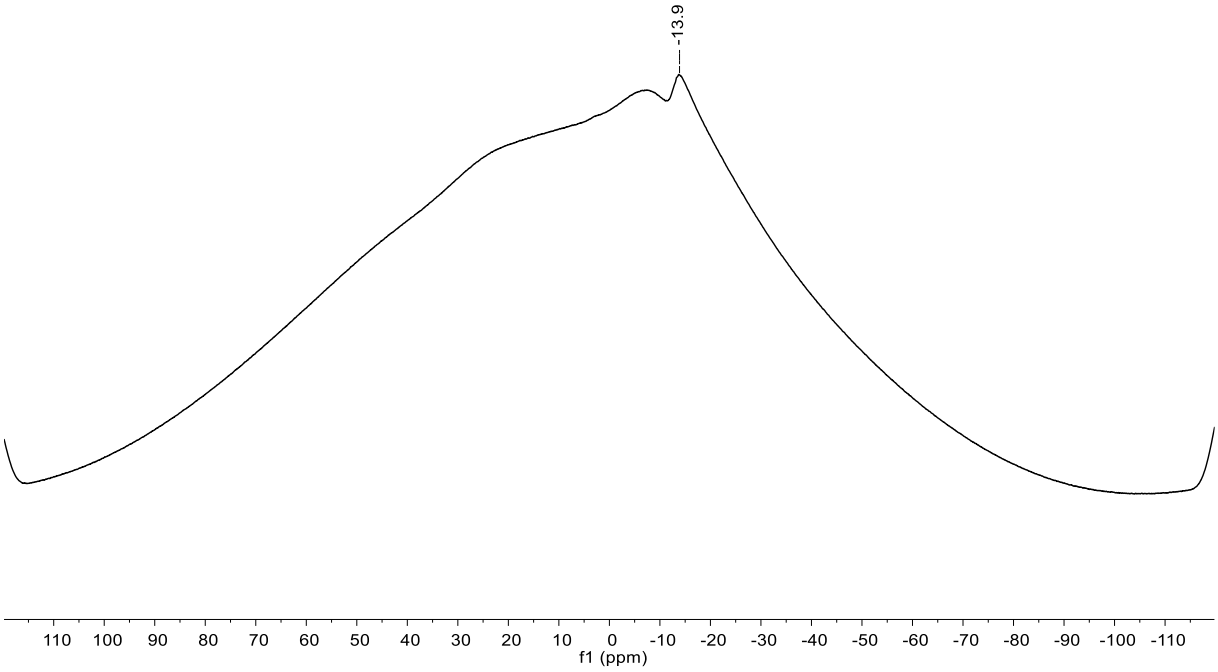

Figure S63: ^{11}B NMR spectrum of [*n*Bu$_4$N][**9**] (96.3 MHz, [D$_8$]THF).

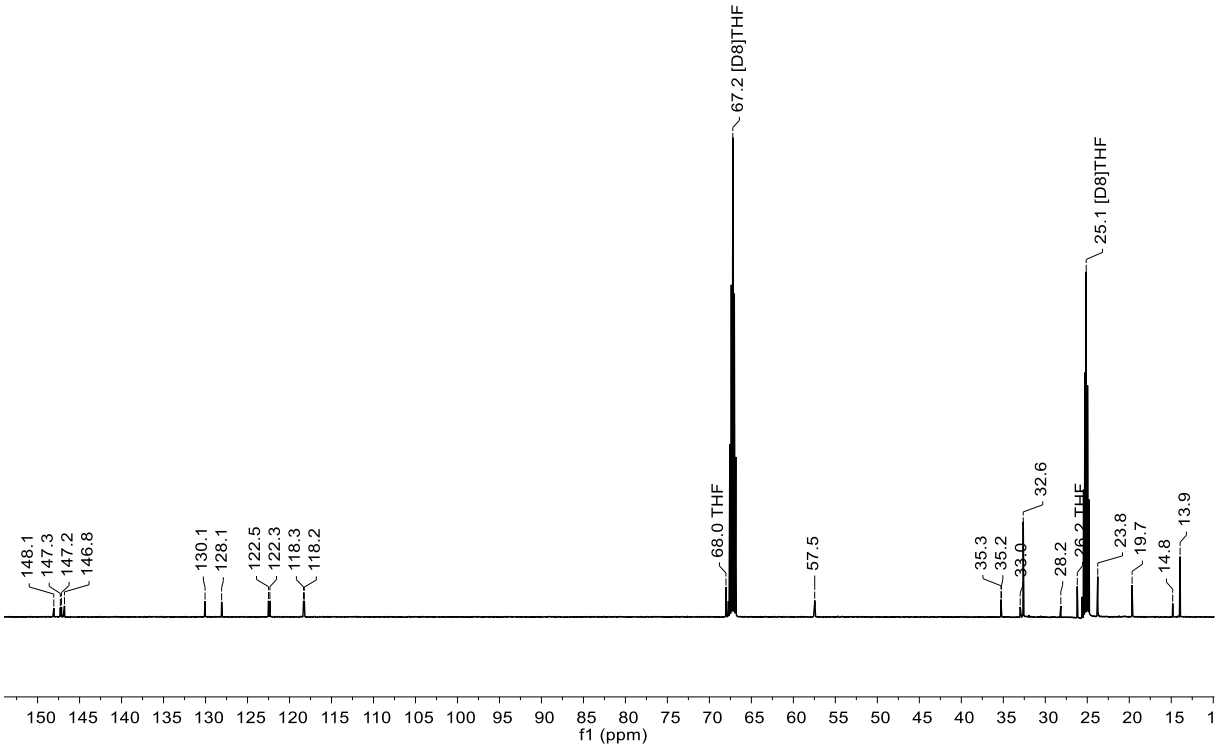

Figure S64: ^{13}C NMR spectrum of [*n*Bu$_4$N][**9**] (125.8 MHz, [D$_8$]THF).

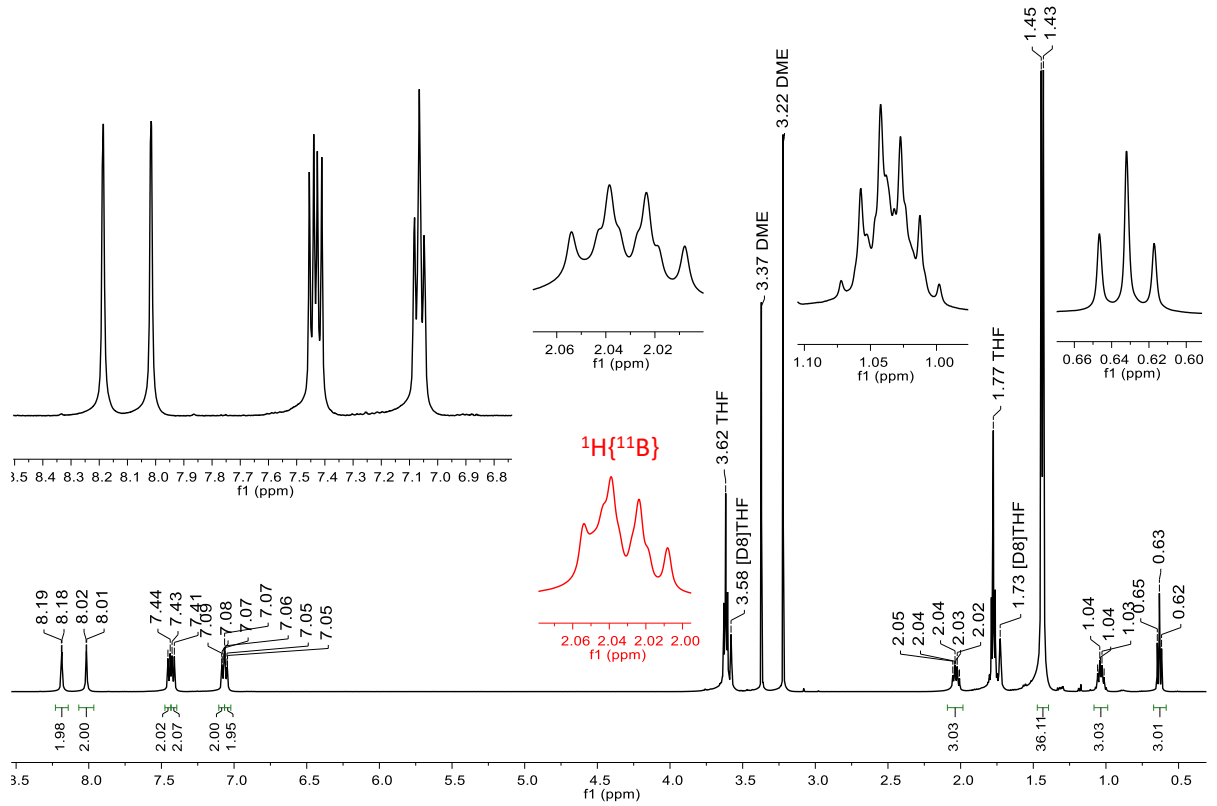

Figure S65: ^{1}H NMR spectrum of Na[**9**] (500.2 MHz, [D$_8$]THF).

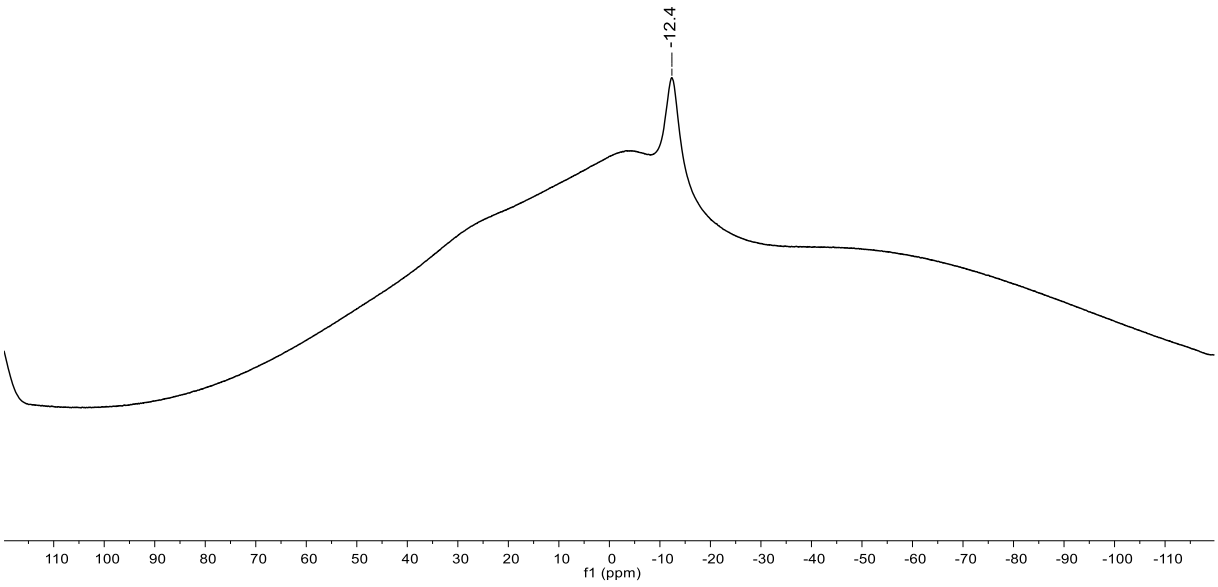

Figure S66: ^{11}B NMR spectrum of Na[**9**] (160.5 MHz, [D_8]THF).

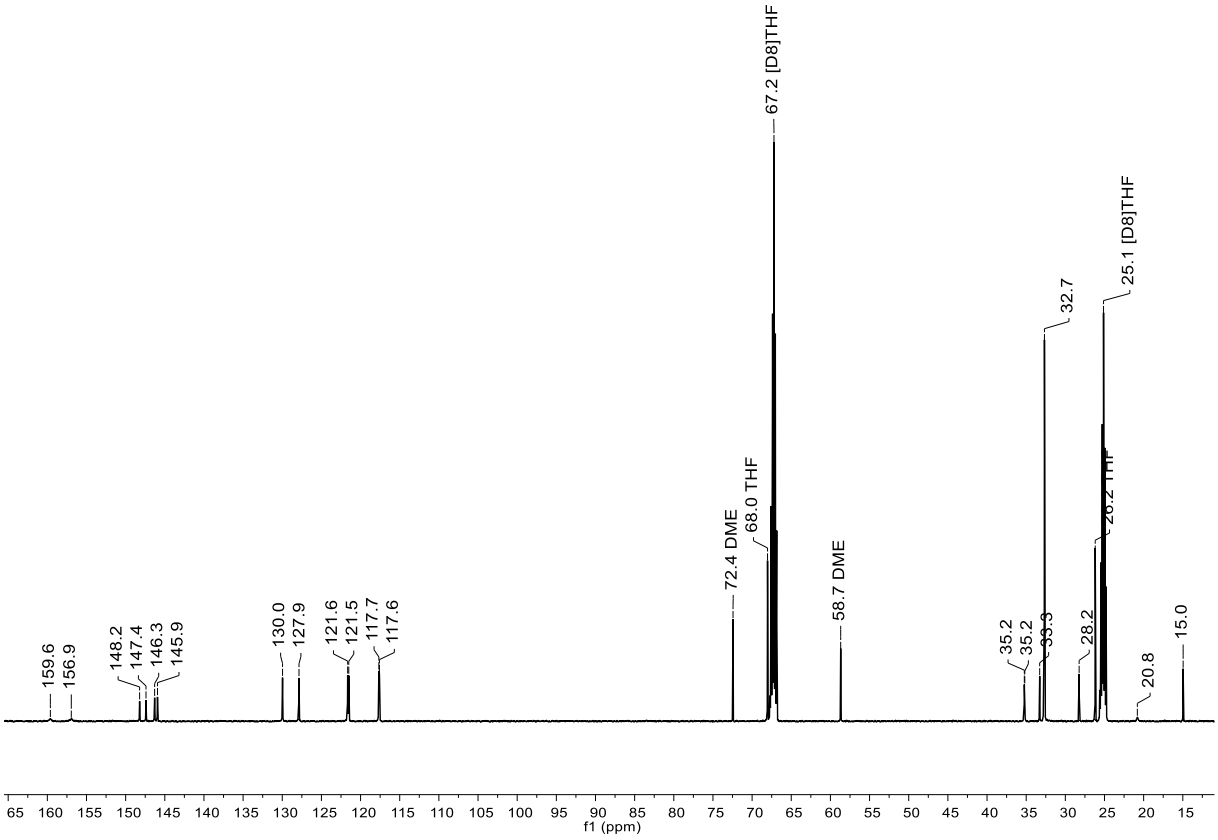

Figure S67: ^{13}C NMR spectrum of Na[**9**] (125.8 MHz, [D_8]THF).

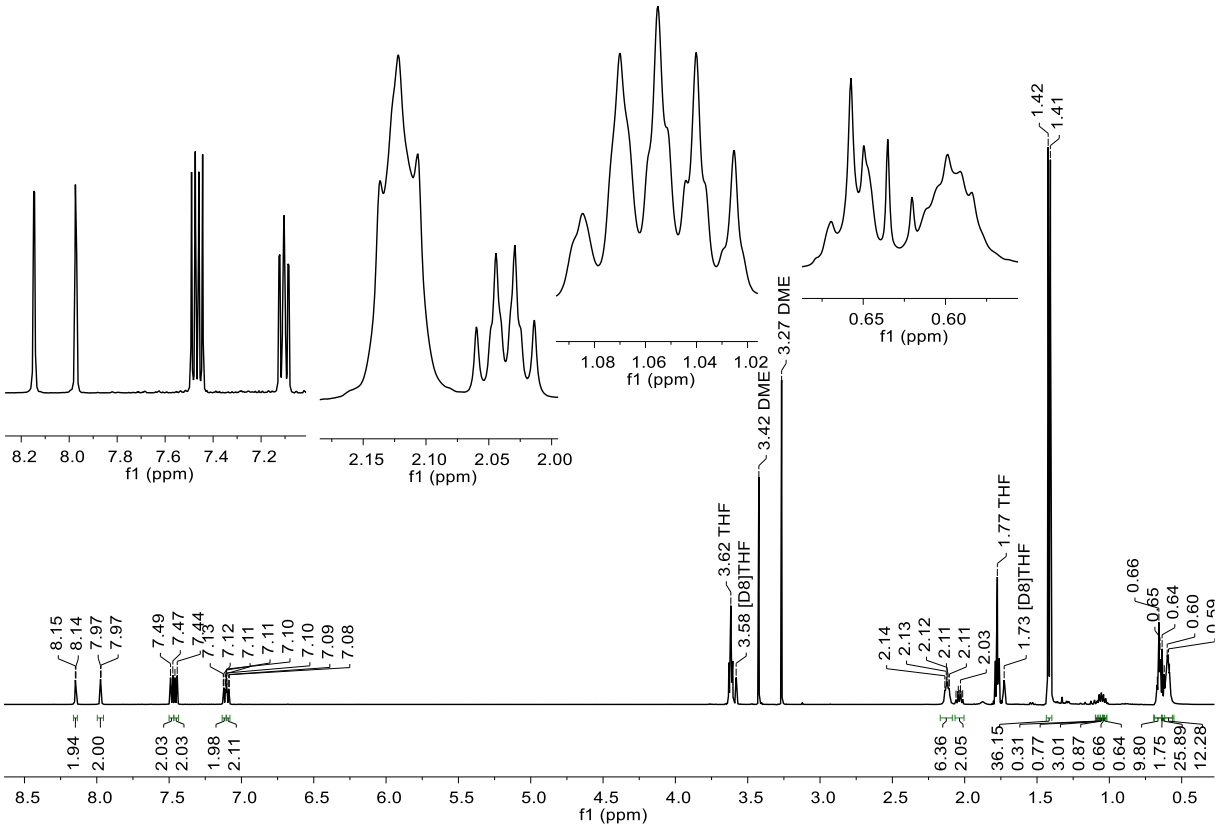

Figure S68: ^{1}H NMR spectrum of [*n*Bu$_4$N]$_x$[Na]$_y$[**9**] (x + y = 1, cf. 1.3.7; 500.2 MHz, [D$_8$]THF).

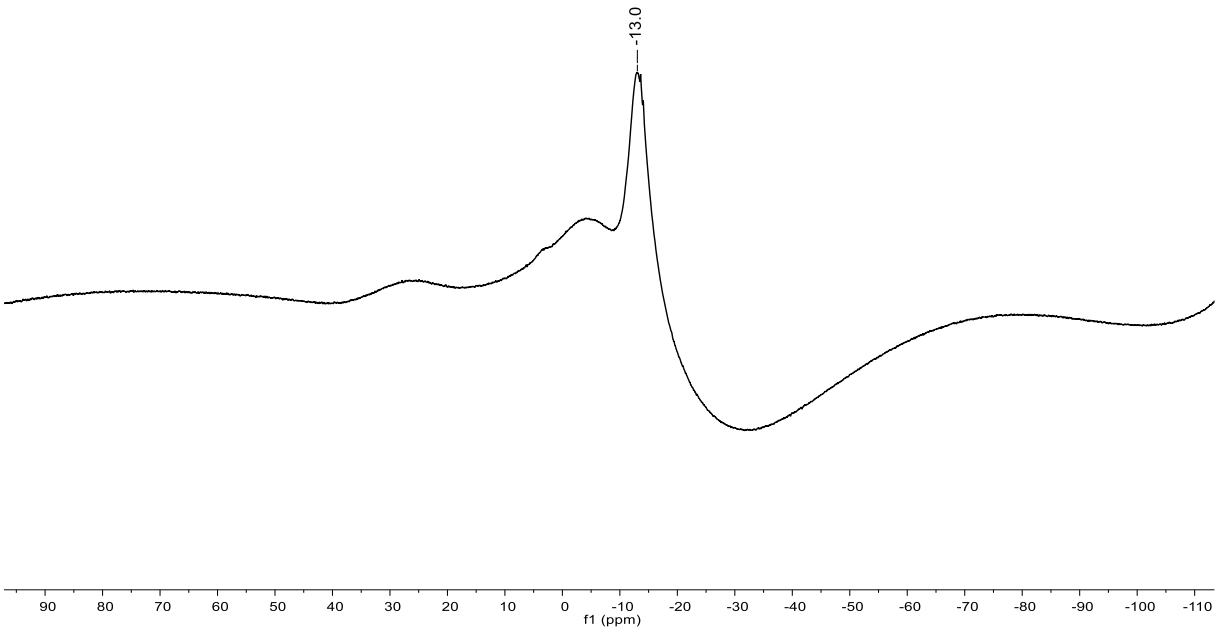

Figure S69: ^{11}B NMR spectrum of [*n*Bu$_4$N]$_x$[Na]$_y$[**9**] (x + y = 1, cf. 1.3.7; 160.5 MHz, [D$_8$]THF).

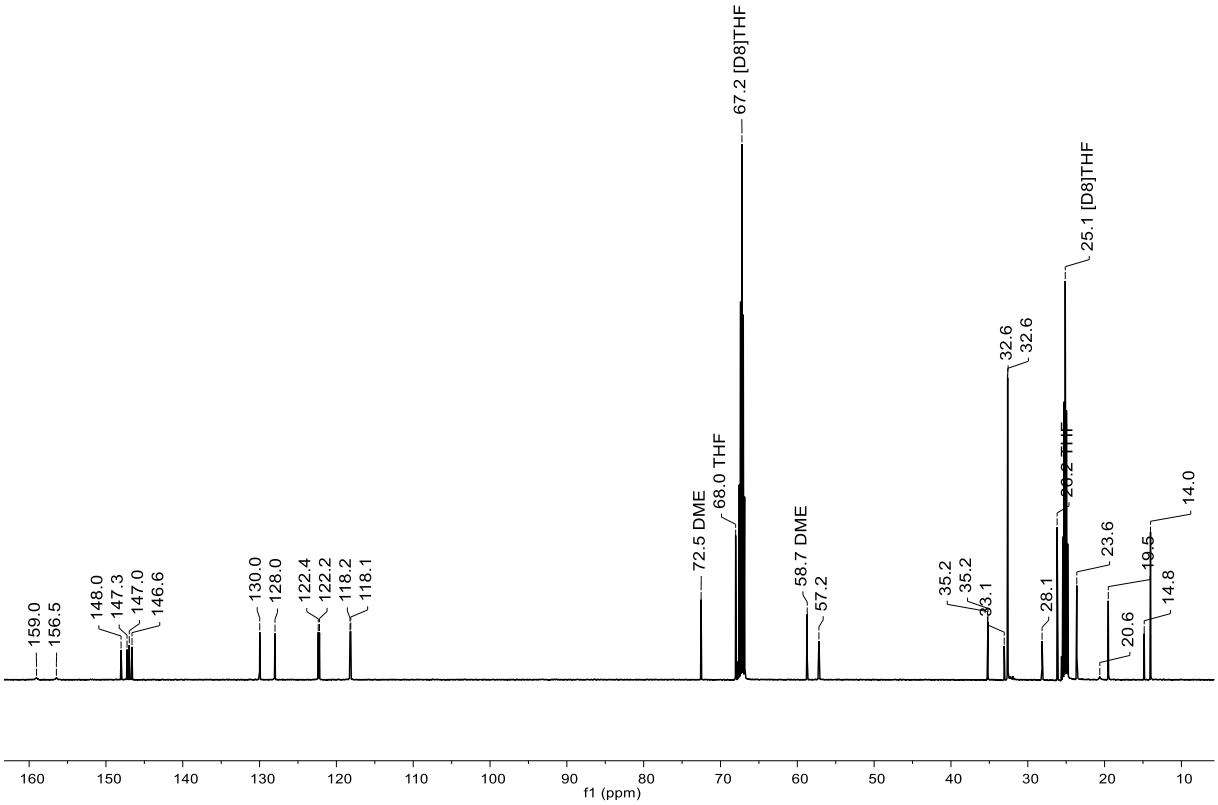

Figure S70: ^{13}C NMR spectrum of $[n\mathrm{Bu}_4\mathrm{N}]_x[\mathrm{Na}]_y$[**9**] (x + y = 1, cf. 1.3.7; 125.8 MHz, $[\mathrm{D}_8]$THF).

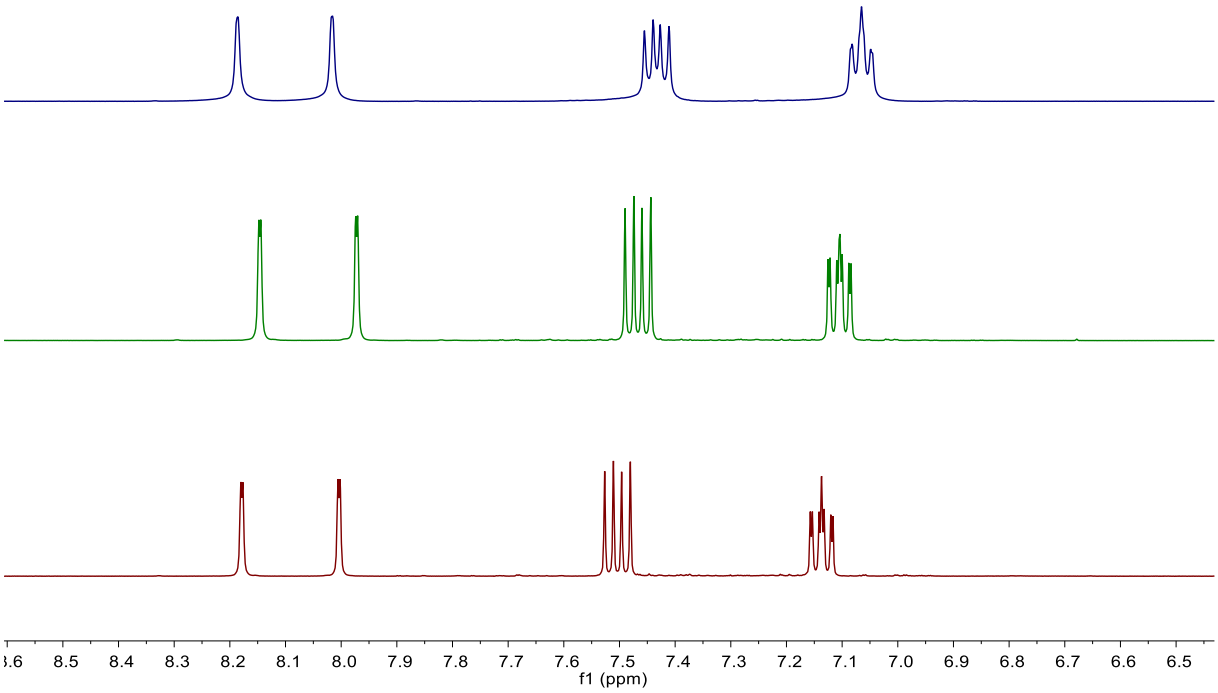

Figure S71: Aromatic regions of the ^{1}H NMR spectra (500.2 MHz, [D_8]THF) corresponding to Na[**9**] (blue, top), [*n*Bu_4N]$_x$[Na]$_y$[**9**] (x + y = 1, cf. 1.3.7; green, middle), or [*n*Bu_4N][**9**] (red, bottom).

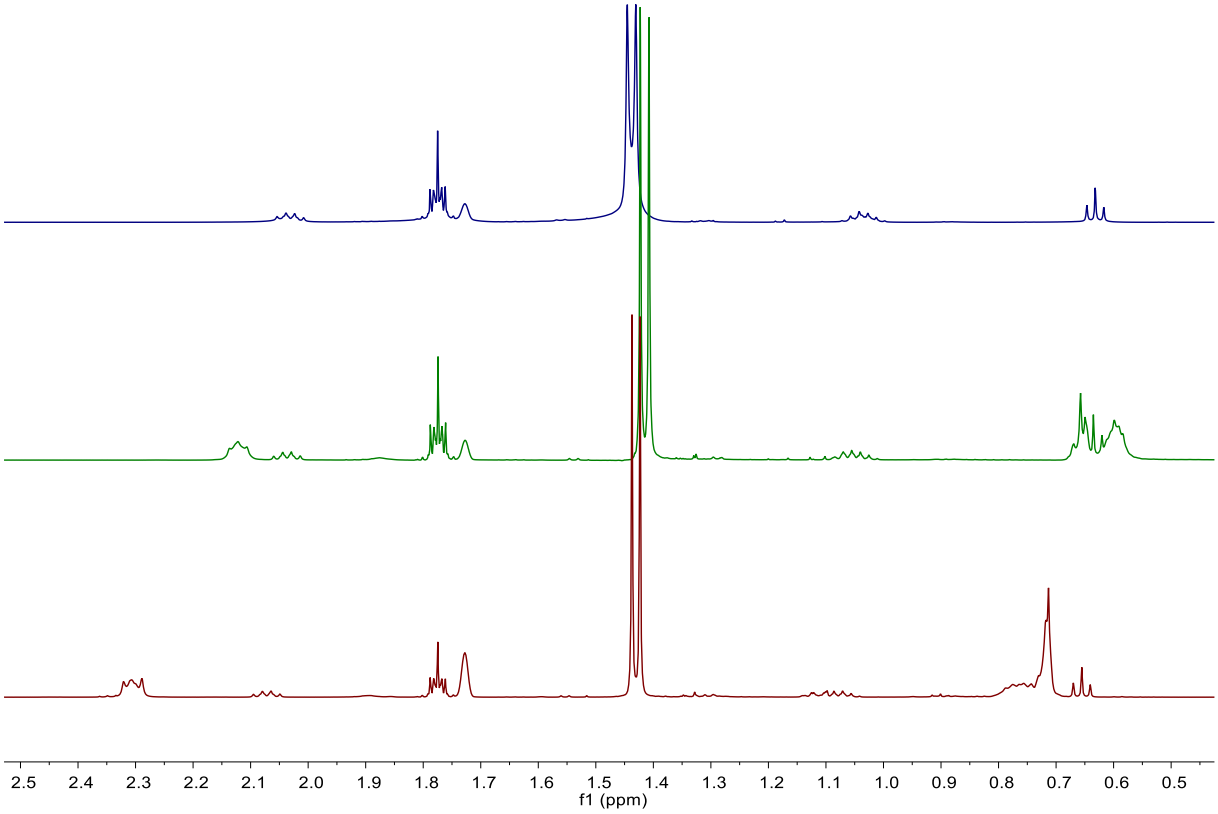

Figure S72: Alkyl regions of the ^{1}H NMR spectra (500.2 MHz, [D_8]THF) corresponding to Na[**9**] (blue, top), [*n*Bu_4N]$_x$[Na]$_y$[**9**] (x + y = 1, cf. 1.3.7; green, middle), or [*n*Bu_4N][**9**] (red, bottom).

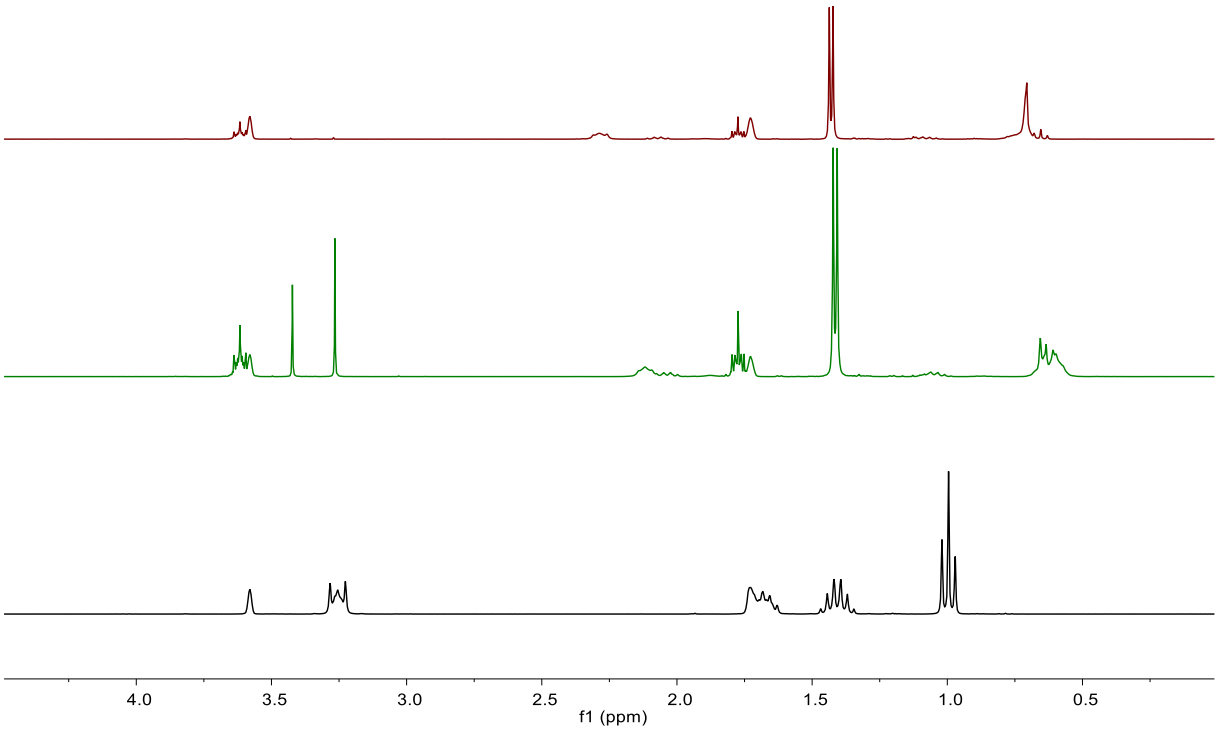

Figure S73: Alkyl regions of the ^{1}H NMR spectra (500.2 MHz, [D_8]THF) corresponding to [*n*Bu_4N][**9**] (red, top), [*n*Bu_4N]$_x$[Na]$_y$[**9**] (x + y = 1, cf. 1.3.7; green, middle), or [*n*Bu_4N][PF_6] (black, bottom).

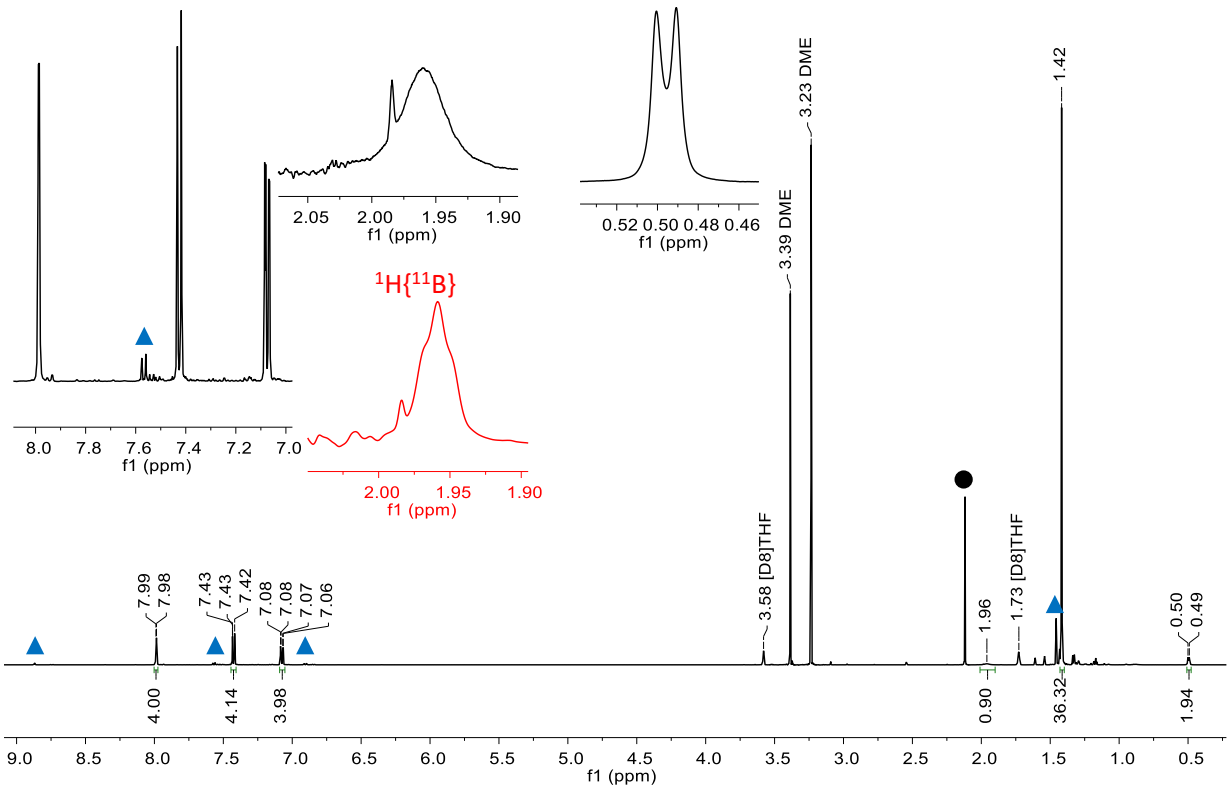

Figure S74: ^{1}H NMR spectrum of the reaction solution of Na_2[**3**] and [Me_4N]Cl recorded three weeks after the compounds were mixed (cf. 1.3.8; 500.2 MHz, [D_8]THF). Marked components: Na_2[**3**] (▲), [Me_4N]Cl (●).

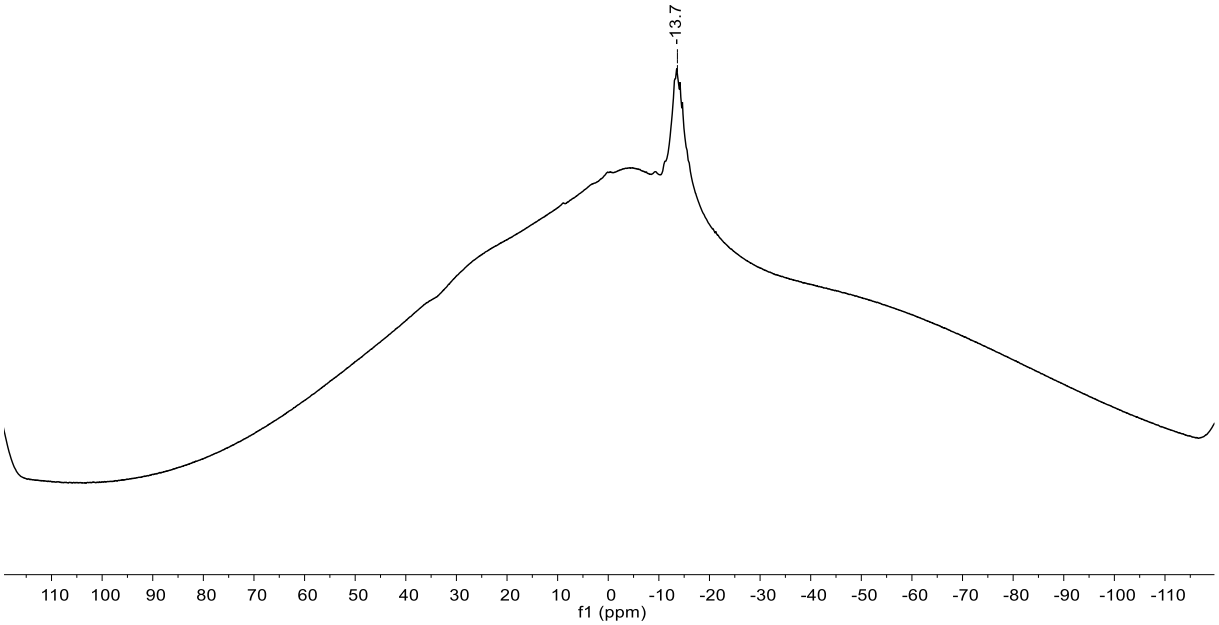

Figure S75: ^{11}B NMR spectrum of the reaction solution of Na_2[**3**] and $[Me_4N]Cl$ recorded three weeks after the compounds were mixed (cf. 1.3.8; 160.5 MHz, $[D_8]$THF).

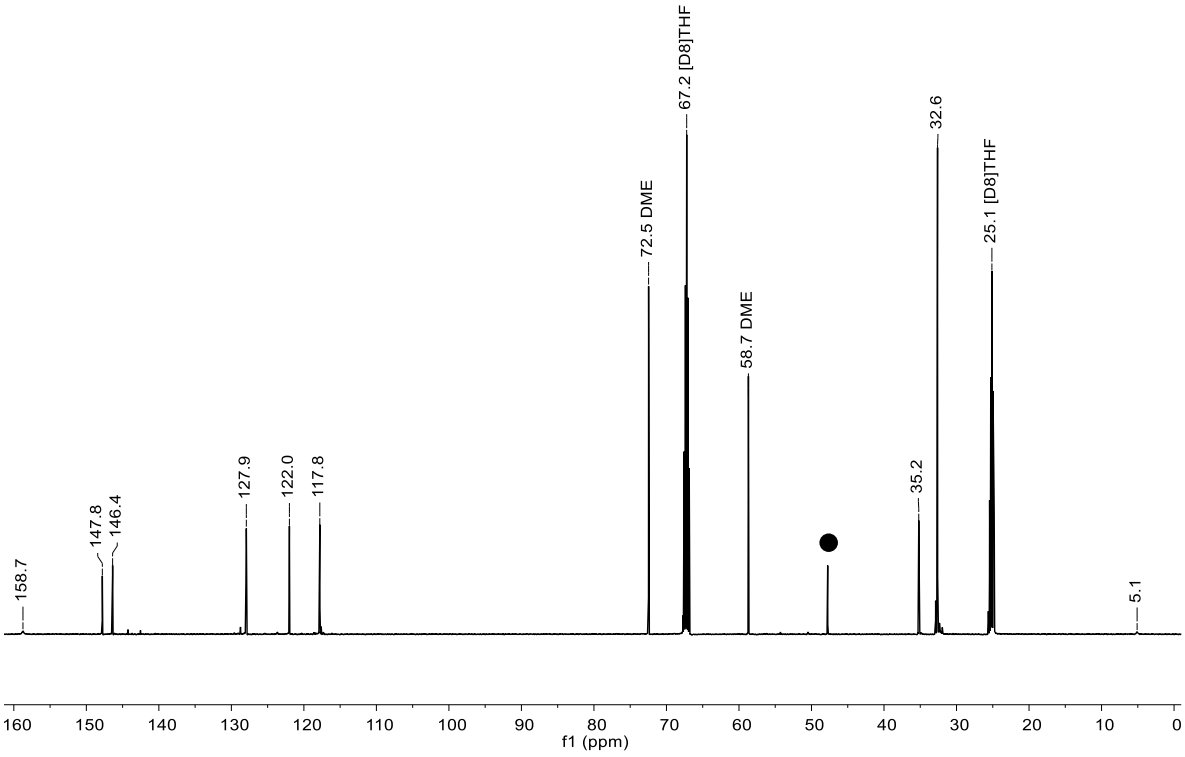

Figure S76: ^{13}C NMR spectrum of the reaction solution of Na_2[**3**] and $[Me_4N]Cl$ recorded three weeks after the compounds were mixed (cf. 1.3.8; 125.8 MHz, $[D_8]$THF). Marked component: $[Me_4N]Cl$ (●).

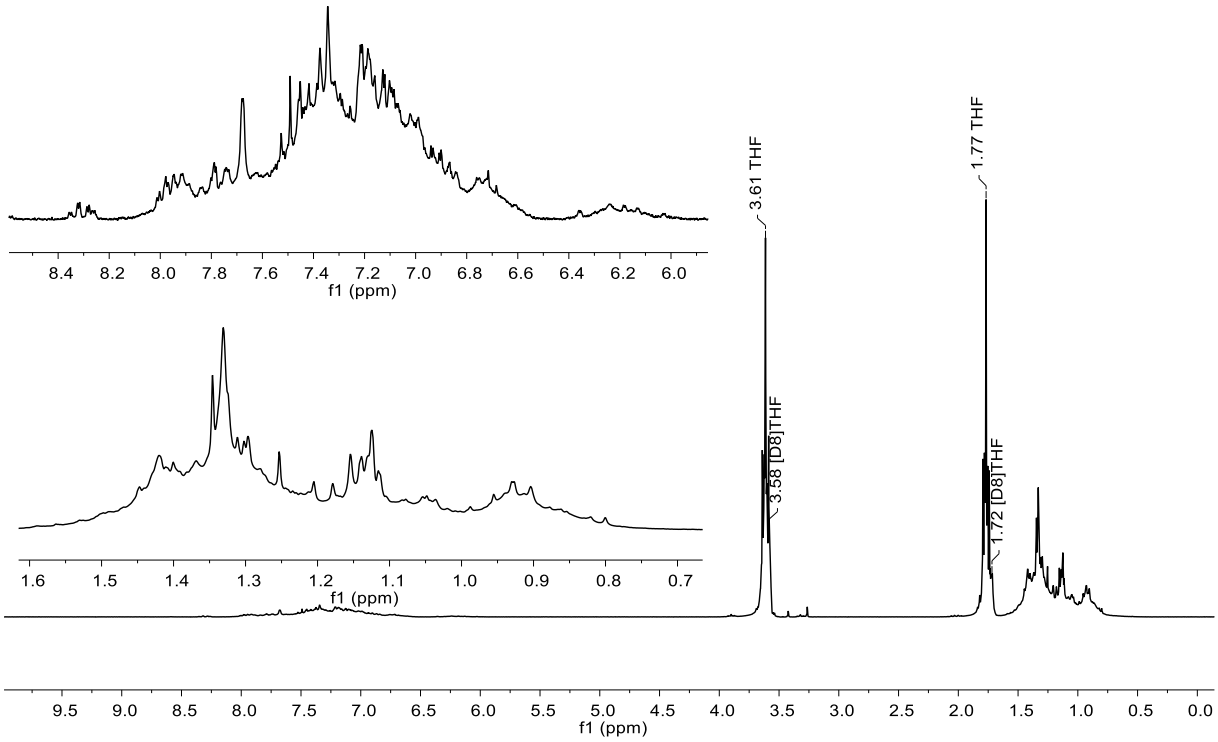

Figure S77: ^{1}H NMR spectrum of the reaction of Li_4[**3**] with dry air immediately after chemiluminescence (250.1 MHz, [D_8]THF).

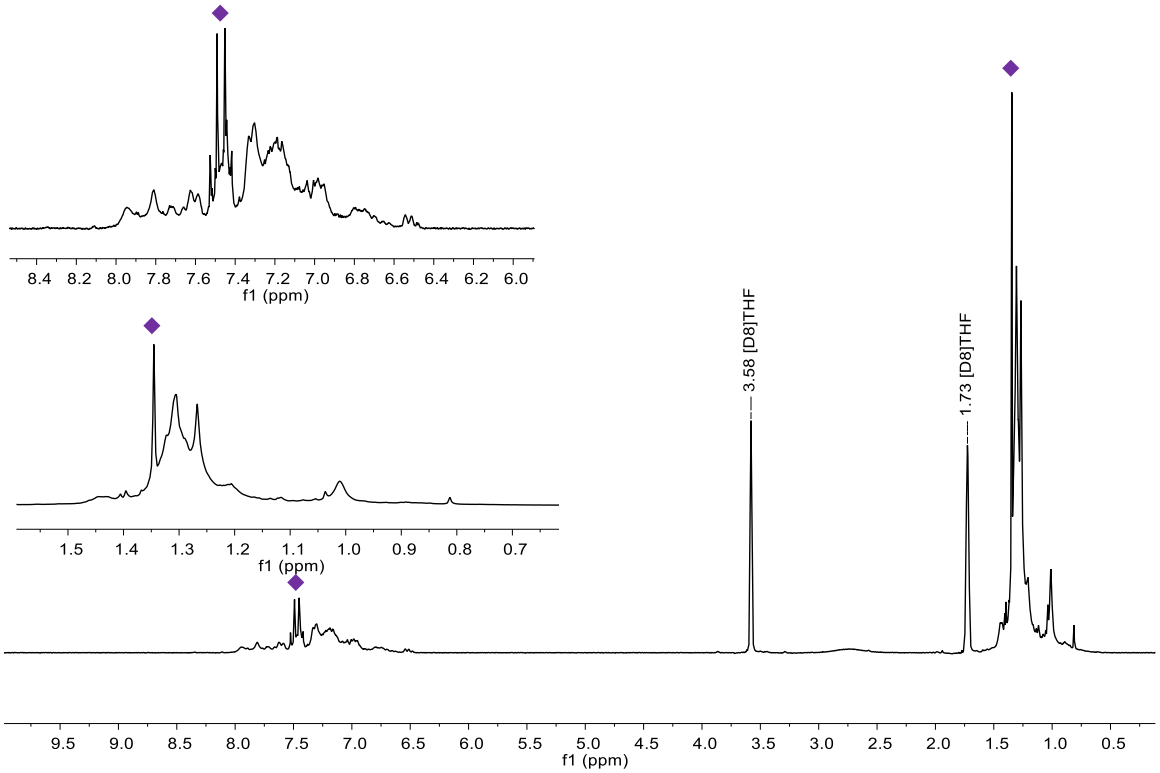

Figure S78: ^{1}H NMR spectrum of the reaction of Li_4[**3**] with dry air after the sample was stored under ambient air for weeks (250.1 MHz, [D_8]THF). Marked compound: 4,4'-di*tert*butyl-1,1'-biphenyl (◆).

3. X-ray crystal structure analyses

Data for all structures were collected on a STOE IPDS II two-circle diffractometer with a Genix Microfocus tube with mirror optics using MoK_α radiation (λ = 0.71073 Å). The data were scaled using the frame-scaling procedure in the *X-AREA* program system.[S11] The structures were solved by direct methods using the program *SHELXS* and refined against F^2 with full-matrix least-squares techniques using the program *SHELXL-97*.[S12]

The crystal of **4** is twinned with a fractional contribution of 0.602(4) for the major domain. There are two crystallographically independent molecules in the asymmetric unit.

In $[Li(thf)_4][\mathbf{5}](THF)_2$, one *tert*-butyl group is disordered over two sets of sites with site occupation factors of 0.610(10) for the major occupied sites. In one thf ligand, four methylene groups are disordered over two sets of sites with site occupation factors of 0.607(12) for the major occupied sites. In one thf ligand, three methylene groups are disordered over two sets of sites with site occupation factors of 0.556(12) for the major occupied sites. In one thf ligand, two methylene groups are disordered over two sets of sites with site occupation factors of 0.62(3) for the major occupied sites. In one of the non-coordinating THF molecules two methylene groups are disordered over two sets of sites with site occupation factors of 0.59(3) for the major occupied sites. Equivalent bond lengths and angles in the thf ligand with four disordered methylene groups were restrained to be equal. The displacement parameters of the disordered atoms were restrained to an isotropic behavior. A rigid-bond restraint was applied to the displacement parameters of the complex cation.

In $[Li(dme)_3][\mathbf{5}](DME)$ the displacement parameters of all dme/DME ligands/molecules were restrained to an isotropic behavior. The non-coordinating DME molecule is disordered about a two-fold rotation axis with equal site occupation factors. Due to the absence of anomalous scatterers, the absolute structure could not be determined reliably (Flack-x-parameter 0.1(5)).

In $[Li(dme)_{1.5}]_2$[**4**OMe]$_2$, one *tert*-butyl group is disordered over two sets of sites with site occupation factors of 0.548(8) for the major occupied sites. The dme ligand connecting two Li cations is located on a center of inversion.

The crystal of $[Na(dme)_2]_2$[**3**] is twinned with a fractional contribution of 0.5040(17) for the major domain. In one dme ligand, the methylene groups are disordered over two positions with a site occupation factor of 0.77(3) for the major occupied sites. The displacement parameters of the disordered atoms were restrained to an isotropic behavior. Bond lengths and angles of the disordered dme ligand were restrained to be similar to those of a non-disordered dme ligand.

In [Na(dme)(thf)][Na(thf)$_3$·thf][**3**], one Na^+ cation is disordered over two sets of sites with a site occupation factor of 0.667(5) for the major occupied site. The dme ligand is located on a center of inversion. One *tert*-butyl group is disordered over two positions with a site occupation factor of 0.611(12) for the major occupied sites. The displacement parameters of the disordered methyl groups were restrained to an isotropic behavior. In one thf ligand, two methylene groups are disordered over two positions with a site occupation factor of 0.613(18) for the major occupied sites. A rigid-bond restraint was applied to the displacement parameters of the thf ligands. The contribution of co-crystallized solvent molecules was suppressed using the *SQUEEZE* routine in *PLATON*.[S13]

In $\{[Na(thf)(dme)_{0.5}]_2[Na(thf)]_{0.5}[Na]_{1.5}$[**3**]$\}_2$, two Na^+ cations are disordered about a two-fold rotation axis over two equally occupied positions. One thf ligand is disordered about a two-fold rotation axis over two equally occupied positions. In one thf ligand, all four methylene groups are disordered over two positions with a site occupation factor of 0.51(4) for the major occupied sites.

In one thf ligand, the C−O bonds were restrained to 1.40(1) Å, the C−C bonds were restrained to 1.50(1) Å, and 1,3-distances were restrained to 2.30(1)Å.

In one dme ligand, the methyl groups are disordered over two positions with site occupation factors of 0.61(5) and 0.80(5) for the major occupied sites.

The contribution of co-crystallized solvent molecules was suppressed using the *SQUEEZE* routine in *PLATON*.[S13] The absolute structure could not be determined reliably (Flack-x-parameter -0.4(2)).

$[Na(thf)_3]_2$[**2**] is located on a center of inversion.

$[Li(dme)]_4$[**3**] is located on a two-fold rotation axis.

$[Li(thf)_2]_2[Li(thf)_{1.5}]_2$[**3**] is located on a two-fold rotation axis. One methylene group of a thf ligand is disordered over two sets of sites with a site occupation factor of 0.51(3) for the major occupied site. The displacement parameters of the disordered atoms and of Li1 and C42 were restrained to an isotropic behavior.

$[Li(dme)]_2[Li(dme)_{1.5}]_2$[**7**] is located on a center of inversion. One methylene group of one dme ligand is disordered over two sets of sites with a site occupation factor of 0.835(9) for the major occupied site. Equivalent C−O/C−C bond lengths and C−C−O bond angles in the disordered dme ligand were restrained to be equal.

In $[Li(Et_2O)][Li(thf)]_2[Li(thf)(Et_2O)]$[**6**], three methylene groups in one thf ligand are disordered over two sets of sites with site occupation factors of 0.563(11) for the major occupied sites. Bond lengths and angles in the disordered thf ligand were restrained to be equal to those of a non-disordered thf ligand. In one Et_2O ligand, all C and H atoms are disordered over two sets of sites with site occupation factors of 0.582(14) for the major occupied sites. The displacement parameters of the disordered atoms were restrained to an isotropic behavior.

In $[Na(thf)_6]$[**9**], one *tert*-butyl group is disordered over two sets of sites with site occupation factors of 0.665(14) for the major occupied sites. Bond lengths and angles of the disordered *tert*-butyl group were restrained to be similar to those of a non-disordered *tert*-butyl group. In one thf ligand, three methylene groups are disordered over two sets of sites with site

occupation factors of 0.53(3) for the major occupied sites. In one thf ligand, two methylene groups are disordered over two sets of sites with site occupation factors of 0.64(3) for the major occupied sites. The displacement parameters of the disordered atoms were restrained to an isotropic behavior. The H atom bonded to B was isotropically refined. Due to the absence of anomalous scatterers, the absolute structure could not be determined reliably (Flack-x-parameter 0.0(6)).

The adduct 9-bromo-9-borafluorene·thf requires no special comments.

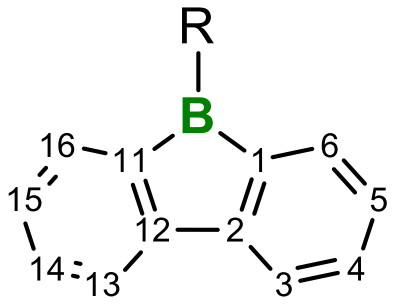

Figure S79: Numbering scheme used for the assignment of B–C and C–C bond lengths and bond angles unless otherwise indicated.

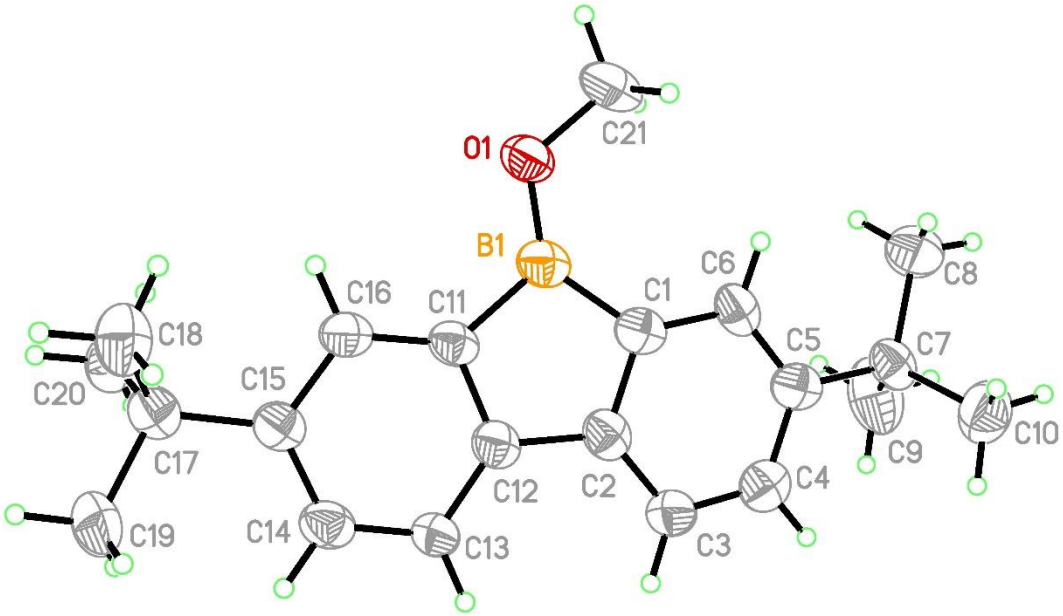

Figure S80: Molecular structure of **4** in the solid state. The two crystallographically independent molecules, $\mathbf{4}_A$ and $\mathbf{4}_B$, possess similar bond lengths and angles within the experimental error margins. We therefore give only the data of $\mathbf{4}_A$. Displacement ellipsoids are drawn at the 50% probability level. Selected bond lengths (Å) and bond angles (°): B1–O1 = 1.356(10), B1–C1 = 1.570(11), B1–C11 = 1.555(10), C1–C2 = 1.409(10), C11–C12 = 1.406(10), C2–C12 = 1.495(10); O1–B1–C1 = 132.0(7), O1–B1–C11 = 121.9(7), C1–B1–C11 = 106.0(6).

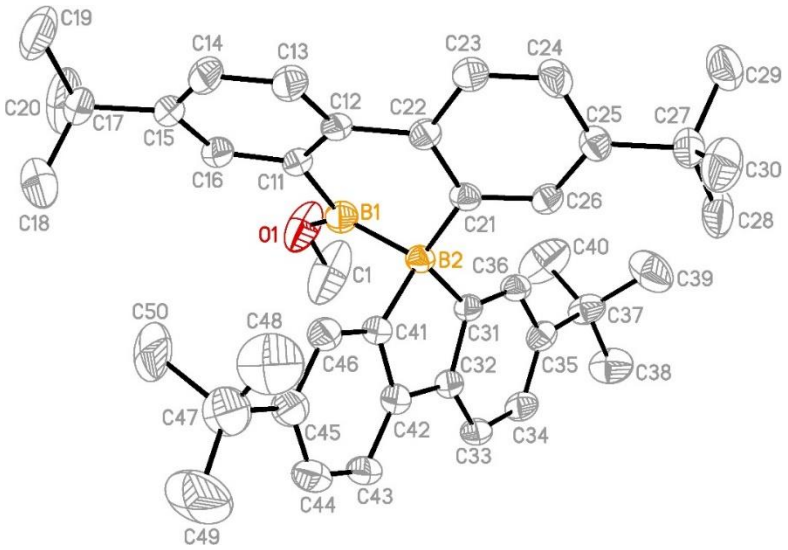

Figure S81: Molecular structure of [**5**]$^-$ in [Li(thf)$_4$][**5**](THF)$_2$ in the solid state. Displacement ellipsoids are drawn at the 50% probability level, hydrogen atoms are omitted for clarity. Selected bond lengths (Å) and bond angles (°): B1–B2 = 1.696(5), B1–O1 = 1.375(4), B1–C11 = 1.582(4), B2–C21 = 1.619(4), B2–C31 = 1.615(4), B2–C41 = 1.639(4); O1–B1–B2 = 132.8(3), O1–B1–C11 = 112.3(3), C11–B1–B2 = 114.3(3), C21–B2–C31 = 118.5(2), C21–B2–C41 = 114.7(2), C21–B2–B1 = 107.6(2), C31–B2–B1 = 118.2(2), C41–B2–B1 = 97.0(2), C31–B2–C41 = 98.6(2).

In the solid state, one [**5**]$^-$ unit is adjoined by one [Li(thf)$_4$]$^+$ ion and one THF molecule, another THF molecule is located next to the [Li(thf)$_4$]$^+$ unit. The chiral [**5**]$^-$ units form a racemic mixture.

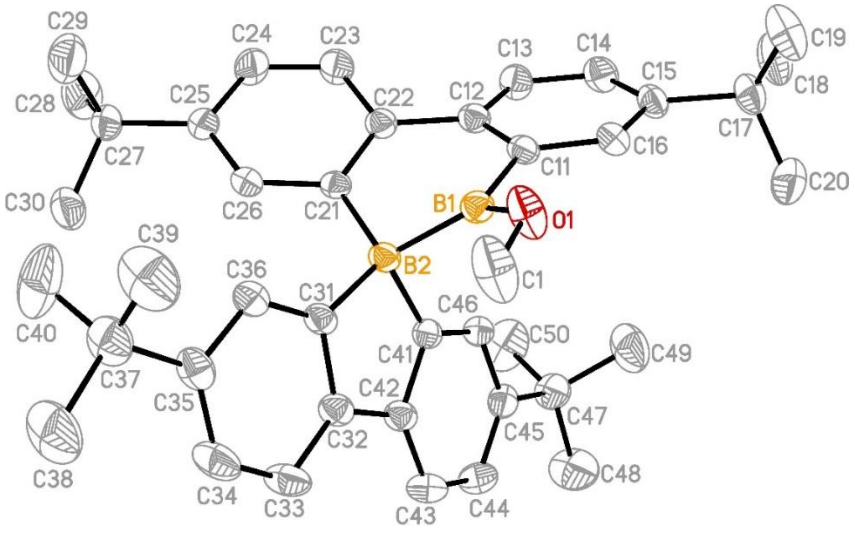

Figure S82: Molecular structure of [**5**]$^-$ in [Li(dme)$_3$][**5**](DME) in the solid state. Displacement ellipsoids are drawn at the 50% probability level, hydrogen atoms are omitted for clarity. Selected bond lengths (Å) and bond angles (°): B1–B2 = 1.703(4), B1–O1 = 1.374(3), B1–C11 = 1.584(3), B2–C21 = 1.627(3), B2–C31 = 1.619(3), B2–C41 = 1.647(3); O1–B1–B2 = 133.0(2), O1–B1–C11 = 113.0(2), C11–B1–B2 = 113.7(2), C21–B2–C31 = 115.61(19), C21–B2–C41 = 114.04(19), C21–B2–B1 = 105.64(18), C31–B2–B1 = 121.26(19), C41–B2–B1 = 101.10(18), C31–B2–C41 = 98.26(17).

In the solid state, one [**5**]$^-$ unit is adjoined by one [Li(dme)$_3$]$^+$ ion and one non-coordinating DME molecule.

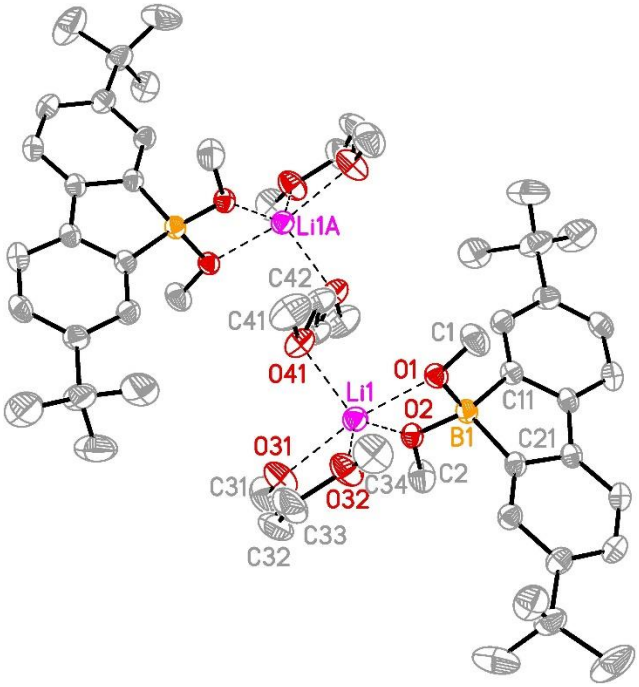

Figure S83: *Description of the solid-state structure of {[Li(dme)$_{1.5}$][**4**OMe]}$_2$*: In the solid state, two contact-ion pairs [Li(dme)][**4**OMe] are bridged by one dme ligand that is located on a center of inversion. In each ion pair, the [**4**OMe]$^-$ anion is acting as a chelating ligand toward its Li1$^+$ counter cation *via* O1 and O2. Li1$^+$ is also coordinated by one chelating dme ligand, rendering it a pentacoordinated cation. Displacement ellipsoids are drawn at the 50% probability level, hydrogen atoms are omitted for clarity. Selected bond lengths (Å) and bond angles (°): B1–O1 = 1.487(3), B1–O2 = 1.487(3), B1–C11 = 1.650(4), B1–C21 = 1.638(4); O1–B1–O2 = 98.88(19), O1–B1–C11 = 115.7(2), O1–B1–C21 = 115.6(2), O2–B1–C11 = 115.6(2), O2–B1–C21 = 113.5(2), C11–B1–C21 = 98.50(19).

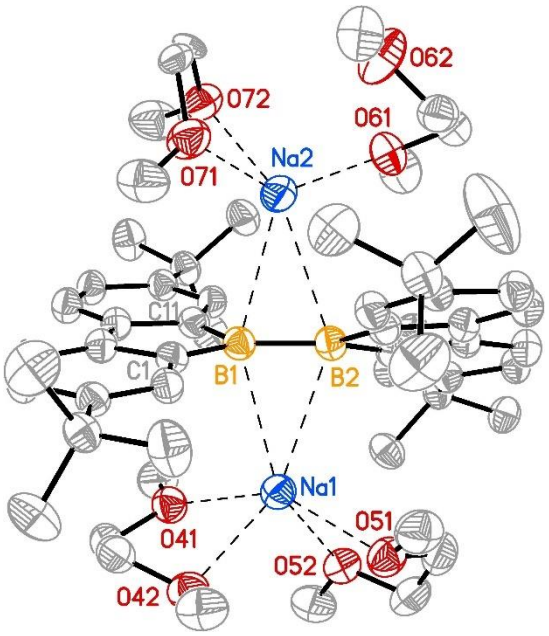

Figure S84: Molecular structure of $[Na(dme)_2]_2$[**3**] in the solid state. Displacement ellipsoids are drawn at the 30% probability level, hydrogen atoms are omitted for clarity. Selected bond lengths (Å), bond angles (°), and dihedral angle (°): B1–B2 = 1.637(7), B1–C1 = 1.575(6), B1–C11 = 1.593(7), B2–C21 = 1.609(7), B2–C31 = 1.584(7), Na1–B1 = 2.796(6), Na1–B2 = 2.902(5), Na2–B1 = 2.744(5), Na2–B2 = 2.791(6), C1–C2 = 1.431(6), C2–C12 = 1.450(6), C11–C12 = 1.435(6), C1–C6 = 1.415(6), C2–C3 = 1.394(6), C3–C4 = 1.368(7), C4–C5 = 1.415(6), C5–C6 = 1.402(6), C11–C16 = 1.412(6), C12–C13 = 1.388(6), C13–C14 = 1.382(7), C14–C15 = 1.400(6), C15–C16 = 1.406(6); C1–B1–C11 = 101.5(4), C1–B1–B2 = 130.0(4), C11–B1–B2 = 128.3(4), C21–B2–C31 = 100.9(4), C21–B2–B1 = 130.1(4), C31–B2–B1 = 128.9(4); C1B1C11//C21B2C31 = 25.4(2).

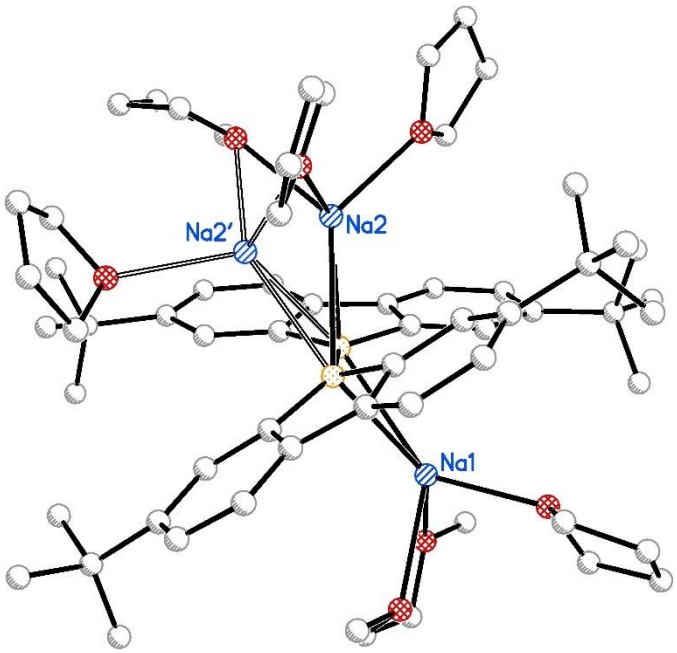

Figure S85: Molecular structure of [Na(dme)(thf)][Na(thf)$_3$·thf][**3**] in the solid state. Na2 is disordered over two sites. The major occupied site (Na2) has a site occupation factor of 0.667(5); Na2' is the minor occupied site.

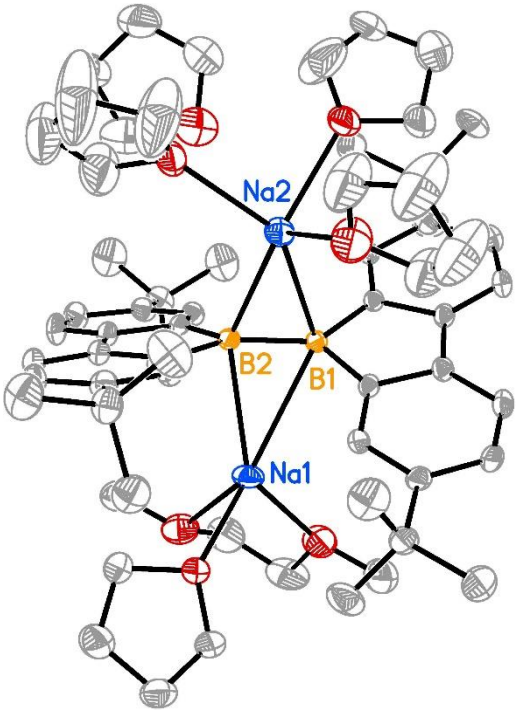

Figure S86: Molecular structure of [Na(dme)(thf)][Na(thf)$_3$·thf][**3**] in the solid state. Displacement ellipsoids are drawn at the 30% probability level, hydrogen atoms are omitted for clarity. Selected bond lengths (Å), bond angles (°), and dihedral angle (°): B1–B2 = 1.637(5), B1–C1 = 1.591(4), B1–C11 = 1.613(4), B2–C21 = 1.596(4), B2–C31 = 1.595(4), Na1–B1 = 2.859(4), Na1–B2 = 2.617(4), Na2–B1 = 2.728(4), Na2–B2 = 2.824(4), Na2'–B1 = 2.896(5), Na2'–B2 = 2.671(5), C1–C2 = 1.433(4), C2–C12 = 1.462(5), C11–C12 = 1.462(4), C1–C6 = 1.413(4), C2–C3 = 1.390(5), C3–C4 = 1.376(5), C4–C5 = 1.402(5), C5–C6 = 1.406(4), C11–C16 = 1.409(5), C12–C13 = 1.390(5), C13–C14 = 1.389(5), C14–C15 = 1.398(5), C15–C16 = 1.399(4); C1–B1–C11 = 100.3(2), C1–B1–B2 = 130.7(3), C11–B1–B2 = 129.0(3), C21–B2–C31 = 100.4(2), C21–B2–B1 = 130.4(3), C31–B2–B1 = 129.1(3); C1B1C11//C21B2C31 = 25.6(4).

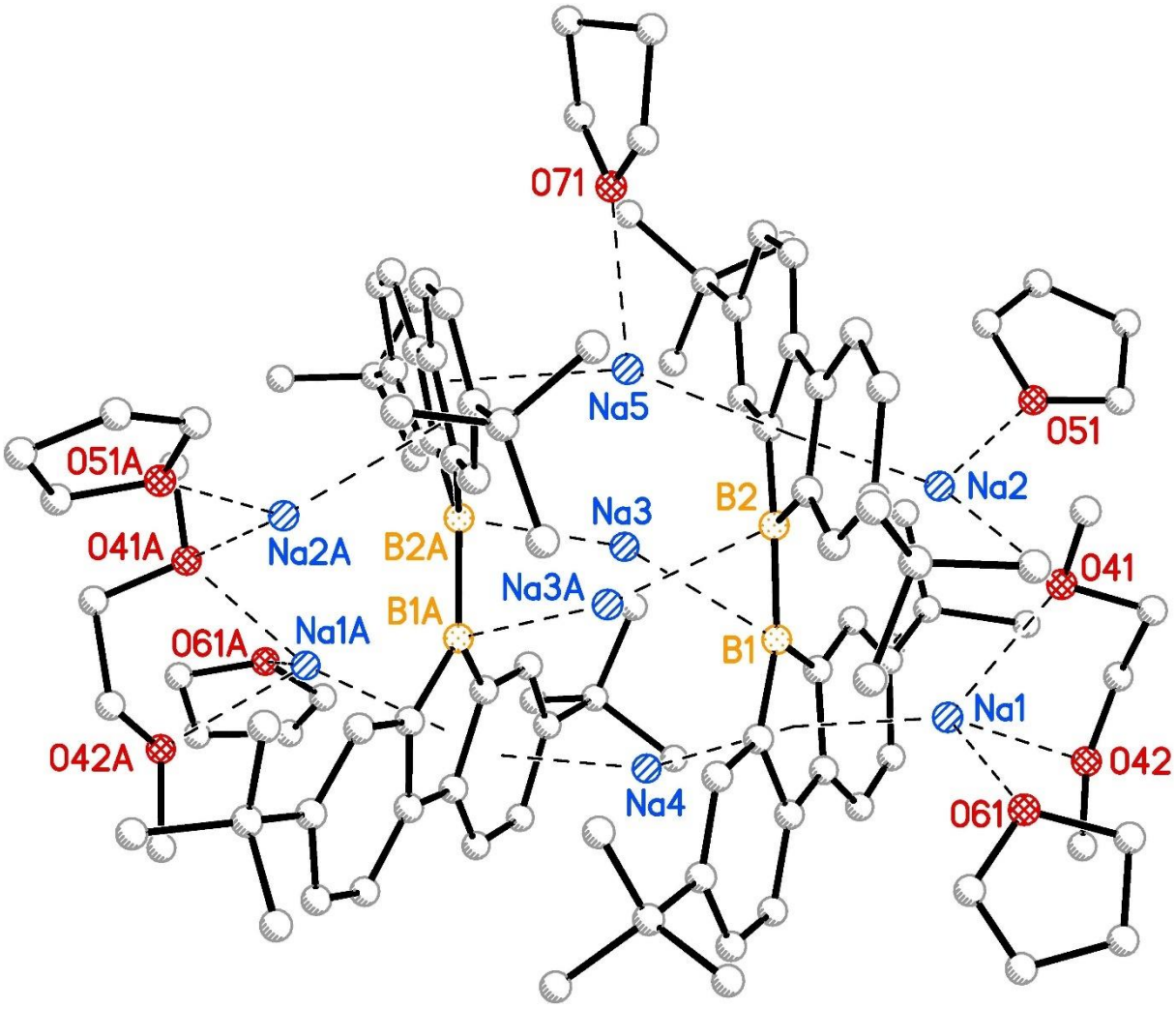

Figure S87: Structure of $\{[Na(thf)(dme)_{0.5}]_2[Na(thf)]_{0.5}[Na]_{1.5}[\mathbf{3}]\}_2$ in the solid state, which serves as a proof for the constitution of the tetraanion $[\mathbf{3}]^{4-}$. $C_2B1//B2C_2$ = 41.0(4)°.

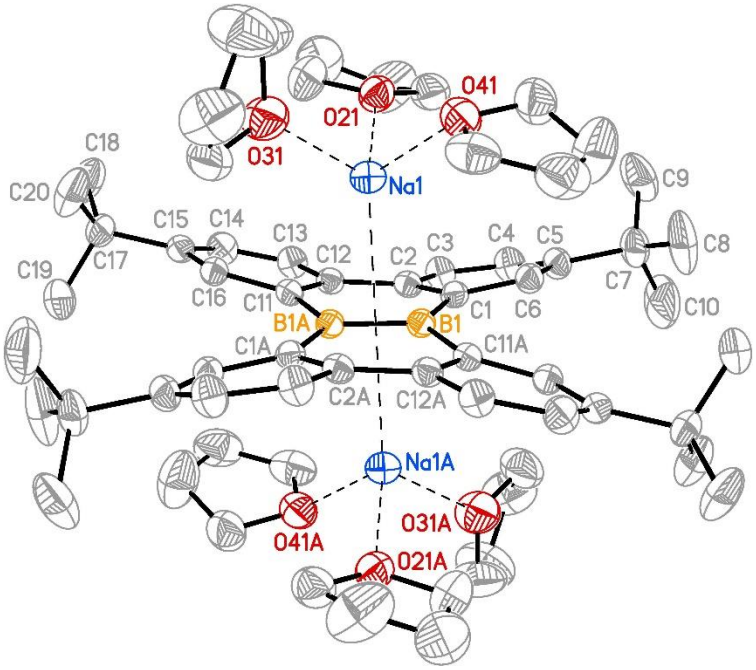

Figure S88: Molecular structure of $[Na(thf)_3]_2$[**2**] in the solid state. Displacement ellipsoids are drawn at the 50% probability level, hydrogen atoms are omitted for clarity. Selected bond lengths (Å) and bond angles (°): B1–B1A = 1.615(4), B1–C1 = 1.563(2), B1–C11A = 1.564(2), Na1–B1 = 2.745(2), Na1–B1A = 2.673(2); C1–B1–C11A = 126.40(15), C1–B1–B1A = 116.80(19), C11A–B1–B1A = 116.73(18). Symmetry operator for generating equivalent atoms with suffix A: 1–x, 1–y, 1–z.

The $[\mathbf{2}]^{2-}$ dianion possesses a dibenzo[*g,p*]chrysene-type molecular scaffold with central B=B double bond, which is capped by two $[Na(thf)_3]^+$ ions. The crystal structure of the analogous compound $[Li(thf)_3]_2$[**2**] has been reported earlier; the bond lengths and torsion angles of the $[\mathbf{2}]^{2-}$ scaffolds in both salts are very similar.[S5]

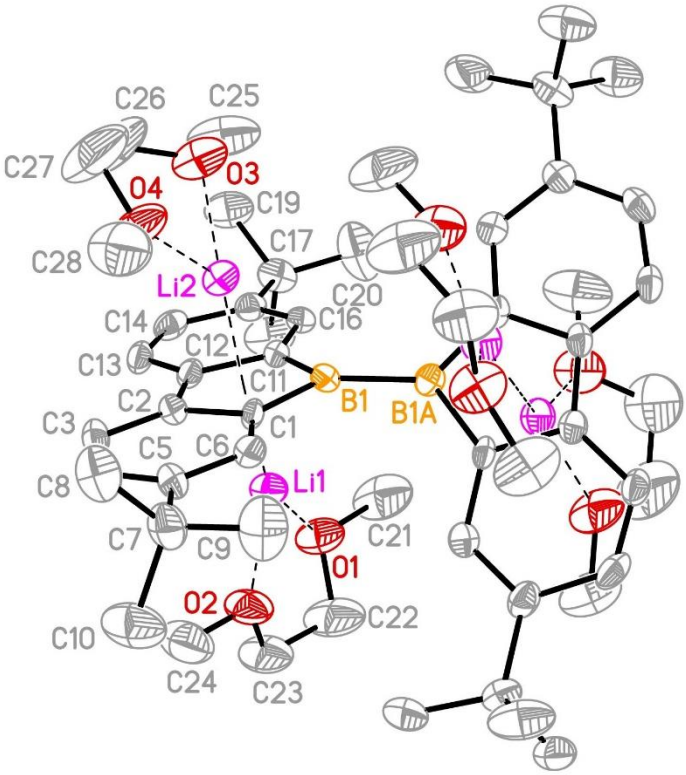

Figure S89: Molecular structure of [Li(dme)]$_4$[**3**] in the solid state. Displacement ellipsoids are drawn at the 50% probability level, hydrogen atoms are omitted for clarity. Selected bond lengths (Å), bond angles (°), and dihedral angle (°): B1–B1A = 1.705(8), B1–C1 = 1.557(5), B1–C11 = 1.541(5), B1–Li1 = 2.278(8), B1–Li2 = 2.352(8), Li1···COG = 1.904(7), Li2···COG = 1.890(7), C1–C2 = 1.466(5), C2–C12 = 1.441(5), C11–C12 = 1.471(5), C1–C6 = 1.444(5), C2–C3 = 1.425(5), C3–C4 = 1.368(5), C4–C5 = 1.451(5), C5–C6 = 1.381(5), C11–C16 = 1.445(5), C12–C13 = 1.426(5), C13–C14 = 1.369(5), C14–C15 = 1.432(5), C15–C16 = 1.374(5); C1–B1–C11 = 100.1(3), C1–B1–B1A = 127.8(2), C11–B1–B1A = 131.7(3); C1B1C11//C1AB1AC11A = 47.0(3). COG = centroid of the respective coordinated C$_4$B ring. Symmetry operator for generating equivalent atoms with suffix A: 1–x, y, –z+3/2.

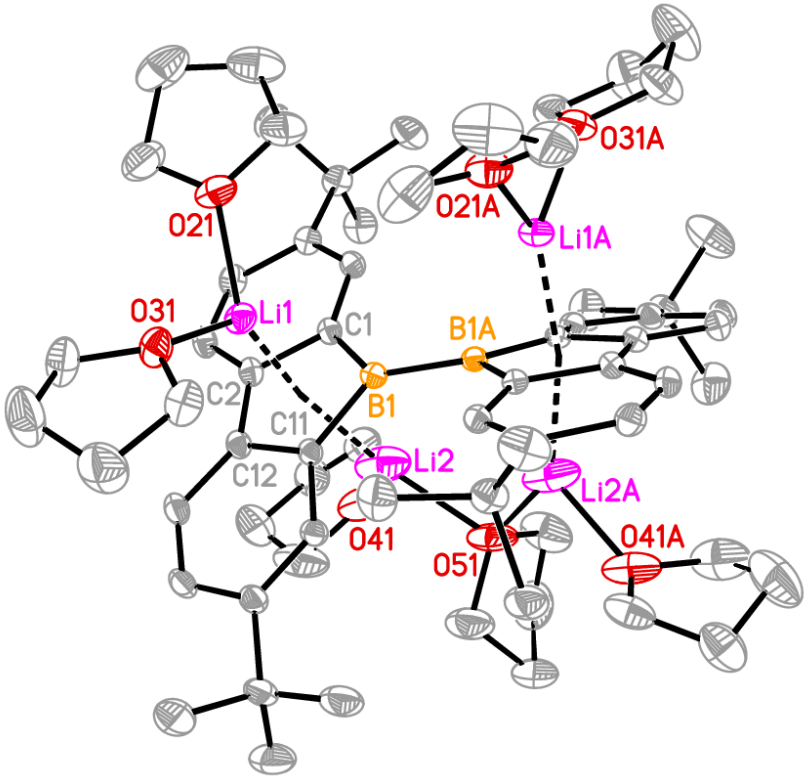

Figure S90: Molecular structure of $[Li(thf)_2]_2[Li(thf)_{1.5}]_2$[**3**] in the solid state. Displacement ellipsoids are drawn at the 30% probability level, hydrogen atoms are omitted for clarity. Selected bond lengths (Å), bond angles (°), and dihedral angle (°): B1–B1A = 1.704(5), B1–C1 = 1.554(4), B1–C11 = 1.560(3), B1–Li1 = 2.325(5), B1–Li2 = 2.193(7), Li1···COG = 1.963(5), Li2···COG = 2.010(7), C1–C2 = 1.464(3), C2–C12 = 1.432(4), C11–C12 = 1.464(3), C1–C6 = 1.435(3), C2–C3 = 1.422(4), C3–C4 = 1.364(4), C4–C5 = 1.439(4), C5–C6 = 1.374(4), C11–C16 = 1.440(3), C12–C13 = 1.416(4), C13–C14 = 1.370(4), C14–C15 = 1.437(4), C15–C16 = 1.380(3); C1–B1–C11 = 99.9(2), C1–B1–B1A = 130.0(3), C11–B1–B1A = 129.0(3); C1B1C11//C1AB1AC11A = 40.33(9). COG = centroid of the respective coordinated C_4B ring. Symmetry operator for generating equivalent atoms with suffix A: 1–x, y, –z+3/2.

The [**3**]$^{4-}$ tetraanion consists of two symmetry-related borafluorenyl moieties that are connected *via* a B–B single bond. Each C_4B ring is coordinated by one $[Li(thf)_2]^+$ ion. One $[(thf)Li(\mu\text{-}thf)Li(thf)]^{2+}$ dication bridges both C_4B rings.

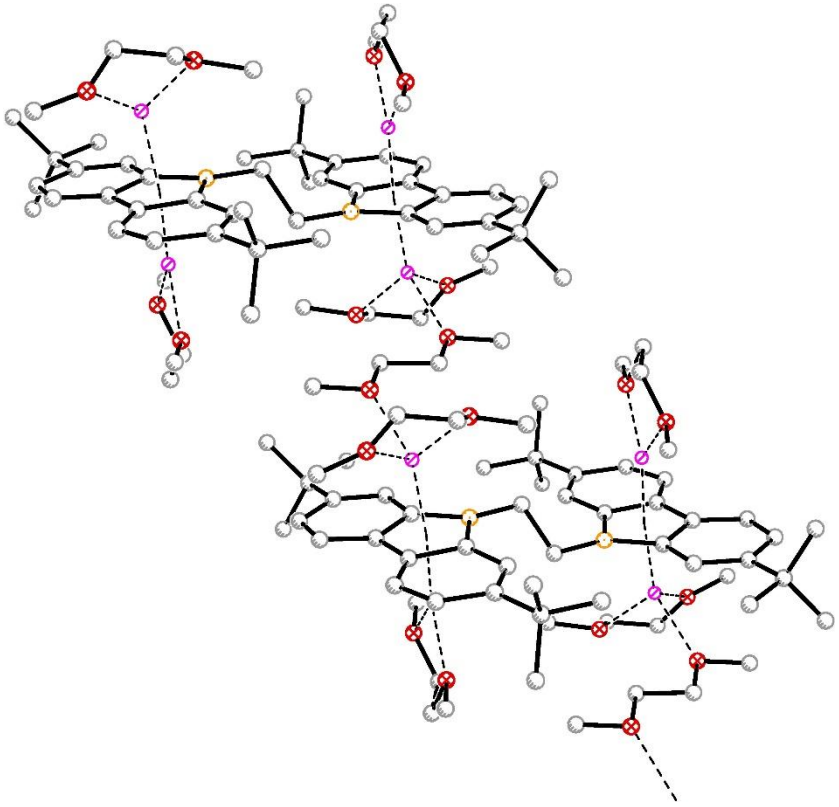

Figure S91: *Description of the polymeric solid-state structure of [Li(dme)]$_2$[Li(dme)$_{1.5}$]$_2$[**7**]:* [**7**]$^{4-}$ consists of two dianionic borafluorenyl moieties that are connected by an ethylene bridge. Each C_4B ring is coordinated by one $[Li(dme)]^+$ cation. From the other side, a $[(dme)Li(\mu\text{-}dme)Li(dme)]^{2+}$ dication connects the C_4B ring with a neighboring [**7**]$^{4-}$ ion to form a coordination polymer.

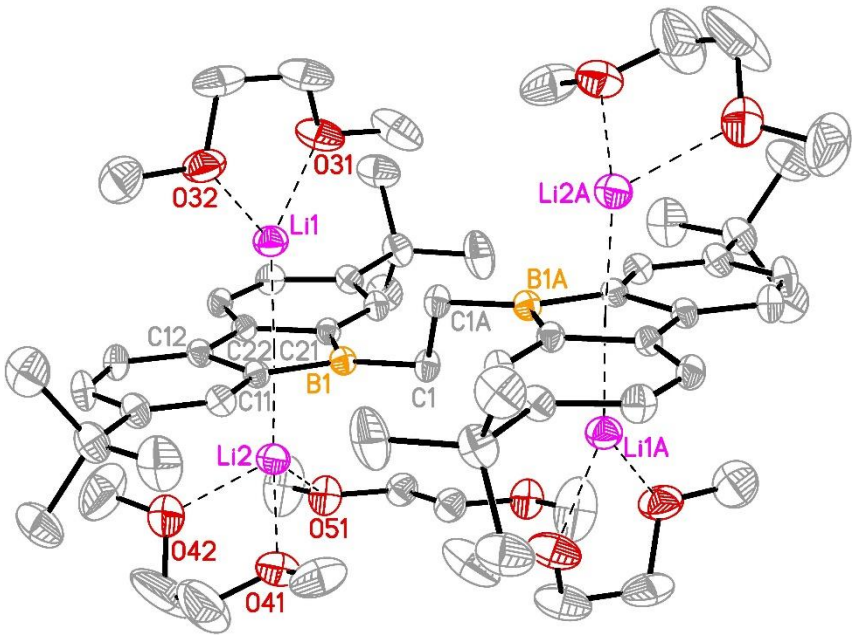

Figure S92: Molecular structure of the monomeric unit of the coordination polymer $[Li(dme)]_2[Li(dme)_{1.5}]_2$[**7**]. Displacement ellipsoids are drawn at the 50% probability level, hydrogen atoms are omitted for clarity. Selected bond lengths (Å) and bond angles (°): B1–C1 = 1.609(2), B1–C11 = 1.536(2), B1–C21 = 1.535(2), Li1–B1 = 2.333(4), Li2–B1 = 2.556(4), Li1···COG = 1.911(4), Li2···COG = 2.085(4), C11–C12 = 1.467(2), C11–C16 = 1.436(2), C12–C13 = 1.416(2), C13–C14 = 1.367(3), C14–C15 = 1.440(3), C15–C16 = 1.371(3), C12–C22 = 1.435(2), C21–C22 = 1.476(2), C21–C26 = 1.431(2), C22–C23 = 1.420(2), C23–C24 = 1.366(3), C24–C25 = 1.441(3), C25–C26 = 1.377(2); C1–B1–C11 = 127.73(15), C1–B1–C21 = 129.48(15), C11–B1–C21 = 102.23(14); COG = centroid of the respective coordinated C_4B ring.

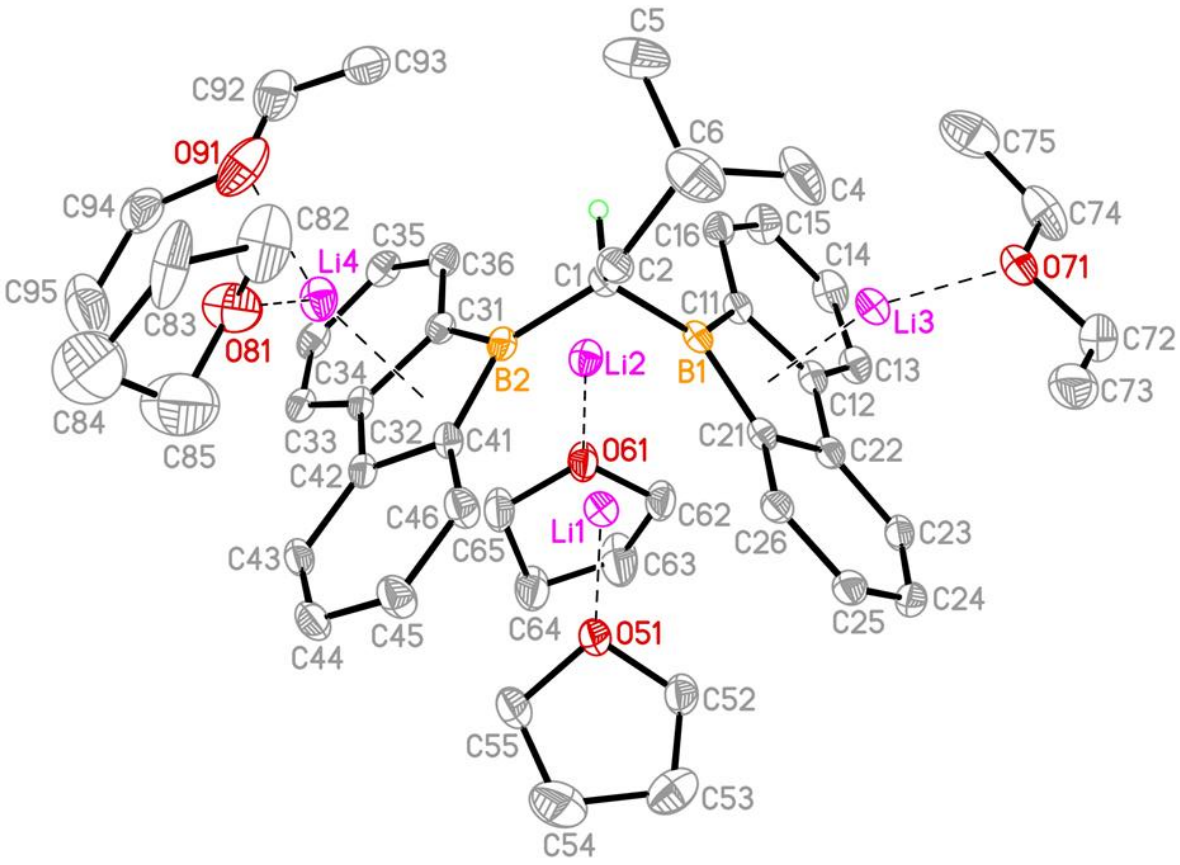

Figure S93: Molecular structure of $[Li(Et_2O)][Li(thf)]_2[Li(thf)(Et_2O)]$[**6**]. Displacement ellipsoids are drawn at the 30% probability level, hydrogen atoms are omitted for clarity. Selected bond lengths (Å) and bond angles (°): B1–C1 = 1.617(4), B1–C11 = 1.549(4), B1–C21 = 1.553(4), B2–C1 = 1.625(4), B2–C31 = 1.541(4), B2–C41 = 1.549(4), B1–Li1 = 2.591(5), B1–Li2 = 2.497(5), B2–Li1 = 2.517(5), B2–Li2 = 2.558(5), Li3···COG = 1.836(5), Li4···COG = 2.005(5), C11–C12 = 1.473(3), C11–C16 = 1.439(4), C12–C13 = 1.414(4), C13–C14 = 1.374(4), C14–C15 = 1.422(4), C15–C16 = 1.376(4), C12–C22 = 1.427(4), C21–C22 = 1.490(3), C21–C26 = 1.448(3), C22–C23 = 1.419(3), C23–C24 = 1.374(4), C24–C25 = 1.420(4), C25–C26 = 1.373(3), C31–C32 = 1.487(3), C31–C36 = 1.438(3), C32–C33 = 1.409(3), C33–C34 = 1.371(4), C34–C35 = 1.419(4), C35–C36 = 1.377(4), C32–C42 = 1.426(4), C41–C42 = 1.480(3), C41–C46 = 1.436(4), C42–C43 = 1.415(3), C43–C44 = 1.375(4), C44–C45 = 1.421(4), C45–C46 = 1.374(4); C1–B1–C11 = 126.9(2), C1–B1–C21 = 131.3(2), C11–B1–C21 = 101.7(2), C1–B2–C31 = 128.4(2), C1–B2–C41 = 129.1(2), C31–B2–C41 = 102.4(2); COG = centroid of the respective coordinated C_4B ring.

The $[\mathbf{6}]^{4-}$ tetraanion consist of two dianionic borafluorenyl moieties that are connected by a C_1 bridge. The peripheral sides of the C_4B rings are coordinated by one $[Li(thf)(Et_2O)]^+$ ion and one $[Li(Et_2O)]^+$ ion. Two $[Li(thf)]^+$ ions are located in the void space between the borafluorenyl fragments.

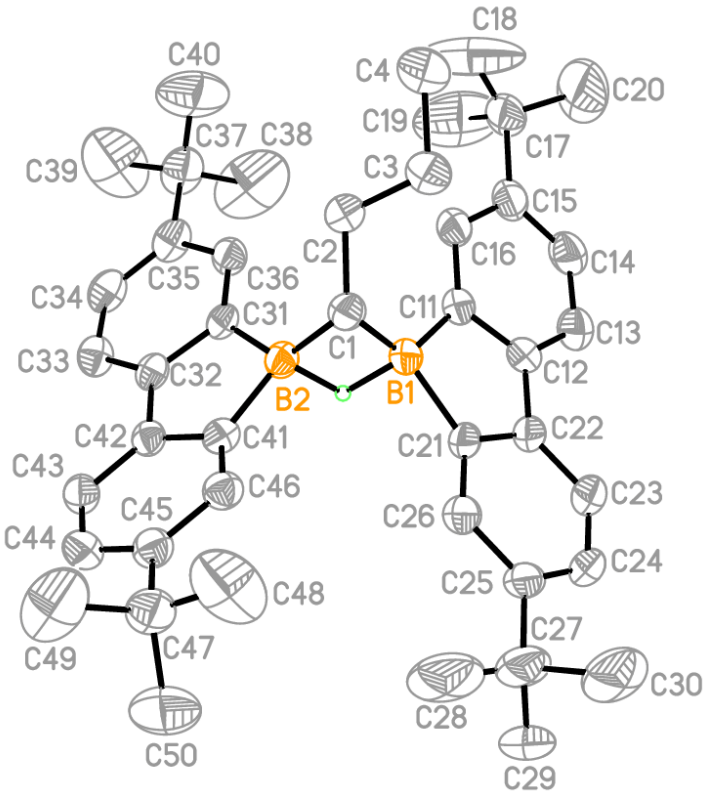

Figure S94: Molecular structure of [**9**]$^-$ in [Na(thf)$_6$][**9**] in the solid state. Displacement ellipsoids are drawn at the 50% probability level, hydrogen atoms (except the boron-bonded one = H1) are omitted for clarity. Selected bond lengths (Å) and bond angles (°): B1–C1 = 1.588(7), B1–C11 = 1.628(7), B1–C21 = 1.622(7), B1···B2 = 1.961(7), B1–H1 = 1.37(6), B2–C1 = 1.606(7), B2–C31 = 1.631(6), B2–C41 = 1.609(7), B2–H1 = 1.38(6); C1–B1–C11 = 124.1(4), C1–B1–C21 = 127.7(4), C11–B1–C21 = 100.1(4), C1–B1–B2 = 52.6(3), C11–B1–B2 = 125.9(4), C1–B1–H1 = 97(2), C11–B1–H1 = 104(2), C21–B1–H1 = 97(2), B2–B1–H1 = 45(2), C1–B2–C31 = 129.8(4), C1–B2–C41 = 119.5(4), C31–B2–C41 = 100.1(3), C1–B2–H1 = 96(2), C31–B2–H1 = 99(2), C41–B2–H1 = 109(2).

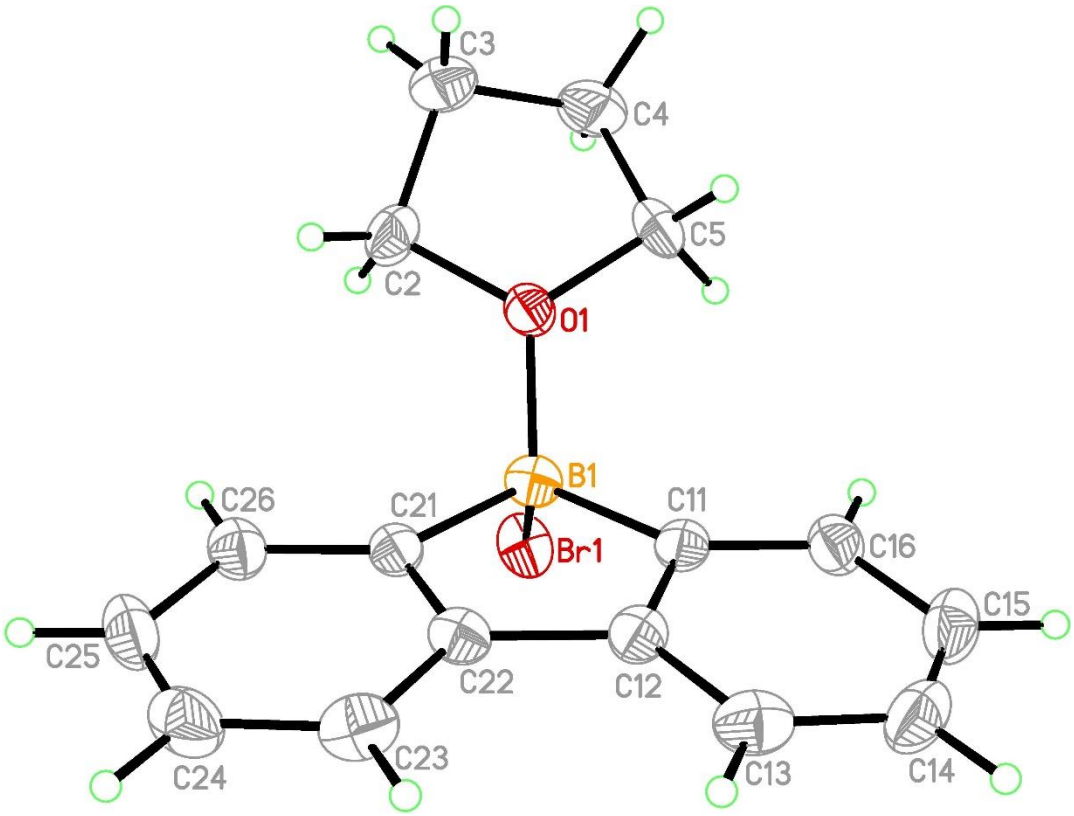

Figure S95: Molecular structure of the adduct 9-bromo-9-borafluorene·thf in the solid state. Displacement ellipsoids are drawn at the 50% probability level. Selected bond lengths (Å) and bond angles (°):B1–O1 = 1.544(5), B1–Br1 = 2.074(4), B1–C11 = 1.601(6), B1–C21 = 1.607(5); Br1–B1–O1 = 106.1(2), Br1–B1–C11 = 112.2(2), Br1–B1–C21 = 113.1(3), O1–B1–C11 = 112.2(3), O1–B1–C21 = 111.3(3), C11–B1–C21 = 102.1(3).

Table S1: Selected crystallographic data for **4** and $[Li(dme)_{1.5}]_2[\mathbf{4}OMe]_2$.

	4	$[Li(dme)_{1.5}]_2[\mathbf{4}OMe]_2$
CCDC number	2085655	2085659
formula	$C_{21}H_{27}BO$	$C_{56}H_{90}B_2Li_2O_{10}$
M_r	306.23	958.77
T (K)	173(2)	173(2)
radiation, λ (Å)	0.71073	0.71073
crystal system	triclinic	monoclinic
space group	P -1	$P\,2_1/n$
a (Å)	6.0433(6)	10.0966(7)
b (Å)	14.0947(17)	19.2209(17)
c (Å)	21.654(2)	15.5627(10)
α (°)	83.705(9)	90
β (°)	89.993(8)	101.712(5)
γ (°)	87.745(9)	90
V (Å^3)	1831.9(3)	2957.3(4)
Z	4	2
D_{calcd} (g cm^{-3})	1.110	1.077
F(000)	664	1044
μ (mm^{-1})	0.065	0.071
crystal size (mm)	0.430 x 0.260 x 0.050	0.290 x 0.290 x 0.260
crystal shape, color	colorless plate	colorless block
reflections collected	22959	11016
independent reflections	22959	5177
R_{int}	-	0.0374
data / restraints / parameters	22959 / 0 / 417	5177 / 36 / 346
R_1, wR_2 ($I > 2\sigma(I)$)	0.1276, 0.2643	0.0741, 0.1554
R_1, wR_2 (all data)	0.2257, 0.3049	0.0929, 0.1649
GOF on F^2	1.191	1.202
Largest difference peak and hole (e Å^{-3})	0.447 and -0.421	0.415 and -0.207

Table S2: Selected crystallographic data for $[Li(thf)_4][\mathbf{5}](THF)_2$ and $[Li(dme)_3][\mathbf{5}](DME)$.

	$[Li(thf)_4][\mathbf{5}](THF)_2$	$[Li(dme)_3][\mathbf{5}](DME)$
CCDC number	2085656	2085657
formula	$C_{65}H_{99}B_2LiO_7$	$C_{57}H_{91}B_2LiO_9$
M_r	1021.00	948.85
T (K)	173(2)	173(2)
radiation, λ (Å)	0.71073	0.71073
crystal system	monoclinic	monoclinic
space group	$P\,2_1/n$	$C\,2$
a (Å)	14.9857(5)	21.8791(7)
b (Å)	22.5034(8)	12.0999(4)
c (Å)	19.1769(6)	22.4269(7)
α (°)	90	90
β (°)	104.595(3)	92.310(3)
γ (°)	90	90
V (Å^3)	6258.3(4)	5932.4(3)
Z	4	4
D_{calcd} (g cm^{-3})	1.084	1.062
F(000)	2232	2072
μ (mm^{-1})	0.067	0.069
crystal size (mm)	0.260 x 0.250 x 0.220	0.270 x 0.270 x 0.220
crystal shape, color	yellow block	orange block
reflections collected	89040	37760
independent reflections	11761	11509
R_{int}	0.0664	0.0275
data / restraints / parameters	11761 / 582 / 807	11509 / 163 / 649
R_1, wR_2 ($I > 2\sigma(I)$)	0.1009, 0.2563	0.0486, 0.1283
R_1, wR_2 (all data)	0.1368, 0.2818	0.0548, 0.1340
GOF on F^2	1.077	1.030
Largest difference peak and hole (e Å^{-3})	0.491 and -0.452	0.356 and -0.236

Table S3: Selected crystallographic data for [Na(thf)(dme)][Na(thf)$_3$·thf][**3**] and [Na(dme)$_2$]$_2$[**3**].

	[Na(thf)(dme)][Na(thf)$_3$·thf][**3**]	[Na(dme)$_2$]$_2$[**3**]
CCDC number	2085662	2085660
formula	$C_{64}H_{98}B_2Na_2O_7$	$C_{56}H_{88}B_2Na_2O_8$
M_r	1047.02	956.86
T (K)	173(2)	173(2)
radiation, λ (Å)	0.71073	0.71073
crystal system	triclinic	monoclinic
space group	P -1	$P\,2_1/n$
a (Å)	13.6323(6)	12.5181(8)
b (Å)	14.3838(7)	19.8592(10)
c (Å)	18.1022(8)	23.0238(17)
α (°)	76.320(4)	90
β (°)	88.421(4)	91.862(6)
γ (°)	70.257(4)	90
V (Å^3)	3240.8(3)	5720.7(6)
Z	2	4
D_{calcd} (g cm^{-3})	1.073	1.111
F(000)	1140	2080
μ (mm^{-1})	0.078	0.084
crystal size (mm)	0.290 x 0.290 x 0.270	0.260 x 0.260 x 0.230
crystal shape, color	red-black block	black block
reflections collected	41751	41497
independent reflections	12148	41497
R_{int}	0.0392	-
data / restraints / parameters	12148 / 177 / 733	41497 / 76 / 633
R_1, wR_2 ($I > 2\sigma(I)$)	0.1054, 0.2852	0.0811, 0.2008
R_1, wR_2 (all data)	0.1331, 0.3115	0.1212, 0.2498
GOF on F^2	1.058	1.036
Largest difference peak and hole (e Å^{-3})	0.814 and -0.491	0.241 and -0.234

Table S4: Selected crystallographic data for $[Na(thf)_3]_2$[**2**] and $\{[Na(thf)(dme)_{0.5}]_2[Na(thf)]_{0.5}[Na]_{1.5}$[**3**]$\}_2$.

	$[Na(thf)_3]_2$[**2**]	$\{[Na(thf)(dme)_{0.5}]_2[Na(thf)]_{0.5}[Na]_{1.5}$[**3**]$\}_2$
CCDC number	2085661	2085658
formula	$C_{64}H_{96}B_2Na_2O_6$	$C_{54}H_{78}B_2Na_4O_{4.50}$
M_r	1029.00	912.74
T (K)	173(2)	173(2)
radiation, λ (Å)	0.71073	0.71073
crystal system	monoclinic	orthorhombic
space group	$P\,2_1/c$	$C\,2\,2\,2_1$
a (Å)	10.5707(4)	21.9750(6)
b (Å)	25.0543(9)	22.3849(8)
c (Å)	11.7196(4)	22.5439(8)
α (°)	90	90
β (°)	97.699(3)	90
γ (°)	90	90
V (Å^3)	3075.86(19)	11089.5(6)
Z	2	8
D_{calcd} (g cm^{-3})	1.111	1.093
F(000)	1120	3936
μ (mm^{-1})	0.080	0.093
crystal size (mm)	0.260 x 0.250 x 0.250	0.220 x 0.210 x 0.190
crystal shape, color	red block	black block
reflections collected	27634	66720
independent reflections	5659	10425
R_{int}	0.0386	0.0448
data / restraints / parameters	5659 / 0 / 334	10425 / 5 / 580
R_1, wR_2 ($I > 2\sigma(I)$)	0.0607, 0.1566	0.1424, 0.3830
R_1, wR_2 (all data)	0.0696, 0.1654	0.1683, 0.4111
GOF on F^2	1.022	1.908
Largest difference peak and hole (e Å^{-3})	0.455 and -0.334	1.467 and -1.621

Table S5: Selected crystallographic data for $[Li(thf)_2]_2[Li(thf)_{1.5}]_2$[**3**] and $[Li(dme)]_4$[**3**].

	$[Li(thf)_2]_2[Li(thf)_{1.5}]_2$[**3**]	$[Li(dme)]_4$[**3**]
CCDC number	2085652	2085651
formula	$C_{68}H_{104}B_2Li_4O_7$	$C_{56}H_{88}B_2Li_4O_8$
M_r	1082.89	938.64
T (K)	173(2)	173(2)
radiation, λ (Å)	0.71073	0.71073
crystal system	orthorhombic	monoclinic
space group	*P b c n*	*C* 2/*c*
a (Å)	14.5844(4)	22.502(3)
b (Å)	20.0136(7)	13.8076(16)
c (Å)	22.2645(7)	22.056(4)
α (°)	90	90
β (°)	90	119.826(11)
γ (°)	90	90
V (Å^3)	6498.7(4)	5945.0(16)
Z	4	4
D_{calcd} (g cm^{-3})	1.107	1.049
F(000)	2360	2040
μ (mm^{-1})	0.068	0.066
crystal size (mm)	0.290 x 0.280 x 0.260	0.190 x 0.110 x 0.100
crystal shape, color	black block	black block
reflections collected	61578	19966
independent reflections	5755	5242
R_{int}	0.0705	0.1242
data / restraints / parameters	5755 / 24 / 376	5242 / 0 / 316
R_1, wR_2 ($I > 2\sigma(I)$)	0.0806, 0.1836	0.0825, 0.1344
R_1, wR_2 (all data)	0.1015, 0.1950	0.1842, 0.1674
GOF on F^2	1.126	0.949
Largest difference peak and hole (e Å^{-3})	0.400 and -0.371	0.250 and -0.188

Table S6: Selected crystallographic data for $[Li(Et_2O)][Li(thf)]_2[Li(thf)(Et_2O)]$[**6**] and $[Li(dme)]_2[Li(dme)_{1.5}]_2$[**7**].

	$[Li(Et_2O)][Li(thf)]_2[Li(thf)(Et_2O)]$[**6**]	$[Li(dme)]_2[Li(dme)_{1.5}]_2$[**7**]
CCDC number	2085653	2085654
formula	$C_{50}H_{72}B_2Li_4O_5$	$C_{62}H_{102}B_2Li_4O_{10}$
M_r	802.45	1056.81
T (K)	173(2)	173(2)
radiation, λ (Å)	0.71073	0.71073
crystal system	monoclinic	triclinic
space group	$P\,2_1/n$	P -1
a (Å)	16.5414(8)	10.6897(6)
b (Å)	16.7794(8)	12.3015(7)
c (Å)	18.6982(9)	12.8582(7)
α (°)	90	76.603(5)
β (°)	112.175(4)	82.096(5)
γ (°)	90	86.590(5)
V (Å^3)	4805.9(4)	1628.54(16)
Z	4	1
D_{calcd} (g cm^{-3})	1.109	1.078
F(000)	1736	576
μ (mm^{-1})	0.067	0.069
crystal size (mm)	0.220 x 0.190 x 0.110	0.270 x 0.140 x 0.090
crystal shape, color	dark red plate	black plate
reflections collected	47279	23168
independent reflections	8466	6623
R_{int}	0.0633	0.0247
data / restraints / parameters	8466 / 118 / 615	6623 / 3 / 362
R_1, wR_2 ($I > 2\sigma(I)$)	0.0727, 0.1535	0.0642, 0.1537
R_1, wR_2 (all data)	0.1035, 0.1649	0.0767, 0.1609
GOF on F^2	1.171	1.088
Largest difference peak and hole (e Å^{-3})	0.431 and -0.298	0.360 and -0.260

Table S7: Selected crystallographic data for $[Na(thf)_6][\mathbf{9}]$ and 9-bromo-9-borafluorene·thf.

	$[Na(thf)_6][\mathbf{9}]$	9-bromo-9-borafluorene·thf
CCDC number	2085663	2085650
formula	$C_{64}H_{99}B_2NaO_6$	$C_{16}H_{16}BBrO$
M_r	1009.04	315.01
T (K)	173(2)	173(2)
radiation, λ (Å)	0.71073	0.71073
crystal system	monoclinic	orthorhombic
space group	*C c*	*Pbca*
a (Å)	20.3838(12)	13.7522(15)
b (Å)	24.3114(10)	7.8787(6)
c (Å)	12.6143(8)	25.9288(19)
α (°)	90	90
β (°)	93.821(5)	90
γ (°)	90	90
V (Å^3)	6237.2(6)	2809.4(4)
Z	4	8
D_{calcd} (g cm^{-3})	1.075	1.490
F(000)	2208	1280
μ (mm^{-1})	0.072	2.914
crystal size (mm)	0.300 x 0.270 x 0.110	0.310 x 0.240 x 0.120
crystal shape, color	colorless plate	colorless plate
reflections collected	29620	11131
independent reflections	10985	2628
R_{int}	0.0438	0.0964
data / restraints / parameters	10985 / 255 / 737	2628 / 0 / 172
R_1, wR_2 ($I > 2\sigma(I)$)	0.0658, 0.1720	0.0398, 0.0780
R_1, wR_2 (all data)	0.0941, 0.1938	0.0717, 0.0861
GOF on F^2	1.017	0.916
Largest difference peak and hole (e Å^{-3})	0.420 and -0.396	0.349 and -0.361

4. EPR spectroscopy

$[Na_2(dme)_{3.75}][\mathbf{3}]$ (4 mg, 4 μmol) was dissolved in THF (0.5 mL) and treated with Na metal (47 mg, 2.0 mmol, 500 equiv). The mixture was set to rest overnight to give a solution of $Na_4[\mathbf{3}]$ (cf. 1.2.8). Unconsumed Na metal was removed manually and the remaining solution was mixed with $[Na_2(dme)_{3.75}][\mathbf{3}]$ (4 mg, 4 μmol, 1 equiv). The solution was diluted with THF (5.5 mL) and approx. 0.2 mL were transferred via syringe into an 3 mm ID quartz EPR tube. The tube was flame-sealed under vacuum. The EPR spectrum of the black solution was recorded using a Bruker EMXnono EPR spectrometer. The standard cavity at room temperature was used with 0.2 G modulation amplitude and a microwave of 2mW at 9.641 GHz; 50min acquisition time The measurement was performed at room temperature.

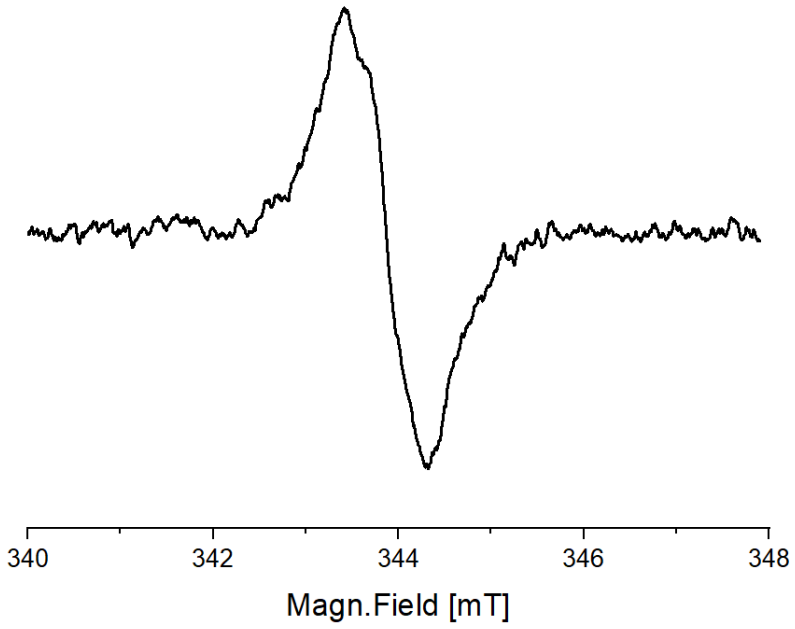

Figure S96: EPR spectrum recorded on a mixture of $Na_4[\mathbf{3}]$ and $Na_2[\mathbf{3}]$ (THF, room temperature).

We attribute the signal to a radical species $Na_3[\mathbf{3^{\bullet}}]$ formed *via* a comproportionation reaction between $Na_4[\mathbf{3}]$ and $Na_2[\mathbf{3}]$. However, due the poor resolution of the EPR spectrum, we could not confirm this assignment further.

5. UV/vis absorption spectra of Na_2[3] and Na_2[2]

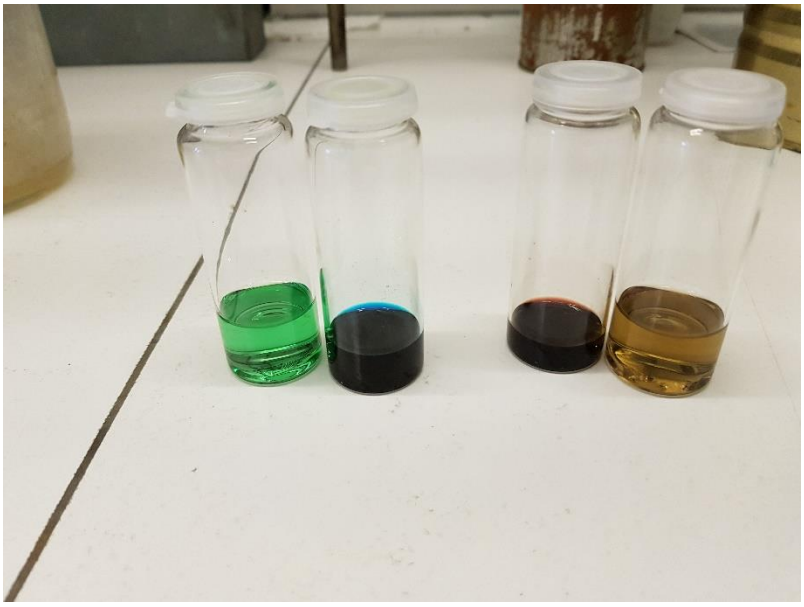

Figure S97: Photo of THF solutions of Na_2[**3**] (far left: 10^{-5} M, middle left: 10^{-4} M) and THF solutions of Na_2[**2**] (middle right: 10^{-4} M, far right 10^{-5} M).

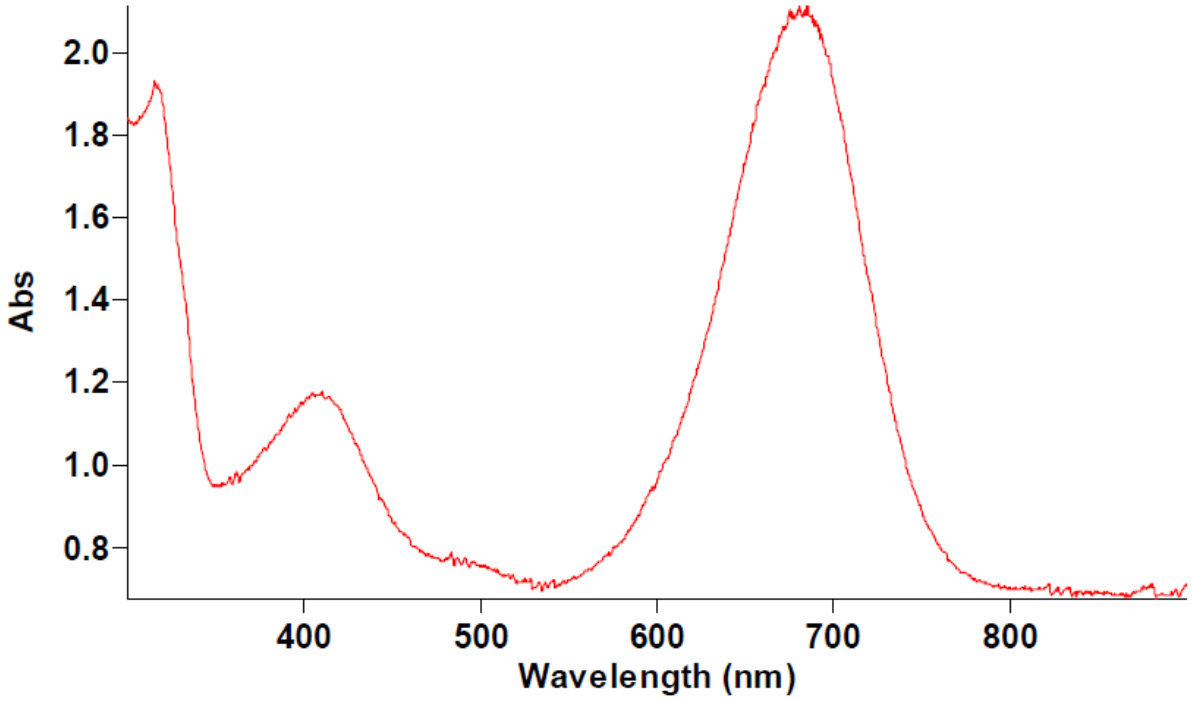

Figure S98: UV/vis absorption spectrum of Na_2[**3**] (THF, room temperature).

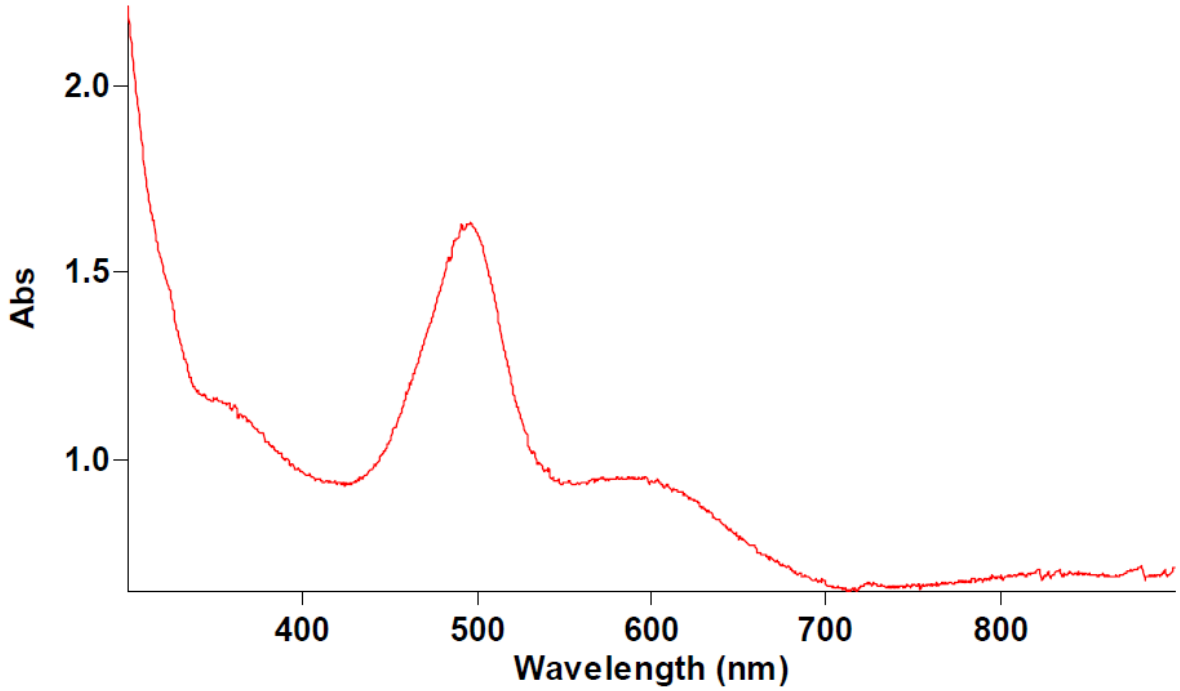

Figure S99: UV/vis absorption spectrum of Na_2[**2**] (THF, room temperature).

6. Investigation of the chemiluminescence of M_4[3] in air (M = Li, Na)

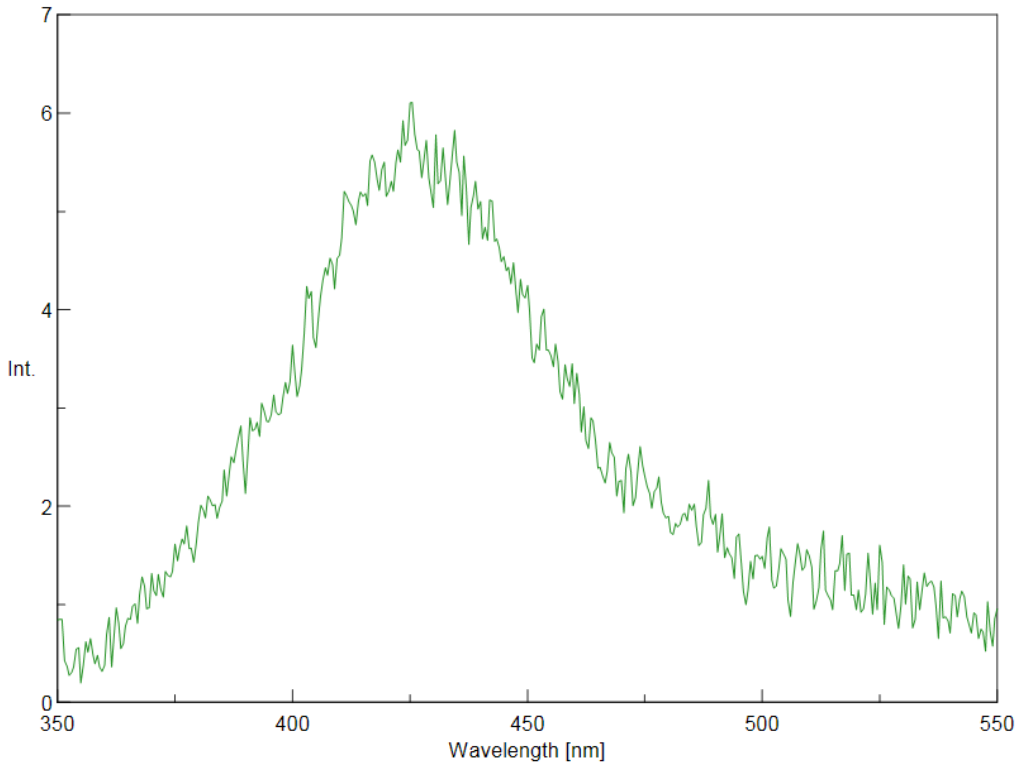

Figure S101: Emission of Na_4[**3**] upon exposure to air, measured during the first 3 min interval of the reaction (THF, room temperature).

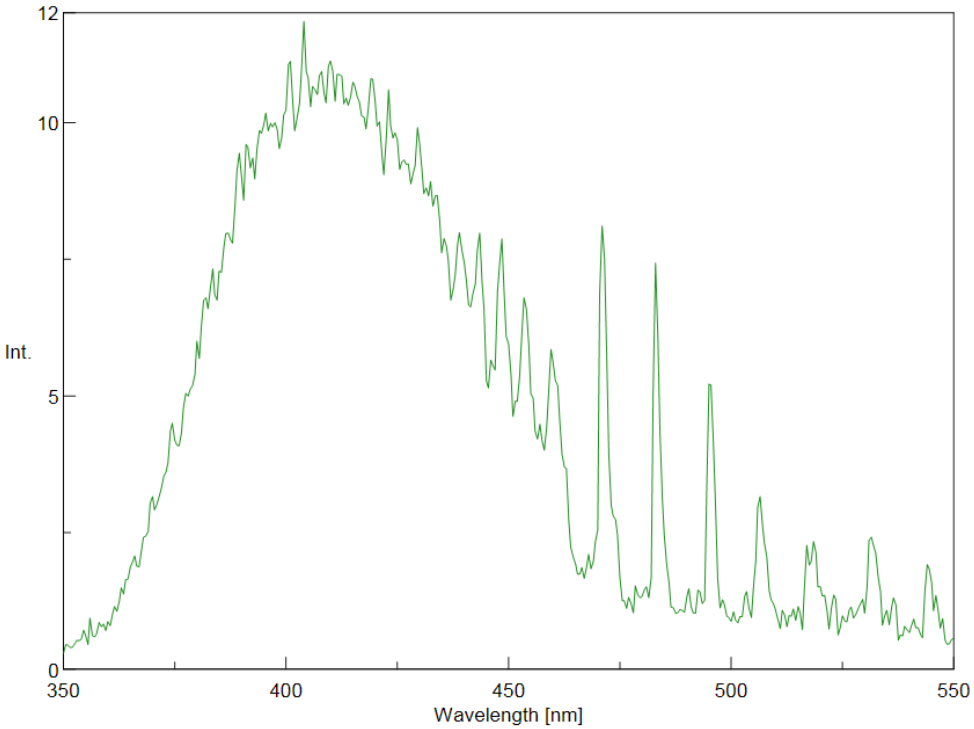

Figure S102: Emission of Na_4[**3**] upon exposure to air, measured during the second 3 min interval of the reaction (THF, room temperature).

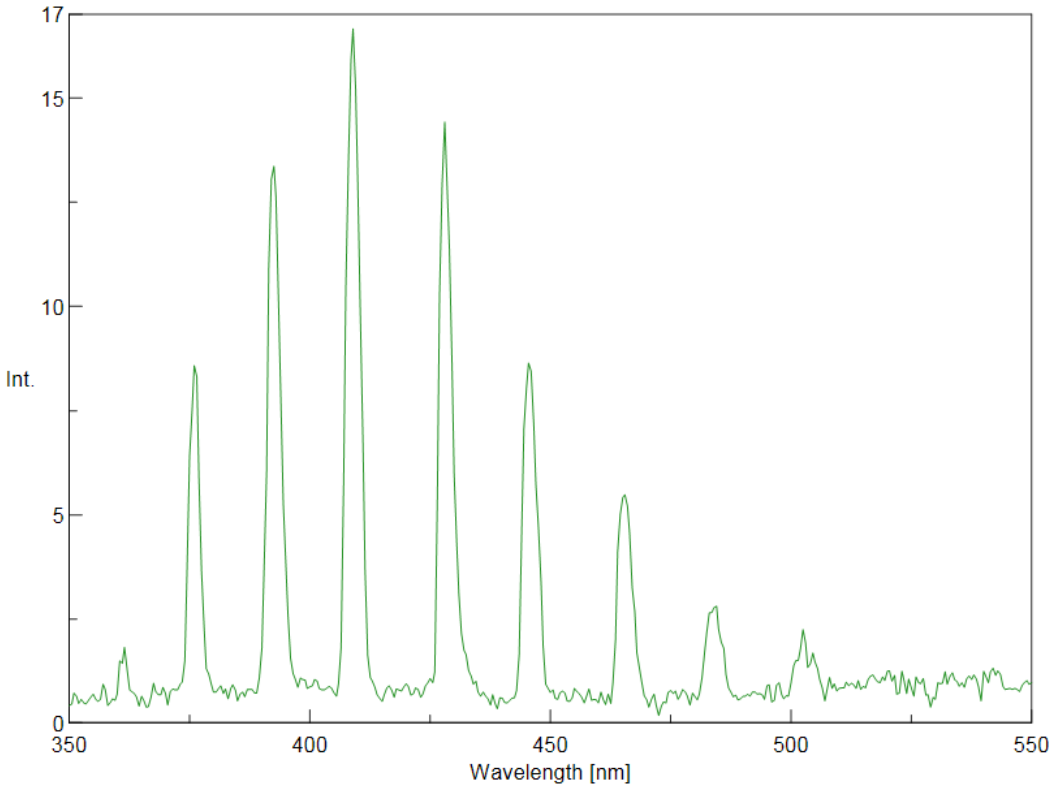

Figure S103: Emission of Na_4[**3**] upon exposure to air, measured during the third 3 min interval of the reaction (THF, room temperature).

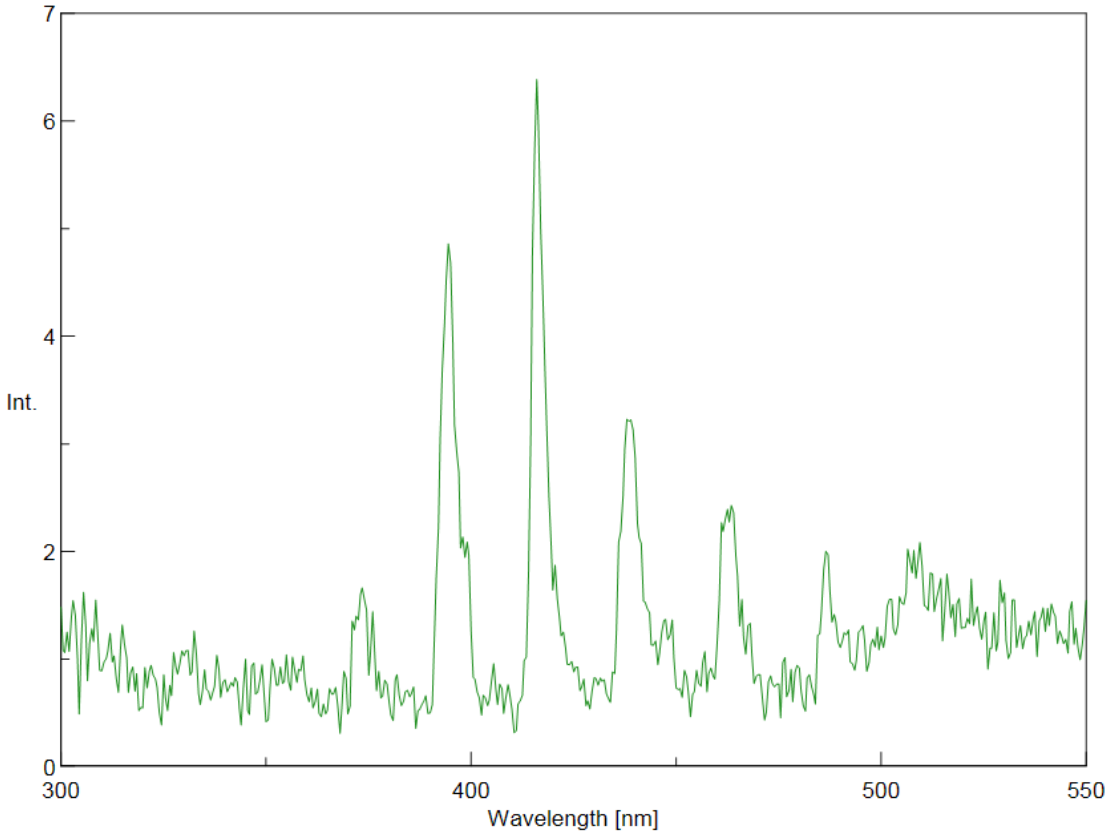

Figure S104: Emission of Na_4[**3**] upon exposure to air, measured during the fourth 3 min interval of the reaction (THF, room temperature).

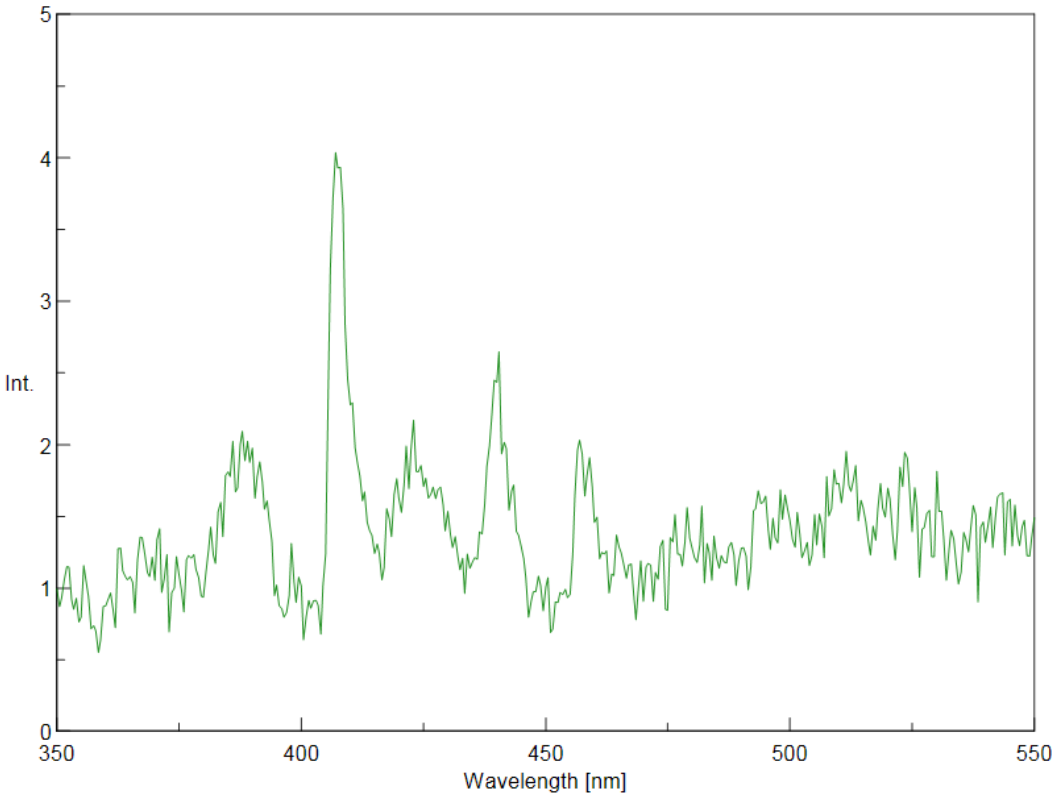

Figure S105: Emission of Na_4[**3**] upon exposure to air, measured during the fifth 3 min interval of the reaction (THF, room temperature).

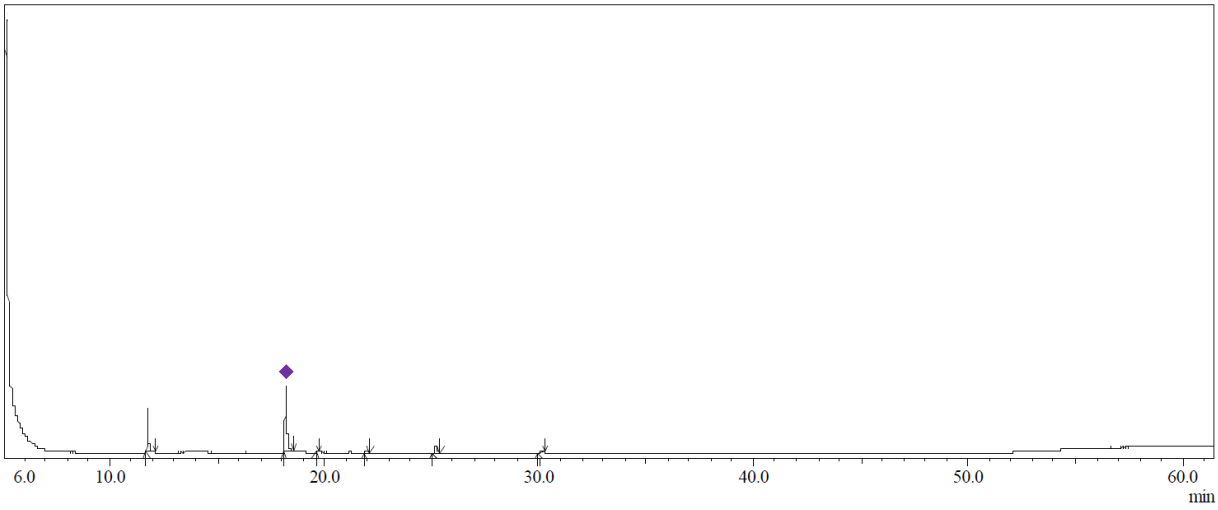

Figure S106: GC-MS chromatogram of the reaction solution Li_4[**3**]/air, immediately after the chemiluminescence had faded (THF). Marked compound: 4,4'-di*tert*butyl-1,1'-biphenyl (◆): rt = 18.20 min, *m/z* = 266 ($[M]^+$).

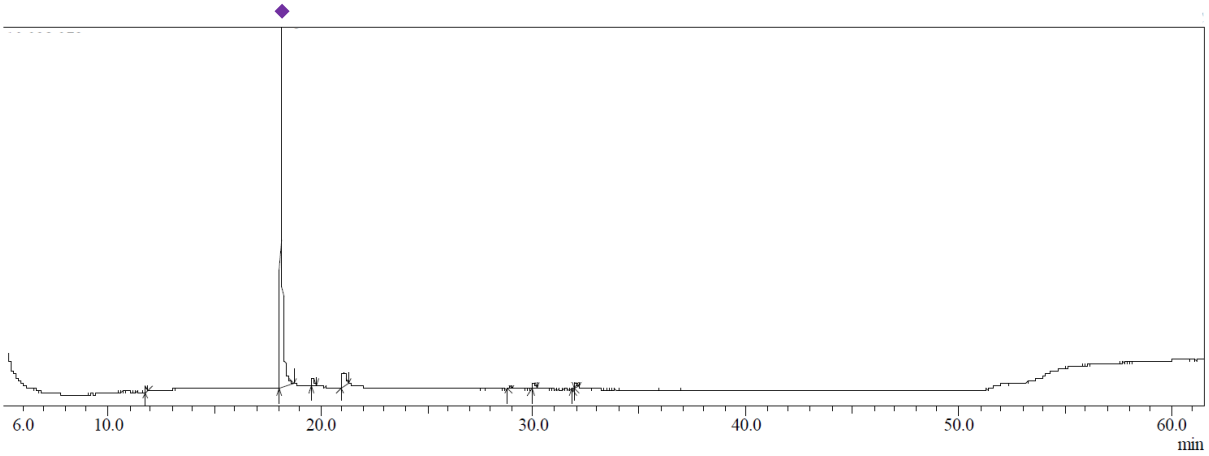

Figure S107: GC-MS chromatogram of the reaction solution Li_4[**3**]/air after the sample had been stored under ambient air for several weeks (THF). Marked compound: 4,4'-di*tert*butyl-1,1'-biphenyl (◆): rt = 18.15 min, *m/z* = 266 ($[M]^+$).

7. Computational details

DFT calculations were carried out with the Gaussian program package.[S14] The PBE0[S15–S18] hybrid functional was used and combined with the D3 atom-pairwise dispersion correction devised by Grimme.[S19,S20] Geometry optimizations and harmonic frequency calculations were computed with the SMD solvation model[S21] using the TZVP basis set.[S22] All Gibbs free energies reported correspond to the total energies of the system calculated with the SMD solvation model,[S21] corrected by thermal contributions from the frequency analyses. All stationary points reported were characterized as minima or first order saddle points by eigenvalue analysis of the diagonalized Hessians. The graphics were produced with Avogadro 1.1.1.

[3]$^{2-}$

Gibbs free energy = −1601.075512 Hartree

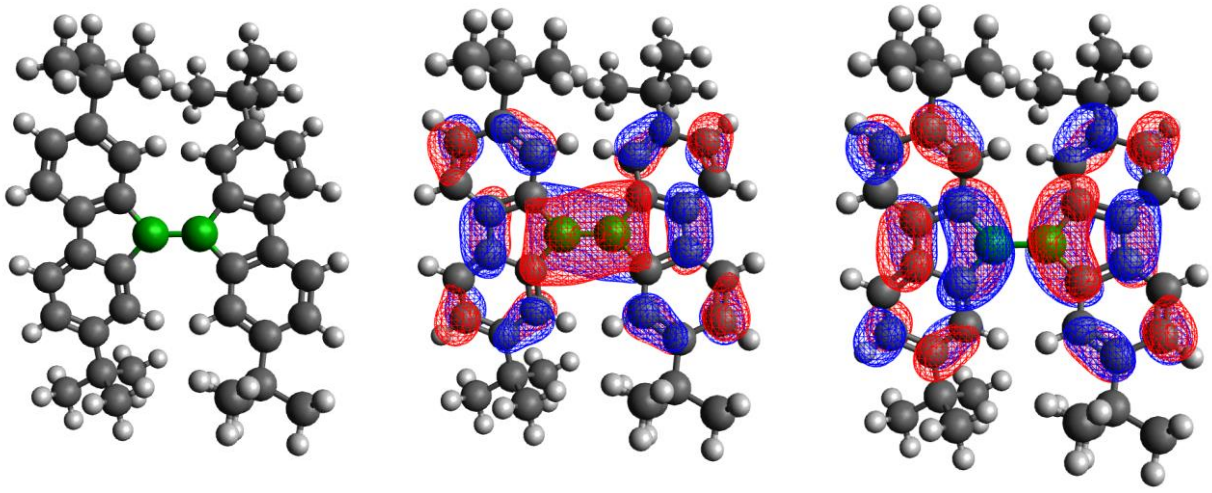

HOMO **LUMO**

Figure S108: Calculated structure of the dianion [**3**]$^{2-}$ and plots of the frontier orbitals (PBE0D/TZVP, SMD solvation model (THF), 0.02 isosurface value). Calculated HOMO energy: −2.173 eV; calculated LUMO energy: −0.063 eV.

B	0.03897	-0.81498	0.00264	C	3.37767	-2.84254	-0.86181	C	-5.79457	2.75225	-0.28435
B	0.03895	0.81498	-0.00237	C	2.55461	-1.74771	-0.58983	H	-5.62181	2.10353	0.57830
C	-1.17747	-1.80380	0.24296	H	2.98425	-0.75185	-0.64120	H	-5.68041	3.78738	0.04685
C	-0.75276	-3.15380	0.08000	C	4.85948	-2.61770	-1.16198	H	-6.82872	2.61190	-0.61734
C	-1.63377	-4.21359	0.27721	C	5.54202	-2.03267	0.08004	C	-5.11296	3.33233	-2.61232
H	-1.30536	-5.24161	0.13755	H	5.46923	-2.72581	0.92262	H	-4.41365	3.13740	-3.42956
C	-2.93667	-3.96478	0.68292	H	6.60176	-1.83652	-0.11545	H	-6.12845	3.14968	-2.97851
H	-3.60952	-4.80248	0.83624	H	5.07257	-1.09464	0.38077	H	-5.03892	4.38998	-2.35204
C	-3.38175	-2.65114	0.92285	C	5.01451	-1.63539	-2.32851	C	1.19781	1.86601	0.26852
C	-2.49426	-1.60480	0.68988	H	4.55163	-0.67198	-2.10809	C	0.66230	3.19251	0.25419
H	-2.81183	-0.58714	0.88080	H	6.07391	-1.45973	-2.54263	C	1.45954	4.29393	0.53600
C	-4.81086	-2.42419	1.41430	H	4.54199	-2.03233	-3.23103	H	1.03873	5.29742	0.53168
C	-5.11292	-3.33211	2.61247	C	5.58446	-3.90875	-1.53668	C	2.80868	4.12330	0.83178
H	-6.12846	-3.14963	2.97860	H	5.56269	-4.63658	-0.72133	H	3.41268	4.99712	1.04555
H	-5.03863	-4.38979	2.35237	H	5.14444	-4.37522	-2.42222	C	3.37776	2.84249	0.86177
H	-4.41369	-3.13688	3.42970	H	6.63299	-3.68939	-1.75846	C	2.55465	1.74766	0.58996
C	-5.04816	-0.98296	1.86042	C	-1.17746	1.80383	-0.24274	H	2.98425	0.75178	0.64147
H	-6.07400	-0.87550	2.22517	C	-0.75264	3.15384	-0.08006	C	4.85956	2.61761	1.16201
H	-4.36750	-0.69841	2.66671	C	-1.63356	4.21365	-0.2775	C	5.54205	2.03214	-0.07983
H	-4.91082	-0.27333	1.04315	H	-1.30507	5.24168	-0.13808	H	6.60176	1.83590	0.11575
C	-5.79466	-2.75236	0.28444	C	-2.93647	3.96487	-0.68317	H	5.07249	1.09410	-0.38031
H	-6.82880	-2.61183	0.61739	H	-3.60923	4.80260	-0.83671	H	5.46940	2.72505	-0.92261
H	-5.62184	-2.10385	-0.57837	C	-3.38168	2.65122	-0.92283	C	5.01447	1.63560	2.32882
H	-5.68062	-3.78758	-0.04654	C	-2.49428	1.60486	-0.68958	H	6.07386	1.45990	2.54300
C	1.19777	-1.86604	-0.26839	H	-2.81196	0.58718	-0.88025	H	4.54198	2.03283	3.23122
C	0.66217	-3.19251	-0.25430	C	-4.81079	2.42427	-1.41428	H	4.55150	0.67218	2.10864

C	1.45936	-4.29393	-0.53628	C	-5.04801	0.98308	-1.86058	C	5.58463	3.90870	1.53633
H	1.03849	-5.29740	-0.53211	H	-4.36736	0.69868	-2.66692	H	6.63315	3.68934	1.75814
C	2.80850	-4.12333	-0.83203	H	-4.91063	0.27336	-1.04340	H	5.56287	4.63631	0.72078
H	3.41245	-4.99715	-1.04596	H	-6.07386	0.87560	-2.22533	H	5.14468	4.37546	2.42176

[2]$^{2-}$

Gibbs free energy = −1601.078020 Hartree

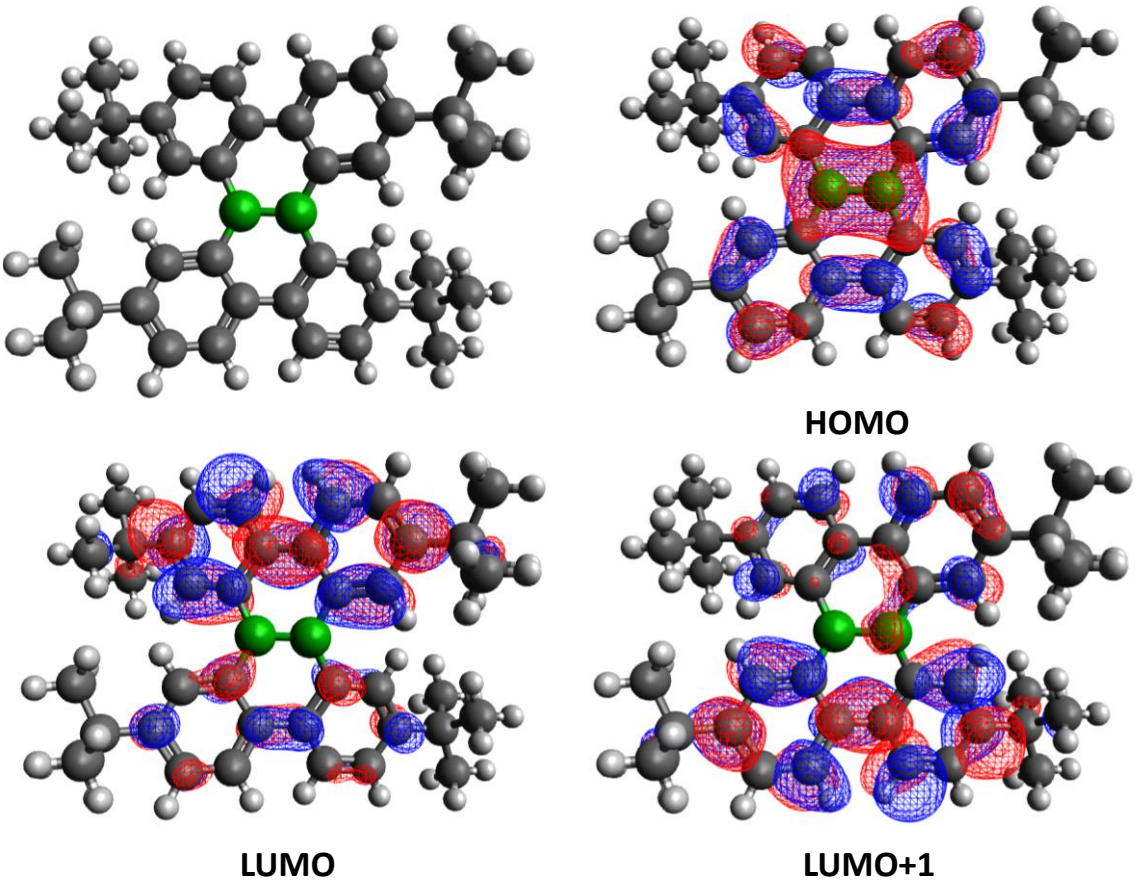

Figure S109: Calculated structure of [**2**]$^{2-}$ (top left) and plots of the frontier orbitals (PBE0D/TZVP, SMD solvation model (THF), 0.02 isosurface value). Calculated HOMO energy: −2.131 eV; calculated LUMO energy: 0.597 eV; calculated LUMO+1 energy: 0.649 eV.

B	0.80989	0.01549	0.01156	H	-5.48502	-1.21311	0.01265	H	3.00699	4.87113	1.26859
C	1.49857	-1.35584	-0.22908	H	-6.82321	-2.20998	0.60625	C	3.42426	2.75624	1.02187
C	0.72311	-2.56469	-0.16861	B	-0.79560	0.00686	0.01375	C	2.83030	1.55621	0.66697
C	1.34756	-3.77098	-0.53859	C	-1.49153	1.37137	-0.25217	H	3.42680	0.65355	0.74806
H	0.76885	-4.68862	-0.55852	C	-0.71994	2.58492	-0.20236	C	4.89228	2.79431	1.44374
C	2.66763	-3.84766	-0.92934	C	-1.34448	3.78165	-0.58837	C	5.76763	2.35375	0.26470
H	3.07873	-4.81177	-1.21418	H	-0.76883	4.70099	-0.61737	H	5.63734	3.02956	-0.58500
C	3.45815	-2.68486	-0.99294	C	-2.66737	3.85170	-0.98780	H	6.82626	2.35522	0.54649
C	2.84870	-1.49392	-0.65118	H	-3.07527	4.81243	-1.28015	H	5.50358	1.34795	-0.06694
H	3.42226	-0.58094	-0.74450	C	-3.44780	2.68816	-1.04532	C	5.33823	4.19077	1.87111
C	-1.47600	-1.36480	0.27270	C	-2.83176	1.50056	-0.68755	H	4.75800	4.55426	2.72344
C	-0.68980	-2.57039	0.22648	H	-3.40625	0.58460	-0.78033	H	6.39090	4.16615	2.16780
C	-1.30692	-3.77436	0.60556	C	-4.91054	2.69232	-1.48647	H	5.23807	4.91347	1.05716
H	-0.72363	-4.68875	0.63759	C	-5.39624	4.08703	-1.87435	C	5.12589	1.84162	2.62111
C	-2.63225	-3.85856	0.99225	H	-4.82250	4.49431	-2.71108	H	4.51550	2.13315	3.47986
H	-3.03252	-4.82416	1.27925	H	-6.44594	4.04023	-2.17870	H	4.86693	0.81378	2.36058
C	-3.42657	-2.70316	1.04394	H	-5.32187	4.78675	-1.03777	H	6.17806	1.85963	2.92497
C	-2.81959	-1.50935	0.69382	C	-5.78872	2.18729	-0.33520	H	5.67422	-3.40878	0.47348

H	-3.40407	-0.59914	0.78090	H	-6.84211	2.16185	-0.63451	C	5.67575	-3.75685	-0.56311
C	-4.89311	-2.72327	1.47174	H	-5.49795	1.18111	-0.02694	H	5.63631	-1.02975	-0.39193
C	-5.09572	-1.80766	2.68403	H	-5.69436	2.84169	0.53564	H	5.23090	-4.75398	-0.58205
H	-4.49202	-2.14930	3.52892	C	-5.09349	1.77116	-2.69770	H	6.71597	-3.84461	-0.89403
H	-6.14699	-1.80460	2.99175	H	-4.48708	2.11701	-3.53897	C	5.62488	-1.43330	-1.40760
H	-4.80470	-0.77945	2.46063	H	-4.79338	0.74664	-2.46952	C	4.90735	-2.77929	-1.46042
C	-5.36828	-4.12392	1.85129	H	-6.14218	1.75608	-3.01358	H	6.66216	-1.55500	-1.73368
H	-5.27938	-4.82040	1.01342	C	1.48676	1.39650	0.25094	H	5.15283	-0.69451	-2.05966
H	-6.42104	-4.08834	2.14650	C	0.69274	2.59663	0.20072	C	4.94827	-3.28908	-2.90594
H	-4.79794	-4.52791	2.69191	C	1.29522	3.80531	0.58382	H	4.47824	-4.27123	-2.99440
C	-5.76726	-2.22346	0.31516	H	0.70088	4.71252	0.61621	H	5.98276	-3.37438	-3.25558
H	-5.65957	-2.87387	-0.55712	C	2.61853	3.90275	0.97522	H	4.41710	-2.60233	-3.57032

8. References

[S1] A. Hübner, H.-W. Lerner, M. Wagner, M. Bolte, *Acta Cryst.* **2010**, *E66*, o444.

[S2] A. Hübner, M. Diefenbach, M. Bolte, H.-W. Lerner, M. C. Holthausen, M. Wagner, *Angew. Chem.* **2012**, *124*, 12682–12686; A. Hübner, M. Diefenbach, M. Bolte, H.-W. Lerner, M. C. Holthausen, M. Wagner, *Angew. Chem. Int. Ed.* **2012**, *51*, 12514–12518.

[S3] T. Kaese, H. Budy, M. Bolte, H.-W. Lerner, M. Wagner, *Angew. Chem.* **2017**, *129*, 7654–7658; T. Kaese, H. Budy, M. Bolte, H.-W. Lerner, M. Wagner, *Angew. Chem. Int. Ed.* **2017**, *56*, 7546–7550.

[S4] G. R. Fulmer, A. J. M. Miller, N. H. Sherden, H. E. Gottlieb, A. Nudelman, B. M. Stoltz, J. E. Bercaw, K. I. Goldberg, *Organometallics* **2010**, *29*, 2176–2179.

[S5] Preparation of the compound **4** is mentioned in the Supporting Information of A. Hübner, M. Bolte, H.-W. Lerner, M. Wagner, *Angew. Chem.* **2014**, *126*, 10576–10579; A. Hübner, M. Bolte, H.-W. Lerner, M. Wagner, *Angew. Chem. Int. Ed.* **2014**, *53*, 10408–10411.

[S6] J. Gilmer, H. Budy, T. Kaese, M. Bolte, H.-W. Lerner, M. Wagner *Angew. Chem.* **2020**, *132*, 5670–5674; J. Gilmer, H. Budy, T. Kaese, M. Bolte, H.-W. Lerner, M. Wagner *Angew. Chem. Int. Ed.* **2020**, *59*, 5621–5625.

[S7] The data were collected in our group in 2010 as part of the PhD thesis of Dr. Alexander Hübner: A. Hübner, Ph.D. thesis, Goethe-Universität Frankfurt (Germany), **2015**.

[S8] These compounds were not isolated and the NMR resonances were assigned by analogy to the Li and Na salts.

[S9] T. Trageser, M. Bolte, H.-W. Lerner, M. Wagner *Angew. Chem.* **2020**, *132*, 7800–7805; T. Trageser, M. Bolte, H.-W. Lerner, M. Wagner *Angew. Chem. Int. Ed.* **2020**, *59*, 7726–7731.

[S10] The corresponding Li salt has been reported in T. Kaese, T. Trageser, H. Budy, M. Bolte, H.-W. Lerner, M. Wagner, *Chem. Sci.* **2018**, *9*, 3881–3891. The NMR resonances of the Na salt were assigned by analogy.

[S11] Stoe & Cie, *X-AREA*. Diffractometer control program system, Darmstadt, Germany, **2002**.

[S12] G. M. Sheldrick, *Acta Crystallogr. Sect. A*, 2008, **64**, 112−122.

[S13] A. L. Spek, *Acta Crystallogr. Sect. D*, 2009, **65**, 148−155.

[S14] M. J. Frisch, G. W. Trucks, H. B. Schlegel, G. E. Scuseria, M. A. Robb, J. R. Cheeseman, G. Scalmani, V. Barone, B. Mennucci, G. A. Petersson, H. Nakatsuji, M. Caricato, X. Li, H. P. Hratchian, A. F. Izmaylov, J. Bloino, G. Zheng, J. L. Sonnenberg, M. Hada, M. Ehara, K. Toyota, R. Fukuda, J. Hasegawa, M. Ishida, T. Nakajima, Y. Honda, O. Kitao, H. Nakai, T. Vreven, J. A. Montgomery, Jr., J. E. Peralta, F. Ogliaro, M. Bearpark, J. J. Heyd, E. Brothers, K. N. Kudin, V. N. Staroverov, T. Keith, R. Kobayashi, J. Normand, K. Raghavachari, A. Rendell, J. C. Burant, S. S. Iyengar, J. Tomasi, M. Cossi, N. Rega, J. M. Millam, M. Klene, J. E. Knox, J. B. Cross, V. Bakken, C. Adamo, J. Jaramillo, R. Gomperts, R. E. Stratmann, O. Yazyev, A. J. Austin, R. Cammi, C. Pomelli, J. W. Ochterski, R. L. Martin, K. Morokuma, V. G. Zakrzewski, G. A. Voth, P. Salvador, J. J. Dannenberg, S. Dapprich, A. D. Daniels, O. Farkas, J. B. Foresman, J. V. Ortiz, J. Cioslowski, D. J. Fox, Gaussian 09, Revision D.01, Gaussian, Inc., Wallingford, CT, USA, **2013**.

[S15] J. P. Perdew, K. Burke, M. Ernzerhof, *Phys. Rev. Lett.* **1996**, *77*, 3865–3868.

[S16] J. P. Perdew, K. Burke, M. Ernzerhof, *Phys. Rev. Lett.* **1997**, *78*, 1396–1396.

[S17] J. P. Perdew, M. Ernzerhof, K. Burke, *J. Chem. Phys.* **1996**, *105*, 9982–9985.

[S18] C. Adamo, V. Barone, *J. Chem. Phys.* **1999**, *110*, 6158–6170.

[S19] L. Goerigk, S. Grimme, *J. Chem. Theory Comput.* **2011**, *7*, 291–309.

[S20] S. Grimme, S. Ehrlich, L. Goerigk, *J. Comput. Chem.* **2011**, *32*, 1456–1465.

[S21] A. V. Marenich, C. J. Cramer, D. G. Truhlar, *J. Phys. Chem. B*, **2009**, *113*, 6378–6396.

[S22] A. Schäfer, C. Huber, R. Ahlrichs, *J. Chem. Phys.* **1994**, *100*, 5829–5835.